Naval Research Laboratory

Stennis Space Center, MS 39529-5004

NRL/FR/7320--03-10,020

Validation Test Report for the 1/16° Global NRL Layered Ocean Model Nowcast/Forecast System

Robert C. Rhodes
Harley E. Hurlburt
Alan J. Wallcraft
E. Joseph Metzger
Jay F. Shriver

Ocean Dynamics and Prediction Branch
Oceanography Division

Ole Martin Smedstad
Jean-Francois Cayula

Planning Systems, Inc.
Stennis Space Center, MS

A. Birol Kara

Florida State University
Talahassee, FL

April 14, 2003

REPORT DOCUMENTATION PAGE

Form Approved
OMB No. 0704-0188

1. REPORT DATE *(DD-MM-YYYY)*	2. REPORT TYPE	3. DATES COVERED *(From - To)*
April 14, 2003		

4. TITLE AND SUBTITLE

Validation Test Report for the 1/16° Global NRL Layered Ocean Model Nowcast/Forecast System

5a. CONTRACT NUMBER

5b. GRANT NUMBER

5c. PROGRAM ELEMENT NUMBER
0601153N

6. AUTHOR(S)

Robert C. Rhodes, Harley E. Hurlburt, Alan J. Wallcraft, E. Joseph Metzger, Jay. F. Shriver, Ole Martin Smedstad,* Jean-Francois Cayula,* and A. Birol Kara†

5d. PROJECT NUMBER

5e. TASK NUMBER
BE 031-03-42

5f. WORK UNIT NUMBER
73-7178-03

7. PERFORMING ORGANIZATION NAME(S) AND ADDRESS(ES)

Naval Research Laboratory
Oceanography Division
Stennis Space Center, MS 39529-5004

8. PERFORMING ORGANIZATION REPORT NUMBER

NRL/FR/7320--03-10,020

9. SPONSORING / MONITORING AGENCY NAME(S) AND ADDRESS(ES)

Office of Naval Research
800 North Quincy Street
Arlington, VA 22217-5660

10. SPONSOR / MONITOR'S ACRONYM(S)

11. SPONSOR / MONITOR'S REPORT NUMBER(S)

12. DISTRIBUTION / AVAILABILITY STATEMENT

Approved for public release; distribution is unlimited.

13. SUPPLEMENTARY NOTES

*Planning Systems, Inc., Stennis Space Center, MS 39529
†Florida St. University, Center for Ocean Atmospheric Prediction Studies, Talahassee, FL 32310

14. ABSTRACT

This report describes validation tests for the eddy-resolving 1/16° global Naval Research Laboratory (NRL) Layered Ocean Model (NLOM) nowcast/forecast system. For the non-assimilative model, maps of sea surface height (SSH) and sea surface temperature (SST) show that the model depicts the observed positions of the major fronts. Comparisons of model SSH variability with altimetry and correlations with tide-gauge SSH time series demonstrate ocean model skill. In addition, model comparisons with daily buoy time series of SST indicate that the model has SST simulation skill when forced by winds and thermal forcing. The realistic non-assimilative model simulation skill indicates that the model will add skill to the data assimilation cycle and, in the case of SSH assimilation, allow the model to be used as the first-guess for the analysis. Validation tests of the assimilative model were performed. SST comparisons with unassimilated buoy time series show that the model has good agreement with the observed data. SSH comparisons with observed sea level from coastal stations and buoys indicate that the model has accurate SSH and the correlations are higher with data assimilation. Nowcast comparisons with analyzed frontal positions from the Naval Oceanographic Office show that the model can be a useful tool to help the analyst improve frontal analyses. Forecast evaluations indicate that the model has SSH predictive skill of at least 30 days in the Kuroshio, about 15 days in the Gulf Stream, and at least 30 days when calculated globally. The NLOM system was also tested for improvement of the Modular Ocean Data Assimilation System (MODAS) synthetic temperature profiles by using the NLOM SSH field as opposed to the MODAS 2-D SSH analysis field. Results indicate that the synthetics from NLOM SSH are, in general, better than MODAS SSH.

15. SUBJECT TERMS

Nowcast/Forecast; NLOM; Kuroshio

16. SECURITY CLASSIFICATION OF:			17. LIMITATION OF ABSTRACT	18. NUMBER OF PAGES	19a. NAME OF RESPONSIBLE PERSON
a. REPORT	b. ABSTRACT	c. THIS PAGE			Bob Rhodes
Unclassified	Unclassified	Unclassified	UL	70	19b. TELEPHONE NUMBER *(include area code)* (228) 688-4704

Standard Form 298 (Rev. 8-98)
Prescribed by ANSI Std. Z39.18

CONTENTS

VALIDATION TEST REPORT FOR THE 1/16° GLOBAL NRL LAYERED OCEAN MODEL NOWCAST/FORECAST SYSTEM

1. INTRODUCTION

The Naval Research Laboratory (NRL) Layered Ocean Model (NLOM) has been under development since 1976 (Hurlburt and Thompson 1980; Wallcraft 1991; Wallcraft and Moore 1997; Moore and Wallcraft 1998; Wallcraft et al. 2002b). NLOM is the centerpiece of the NRL baseline global ocean prediction system, which is the first in a progression of numerical ocean model-based nowcast/forecast systems planned for Naval operations. The process began in FY99 without an ocean model as an ocean analysis capability (the Modular Ocean Data Assimilation System, MODAS). This was followed in FY01 with delivery of the 1/16° global model (NLOM) that had the resolution required to properly resolve mesoscale ocean dynamics. It has been running daily at the Naval Oceanographic Office (NAVOCEANO) since 18 October 2000 and became an operational product on 27 September 2001. NLOM will be followed in FY03 by a 1/8°global version of the Navy Coastal Ocean Model (NCOM) with higher vertical resolution in the mixed layer for improved upper-ocean prediction. NCOM will assimilate sea surface height (SSH) from NLOM, and together they will form a two-model system in which each provides value added and each is used in operational applications (Rhodes et al. 2002).

Operational applications for the NLOM system will include improved nowcasts and forecasts of major front and eddy systems like the Gulf Stream and Kuroshio Extension, accurate high-resolution SSH and sea surface temperature (SST) products to improve MODAS 3-D temperature and salinity synthetics. By improving MODAS synthetics, NLOM will provide more accurate and more dynamically realistic initialization for global NCOM. The front and eddy nowcasts will be used by the Warfighting Support Center (WSC) at NAVOCEANO to improve global front and eddy analysis products, and the system will provide a "first of its kind" forecast capability for ocean fronts and eddies.

This report discusses the various system components, including NLOM, and some of the validation results for the NLOM system. For the model running in a non-assimilative simulation mode, comparisons include mean SSH with and without assimilation, time series from tide gauge data, root-mean-square (RMS) SSH with observed data from altimetry, and SST comparisons with buoy data. In the assimilative model runs, SSH comparisons with unassimilated global tide-gauge sea-level data and SST comparisons with the global MODAS analysis and unassimilated buoy data are shown. Comparisons of nowcast positions of major fronts and eddies from NLOM will be compared to NAVOCEANO frontal analysis products, and forecast validation statistics for 30-day NLOM front and eddy forecasts in the Gulf Stream and Kuroshio are discussed. Validation of global SSH forecasts is also discussed. Additional evaluations of MODAS synthetic temperature profiles calculated using the NLOM SSH fields are provided and recommendations for future systems, including the increase in horizontal resolution of NLOM, are made. The results are based on initial evaluations. Additional discussion and evaluation of the 1/16° NLOM nowcast/forecast system are found in Hurlburt and Wallcraft (2000a,b), Hurlburt et al. (2001, 2002), Metzger et al. (2001), Rhodes et al. (2002), Smedstad et al. (2002), Wallcraft et al. (2002a), and Zamudio et al. (2002).

Manuscript approved October 19, 2002.

2. SYSTEM COMPONENTS

NRL Layered Ocean Model

The NRL Layered Ocean Model is a descendent of the primitive equation model by Hurlburt and Thompson (1980). Since then, the capability of the model has been greatly expanded (Wallcraft 1991, Wallcraft and Moore 1997, Moore and Wallcraft 1998, Wallcraft et al. 2002b). It is available in both reduced gravity versions, in which the lowest layer is infinitely deep and at rest, and in finite-depth versions, which allow for realistic bottom topography. The 1/16° NLOM nowcast/forecast system has seven layers including the mixed layer.

The model has a global domain that extends from 72°S to 65°N. The horizontal resolution of each model variable is 1/16° in latitude by 45/512° in longitude. At this resolution, the model is eddy-resolving. There is strong evidence that NLOM and other popular ocean models need to use grid cells for each prognostic variable that are, at most, about 7 km across at midlatitudes. NRL research has shown that doubling the horizontal resolution to 4 km per cell gives substantial improvement but doubling again to 2 km gives only modest additional improvement (Hurlburt and Hogan 2000). For the NLOM grid, these resolutions translate to 1/16°, 1/32°, and 1/64°, respectively. This is for the global and basin-scale. Much finer resolution is needed in coastal regions. At 4 km, the optimal resolution is finer than might be expected based on the size of ocean eddies. In relation to ocean eddy size, it is similar to the resolution currently used by the leading weather forecasting models in relation to the size of atmospheric highs and lows. More specifically, our research has shown that fine resolution of the ocean eddy scale is required to obtain coupling between upper-ocean currents and seafloor topography via turbulent flow instabilities. This coupling can strongly affect the pathways of upper ocean currents and fronts, including the Gulf Stream and the Kuroshio. The high resolution is also required to obtain sharp fronts that span major ocean basins (Hurlburt et al. 1996), and it can affect the large-scale shape of ocean gyres such as the Sargasso Sea in the Atlantic (Hurlburt and Hogan 2000). As discussed later, simulation skill for the preceding is crucial for an ocean model to act as an effective dynamic interpolater for satellite altimeter data and for successful forecasting of ocean eddies and the meandering of ocean currents and fronts. Results from a 1/4° global model did not demonstrate these skills (Hurlburt et al. 2000).

The model is thermodynamic, and horizontal density gradients within a layer can be modified by advection, diffusion, entrainment, or relaxation to a density climatology such as MODAS. The latter helps NLOM maintain accurate SSH. Unlike models with fixed levels in the vertical, such relaxation does not damp the anomalies because NLOM carries most of the information about anomalies in layer thickness variations. For example, NLOM maintained a Rossby wave generated by the 1982-1983 El Niño for at least a decade (Jacobs et al. 1994) without oceanic data assimilation except for relaxation to climatological density. The model equations and additional details concerning NLOM are found in Hurlburt et al. (1996), Metzger and Hurlburt (1996), Moore and Wallcraft (1998), and Shriver and Hurlburt (1997). A mixed layer model and sea surface temperature were added to NLOM (Wallcraft et al. 2002b) and is part of the system transitioned to NAVOCEANO.

The model was originally spun up at 1/2° resolution using the Hellerman and Rosenstein (HR) (1983) monthly wind stress climatology. After reaching statistical equilibrium at 1/2°, the model was continued at 1/4°, 1/8°, and 1/16° resolution using HR stresses until equilibrium was reached. From this point, the model with a mixed layer was run for additional spin-up using HR stresses and Comprehensive Ocean Atmosphere Data Set (COADS) thermal forcing before interannual wind and thermal forcing began in 1979. A hybrid

approach was used when 6-12 hourly interannual atmospheric forcing began on 1 January 1979. This consisted of a combination of first, European Centre for Medium-Range Weather Forecasts (ECMWF) (1979-1989) and then FNMOC NOGAPS (1990-present) and HR surface stresses, where the long-term mean (1979-1993 for ECMWF and August 1990-July 1999 for FNMOC) was subtracted from the ECMWF and FNMOC stresses and replaced with the HR annual mean. This hybrid approach has been previously used successfully with the HR and ECMWF 1000-mb winds (Metzger et al. 1992, 1994; Hurlburt et al. 1996)

The 6-hourly ECMWF/HR hybrid winds and ECMWF thermal forcing were used to force the model over the 1979-1989 time frame. In 1990, a switch was made to 12-hourly FNMOC NOGAPS wind forcing with ECMWF thermal forcing, followed by a switch to NOGAPS thermal forcing in 1998. SSH assimilation began in 1997, and SST assimilation began in 1998. This was continued until October 2000 when the system was transitioned to NAVOCEANO, and it is now running in real time. It is updated daily as part of the operational run stream forced by NOGAPS wind and thermal forcing and with assimilation of SSH and SST.

NLOM Data Assimilation

The NLOM system assimilates both SSH and SST but by using different methods. The SSH assimilation is daily, using a 3-day data window. It consists of an optimum interpolation (OI)-based data assimilation scheme that uses an OI deviation analysis with the model as the first guess, the statistical inference technique of Hurlburt et al. (1990) for vertical projection, geostrophic balance for velocity deviations outside an equatorial band, and slow analysis insertion to further reduce gravity wave generation (Smedstad and Fox 1994). The spatially varying covariance functions for the OI analyses were calculated from TOPEX/POSEIDON and ERS-2 data over 1993-1999 by Jacobs et al. (1999, 2001). Since the altimeter data are deviations from their mean over 1993-1999, a slightly modified model mean SSH over the same time frame is added to the altimetric deviations. The model mean is consistent with hydrographic climatology because of the density relaxation within the layers (Section 2), but it has sharper means for fronts, boundary currents, and currents that extend into the ocean interior. The mean SSH and its creation are discussed in more detail by Smedstad et al. (2002). Jacobs and Mitchell (1997) discuss the combining of altimeter data from multiple satellites with different orbits and life spans. The SST assimilation is performed by relaxing the NLOM SST to the real-time MODAS SST analysis performed daily at NAVOCEANO. Data assimilation began with altimetry SSH assimilation in 1997, and SST assimilation began in the fall of 1998 and continues to the present.

The assimilation cycle for the operational system goes back three days in time and uses analysis wind and thermal forcing as data are assimilated up to the nowcast time. This technique allows the use of additional and more accurate altimeter data that is updated as more precise orbit calculations became available. It also allows more accurate nowcasts to initialize model forecasts. The system performs a daily 4-day forecast, except for once a week when a 30-day forecast is made. During the forecast period, a relaxation to climatologically corrected persistence is performed for SST with a relaxation time scale of 1/4 the forecast length (i.e., 1 day for a 4-day forecast and 1 week for a 4-week forecast). This is a necessary step for the longer term (30-day) SST forecast because the forecast atmospheric thermal forcing is only available out to four days and SST is very sensitive to atmospheric forcing. This allows the model to have more accurate SST forecasts. During a forecast, the position of oceanic fronts, current/frontal meanders and eddies can change substantially. The SST relaxation is weak enough that it allows the model to keep the SST forecasts of these features better in phase with the forecasts of SSH and surface currents than climatologically corrected persistence, a model value added in SST forecasting. There is no relaxation for SSH because the model is used to forecast the movement of fronts and eddies that are due to flow instabilities. These are more sensitive to initial conditions than to atmospheric forcing.

3. TESTING RESULTS

Non-Assimilative Model Validation

Model Mean

Figures 1 and 2 show the 1997-1999 mean hemispheric SSH from the non-assimilative global simulation driven by FNMOC forcing and the assimilative model with TOPEX and ERS-2 altimeter data assimilated. (For convenience, all figures in this report are grouped at the end of the text.) In the Pacific Ocean (Fig. 1) the model is able to simulate the basic upper ocean circulation patterns without data assimilation. The non-assimilative (Fig. 1(a)) and data-assimilative (Fig. 1(b)) model means are very similar since a slightly modified model mean SSH over 1993-1999 is added to the altimetric deviations from their own 1993-1999 mean. Besides the modifications to the mean, these means can differ because of differences in the 1997-1999 mean deviation from the 1993-1999 mean used for SSH assimilation. Model skill in simulating the position and strength of major gyres, fronts, and eddies without assimilation is required for the model to be a skillful dynamic interpolator of the satellite altimeter data. An accurate model mean is also very important for use in areas of strong fronts because the model can provide a mean over the same period as the altimeter. A fully eddy-resolving model also gives a sharper mean front than is possible from a hydrographic climatology when added to the altimeter anomalies. This allows a more realistic SSH change across the front.

Starting in the Northern Hemisphere (NH), the cyclonic subpolar gyre and anticyclonic subtropical gyre dominate the large scale. The subpolar gyre is bounded by the Alaska Stream on the north, the East Kamchatka Current on the west, and the Oyashio Current on the west and southwest. A weak subarctic front/ North Pacific Current separates these two gyres along 41°-45°N. The subtropical gyre is bounded by the Kuroshio on the west, the subarctic front on the north, and the North Equatorial Current (NEC) along 10°-18°N on the south. These features are seen in both the assimilative and non-assimilative model experiments.

In both experiments, at ~14°N the NEC splits at the Philippines coast into the northward-flowing Kuroshio and the southward-flowing Mindanao Current (MC). The MC is the western boundary current of the zonally elongated northern tropical gyre with the NEC on the north and the North Equatorial Countercurrent (NECC) on the south along 5°-10°N.

For both the non-assimilative and assimilative cases in the Southern Hemisphere (SH), the South Equatorial Countercurrent (SECC) is centered at 7°-10°S and is much weaker than the NECC. The core of this current is confined mostly to the west of the dateline. The Antarctic Circumpolar Current (ACC) is shown in the non-assimilative model south of 40°S and has many mesoscale mean meanders similar, to the assimilative case due to topographic steering (Tilburg et al. 2001, 2002)

In the NH Atlantic Ocean (Fig. 2), both model simulations produce a realistic subtropical gyre shape and separation of the Gulf Stream at Cape Hatteras. In the Gulf of Mexico, the models simulate the Loop Current and its associated eddies. The North Brazil retroflection is seen near 7°N, 48°W and, in both cases, the model realistically simulates the ring generation characteristic of this region (Fratantoni et al. 1995). Finally, both the non-assimilative and assimilative models show good agreement on simulating the Agulhas Retroflection at the southern tip of Africa.

Figure 3 shows snapshots of SSH from the non-assimilative model for the Gulf Stream (Fig. 3(a)) and the Kuroshio Extension (Fig 3(b)). These areas are both dominated by flow instabilities. If the model is

going to have any skill in forecasting the movement of fronts and eddies, the model must accurately simulate these features. The Gulf Stream plot includes an overlay of the mean ±1 standard deviation of the position of the Gulf Stream north wall derived from satellite infrared (IR) imagery. The model does an excellent job in comparison to the mean in simulating the position of the Gulf Stream pathway from Cape Hatteras to the Grand Banks. Also, many warm and cold Gulf Stream eddies are simulated by the model on this day. The eddies are realistic in size and shape, and warm core eddies (which have been particularly difficult for models) are well simulated by the non-assimilative 1/16° NLOM.

The Kuroshio Extension (Fig. 3(b)) simulated by the model has a realistic pathway that extends out past 180°E, which is consistent with observations. It also simulates both the meander and straight path modes near 138°E. The Oyashio and subarctic fronts are also well represented by the non-assimilative model. In this snapshot, the model shows the meander mode pathway off the coast of Japan and simulates many warm and cold eddies that are realistic in size and shape, similar to the Gulf Stream results.

RMS Sea Surface Height Variability Compared with Altimetry

Figures 4 and 5 show the hemispheric RMS SSH variability from 1997-1999 for the non-assimilative and assimilative models compared with variability from observed TOPEX/Poseidon satellite altimetry data. This is shown as further evidence that the non-assimilative model is producing not only realistic pathways of major ocean features but is also simulating the variability in areas of strong flow instabilities. One important component of the NLOM data assimilation is the statistical inference technique (Hurlburt et al. 1990), which uses model statistics to derive the relationship between variability in the model upper layer and that in the lower layers. If the model is not properly simulating the observed variability of the ocean, then the statistical inference will be less effective. This is another example of the need for model skill in simulating the ocean to be a useful part of the data assimilation system.

In the Pacific (Fig. 4), the non-assimilative model (Fig. 4(a)) generally shows good agreement with the variability from the assimilative model (Fig. 4(b)) and the TOPEX data (Fig 4(c)). The largest variability is indicated in areas of strong flow instabilities like the Kuroshio Extension and off the east coast of Australia. In both of these areas, the non-assimilative model has similar variability patterns compared with the assimilative case and the TOPEX data. The TOPEX data are a smoother representation of the variability because of the horizontal track spacing of the altimeter. In particular, the non-assimilative model variability in the Kuroshio region is consistent with the other two, with high variability out to 160°E.

In the Atlantic (Fig. 5), several areas of high variability are well simulated by the non-assimilative model (Fig. 5(a)). In the Gulf Stream region, the model has realistic variability along the Gulf Stream pathway from Cape Hatteras to the Grand Banks compared with the assimilative model (Fig. 5(b)) and the TOPEX data (Fig 5(c)). However, the non-assimilative model has higher variability just east of Cape Hatteras and lower variability south and southwest of the Grand Banks when compared to the data. The region of high variability does extend out to ~45°W, which is consistent with the data. Other areas of high variability found in all three cases are the Gulf of Mexico, the southern east coast of South America (~40°S), and the Agulhas Retroflection south of Africa (~20°E).

Sea Surface Temperature Compared with Buoy Data

The non-assimilative mode NLOM was also tested for skill in nowcasting SST forced by operational atmospheric fluxes and with no relaxation to observed SST. Similar to SSH nowcasting discussed earlier,

the model must have skill in simulating the observed monthly and seasonal changes of SST or the model will always "fight" the relaxation to observed SST and lack SST forecasting skill. Figure 6 shows yearlong daily time series comparisons of non-assimilative 1/16° global NLOM forced with operational wind and thermal forcing from ECMWF with observed buoy data for 1998.

The results indicate that free-running NLOM SST data compare well with the buoy SST data. This is a very encouraging result. It shows the skill of the model, but it also indicates that operational wind and thermal forcing is accurate enough to force an ocean model and simulate seasonal and interannual variations in SST. The results for the three buoys are very consistent and indicate the model having the correct phase and amplitude for the seasonal steric signal as the ocean warms in the summer and cools in the winter. The model comparison with the buoy at 38°N, 130°W (Fig. 6(a)) has the lowest RMS error at 0.59°C, followed by the buoy at 46°N, 131°W with RMS error of 0.66°C, and the buoy at 41°N, 137°W with RMS error of 0.92°C. Each of the buoys had a correlation of 0.98. These results indicate that when data assimilation is added to the model system, the model should be able to accept the observed SST data and also add some skill to SST nowcasts and forecasts as a component of the data-assimilative system.

Assimilative Model Validation

Sea Surface Temperature Comparisons with MODAS Analysis

For SST assimilation, the NLOM system is relaxed to the MODAS analysis performed daily at NAVOCEANO. For this report, the criterion for model performance was that the NLOM system have good agreement with the MODAS analysis. Figures 7-12 show comparisons of the assimilative NLOM system and the MODAS analysis with observed buoy SST data for 1999. This is an independent comparison because, at the present time, the daily MODAS analysis assimilates only satellite MCSST data, and buoy data are not assimilated.

In all cases, the NLOM SST tracks the MODAS analysis very well. In most cases, the model and MODAS compare favorably to the buoy data. Figures 7-10 depict buoys that are in equatorial areas. The NLOM and MODAS results do not depict the high-frequency variability and are therefore smoother than the buoy data, but for most of the equatorial buoys, NLOM and MODAS show good agreement with the buoys. Outside the equatorial area (Figs. 11 and 12) the results are similar. The overall results show that the median RMS error for MODAS and NLOM vs buoy data are almost identical (0.35°C and 0.33°C, respectively), which is the test criterion for SST nowcasts. Some of the larger MODAS and NLOM errors with respect to the buoys are most likely due to cloudy periods when there was no MCSST data for long periods of time. However, the MODAS product at NAVOCEANO will improve as real-time buoy data are included in the analysis in the future.

Sea Surface Height Comparisons with Island Sea-level Data

The assimilative NLOM system was compared to observed tide-gauge sea-level data—one means of showing model skill in nowcasting SSH. Table 1 depicts observed monthly SSH correlation (r) from 1997-1999 for 74 tide-gauge stations around the world from the Joint Archive for Sea Level Data (JASL) database. Comparison of results from the non-assimilative simulation (Free) and the assimilative model (Assim) shows improvement in the real-time results when satellite altimeter data are assimilated. As discussed earlier, the non-assimilative model has simulation skill, as indicated by the correlation results that have a median $r = 0.72$. Comparison with the observations shows that the assimilation improves the correlation at 74% of the locations. The median correlation for the assimilative model is $r = 0.81$. Figure 13 shows the location

Table 1 — The 1997-1999 correlation coefficients between observed JASL sea level data and the non-assimilative 1/16° global NLOM (Free) and the assimilative 1/16° global NLOM (Assim). Both model simulations are forced with NOGAPS wind and thermal fields. The JASL data are monthly averages and a 30-day running mean has been applied to the model results. The median correlation of non-assimilative (assimilative) NLOM is 0.72 (0.81).

Station Name		Location	Correlation	
			Free	Assim
NAHA	JAPAN	26°13'N 127°40'E	0.63	0.75
ABURATSU	JAPAN	31°34'N 131°25'E	0.57	0.69
KUSHIMOTO	JAPAN	33°28'N 135°47'E	0.35	0.45
MERA	JAPAN	34°55'N 139°50'E	0.29	0.49
PETROPAVLOVSK	RUSSIA	53°01'N 158°38'E	0.84	0.88
ADAK	ALASKA	51°52'N 176°38'W	0.57	0.77
UNALASKA	ALASKA	53°54'N 166°30'W	0.69	0.79
SEWARD	ALASKA	60°05'N 149°27'W	0.76	0.82
YAKUTAT	ALASKA	59°33'N 139°44'W	0.83	0.89
PRINCE RUPERT	CANADA	54°19'N 130°20'W	0.83	0.87
TOFINO	CANADA	49°09'N 125°55'W	0.89	0.88
BAMFIELD	CANADA	48°50'N 125°08'W	0.88	0.88
NEAH BAY	WASHINGTON	48°22'N 124°37'W	0.88	0.88
CRESCENT CITY	CALIFORNIA	41°45'N 124°12'W	0.81	0.83
SAN FRANCISCO	CALIFORNIA	37°48'N 122°28'W	0.64	0.68
SAN DIEGO	CALIFORNIA	32°43'N 117°10'W	0.85	0.81
WAKE	USA TRUST	19°17'N 166°37'E	-0.13	0.81
SAIPAN	NORTH MARIANA	15°14'N 145°45'E	0.73	0.80
GUAM	MARIANAS	13°26'N 144°39'E	0.86	0.91
LEGASPI	PHILIPPINES	13°09'N 123°45'E	0.78	0.72
KWAJALEIN	MARSHALL	8°44'N 167°44'E	0.63	0.81
YAP	F. S. M.	9°31'N 138°08'E	0.81	0.95
POHNPEI	F. S. M.	6°59'N 158°15'E	0.80	0.87
KAPINGAMARANGI	F. S. M.	1°06'N 154°47'E	0.96	0.88
MALAKAL	BELAU	7°20'N 134°28'E	0.80	0.95
NAURU	NAURU	0°32'S 166°54'E	0.91	0.84
RABAUL	P. N. G.	4°12'S 152°11'E	0.93	0.79
HONIARA	SOLOMONS	9°26'S 159°57'E	0.87	0.84
MIDWAY	USA TRUST	28°13'N 177°22'W	0.49	0.74
FRENCH FRIGATE SHOAL	HAWAII	23°52'N 166°17'W	0.42	0.83
HONOLULU	HAWAII	21°18'N 157°52'W	0.31	0.63
HILO	HAWAII	19°44'N 155°04'W	-0.14	0.62
MAJURO	MARSHALL	7°06'N 171°22'E	0.68	0.91
CHRISTMAS	KIRIBATI	1°59'N 157°28'W	0.93	0.95
TARAWA	KIRIBATI	1°22'N 172°56'E	0.89	0.74
KANTON	KIRIBATI	2°49'S 171°43'W	0.88	0.89
FUNAFUTI	TUVALU	8°32'S 179°13'E	0.78	0.95
NUKU HIVA	FREN POLYNESIA	8°56'S 140°05'W	0.73	0.81
PENRHYN	COOK ISL	8°59'S 158°03'W	0.66	0.88
PAGO PAGO	SAMOA	14°17'S 170°41'W	0.83	0.95
PAPEETE	FREN POLYNESIA	17°32'S 149°34'W	0.77	0.91
SUVA	FIJI	18°08'S 178°26'E	-0.15	0.60
CABO SAN LUCAS,B.C.	MEXICO	22°53'N 109°54'W	0.89	0.90
BUENAVENTURA	COLOMBIA	3°54'N 077°06'W	0.86	0.80
TUMACO	COLOMBIA	1°50'N 078°44'W	0.90	0.92
BALTRA	ECUADOR	0°26'S 090°17'W	0.92	0.96
SANTA CRUZ	ECUADOR	0°45'S 090°19'W	0.93	0.95
LA LIBERTAD	ECUADOR	2°12'S 080°55'W	0.87	0.88
CALLAO	PERU	12°03'S 077°09'W	0.84	0.88
ANTOFAGASTA	CHILE	23°39'S 70°24'W	0.78	0.72
VALPARAISO	CHILE	33°02'S 71°38'W	0.81	0.76
EASTER ISLAND	CHILE	27°09'S 109°27'W	-0.50	0.33
NOUMEA	NEW CALEDONIA	22°17'S 166°26'E	0.75	0.56
NUKU'ALOFA	TONGA	21°08'S 175°10'W	0.64	0.72
NORFOLK ISLAND	AUSTRALIA	29°40'S 167°56'E	-0.17	0.65
KEY WEST	FLORIDA	24°33'N 81°48'W	0.58	0.77
VIRGINIA KEY	FLORIDA	25°44'N 80°10'W	0.58	0.72
SAN JUAN	PUERTO RICO	18°28'N 66°07'W	0.59	0.86
LIMETREE BAY	US VIRGIN ISLANDS	17°42'N 64°45'W	0.46	0.87
SETTLEMENT POINT	BAHAMAS	26°46'N 79°00'W	0.37	0.72
CARTAGENA	COLUMBIA	10°23'N 75°32'W	0.38	0.66
LAS PALMAS	CANARY ISLANDS	28°09'N 15°24'W	0.73	0.50
TENERIFE	CANARY ISLANDS	28°29'N 16°14'W	0.60	0.75
BERMUDA	UK	32°22'N 64°42'W	0.66	0.89
SOUTH PASS	LOUISIANA	29°00'N 89°08'W	0.72	0.73
PORT LOUIS	MAURITIUS	20°09'S 57°30'E	-0.03	0.84
MALE	MALDIVES	04°11'N 73°32'E	0.62	0.61
GAN	MALDIVES	0°41'S 73°09'E	0.63	0.83
MASIRAH	OMAN	20°41'N 58°52'E	0.26	0.58
SALALAH	OMAN	16°56'N 54°00'E	0.90	0.86
HANIMADHOO	MALDIVES	6°46'N 73°10'E	0.84	0.86
LAMU	KENYA	02°16'S 40°54'E	0.01	0.62
ZANZIBAR	TANZANIA	6°09'S 39°11'E	0.36	0.63
COCOS ISLANDS	AUSTRALIA	12°07'S 96°53'E	0.69	0.83

of the tide gauge stations in Table 1 color-coded by correlation for the non-assimilative (Fig. 13(a)) and the assimilative (Fig. 13(b)) model. The results indicate that the high correlations are spread around the globe, and the improvement with assimilation is seen by many locations changing to colors that represent the higher correlation values. Generally, in locations where altimeter data did not improve the correlations, the correlations were already high in the non-assimilative model run.

Table 2 shows additional comparisons with daily averaged SSH from buoys also available from JASL. These results are similar to the monthly averaged tide-gauge data and indicate the skill of the assimilative NLOM system in nowcasting SSH. Again for 65% of the cases, the assimilative model has higher correlation values than the non-assimilative model. The NLOM system's ability to nowcast SSH is one of the strengths of the system and is a critical evaluation criterion for using NLOM SSH in MODAS to calculate 3-D synthetic temperature profiles.

Sea Surface Height Nowcast Comparisons with NAVOCEANO Frontal Analyses

One of the most critical evaluations of the NLOM system is the ability of the system to nowcast the positions of major fronts and eddies on the global scale. The Warfighting Support Center (WSC) at NAVOCEANO relies on satellite infrared SST data to locate fronts and eddies for the global ocean and releases frontal analysis products to the Fleet. The NLOM system will allow the WSC analysis to use daily nowcasts and animations of SSH as another powerful tool to improve the quality of frontal analysis products. This is particularly significant because SSH is a better indicator of subsurface frontal location than SST. An example in which this has an impact is discussed later in this subsection. Specifically, NLOM provides a daily map of the ocean mesoscale SSH field that can be used as a tool to help the WSC interpret cloud-filled IR images. In addition, by using animations of the last month's NLOM SSH field, the analyst can better track front and eddy movements to help analyze the space and time continuity of the ocean mesoscale in areas where frontal analysis is required.

Figure 14 shows the NLOM SSH nowcast for the Kuroshio Extension overlaid with the daily WSC frontal analysis product for 20 October 2000 (Fig. 14(a)) and for 30 October 2000 (Fig. 14(b)). The model field color palette was chosen to emphasize the location of the Kuroshio and associated eddies. One must be careful in interpreting these results because of the uncertain quality of the WSC frontal analysis. Due to clouds, the analyst may not have seen the front for several days and may be depending on a previous (older) frontal analysis. In areas where there is good agreement, we can be reasonably sure that the NLOM Kuroshio front is accurate. In areas where agreement is not as good, there may be a question of the quality of the WSC analysis and one is not sure of the correct path.

However, on closer analysis, some obvious clues seem to indicate the value that NLOM will have for frontal analysis. For both 20 October and 30 October 2000, the NLOM Kuroshio pathway is in agreement with the WSC frontal analysis from 130°E to ~160°E and also from 170°E to 180°E. Both products show the Kuroshio in meander mode and show the classic "double meanders" at 145°E and 150°E. The area of disagreement between 160°E to 170°E is in an area where the frontal analysis becomes very difficult because of warm eddies that are frequently located just north of the main Kuroshio front. In this case, the analyst seems to have observed the warm eddy near 165°E, 37°N in IR data and possibly incorrectly identified it as a Kuroshio meander. This is especially seen in Fig.14(b) where the eddy is well represented by NLOM. The analyst takes the Kuroshio north wall up to 38°N and seems to wrap around the eddy seen in NLOM. On closer analysis and by looking at NLOM SSH animations (which are available to the WSC analysts), it is learned that the observed feature is really a bifurcation of the Kuroshio at the Shatsky Rise, which is a

Table 2 — The 1997-1999 correlation coefficients for daily averaged NODC buoy sea-level data and the non-assimilative–1/16° global NLOM (Free) and assimilative 1/16° global NLOM (Assim.) Both model simulations are forced with NOGAPS wind and thermal fields. The median correlation of non-assimilative (assimilative) NLOM is 0.49 (0.72).

	Buoy	Location	Correlations 1997–1999	
			Free	Assim.
1	Atlantic	16°N, 062°W	0.51	0.85
2	Atlantic	18°N, 065°W	0.54	0.77
3	Atlantic	26°N, 097°W	0.38	0.44
4	Atlantic	27°N, 079°W	0.28	0.63
5	Atlantic	28°N, 016°W	0.57	0.57
6	Atlantic	32°N, 065°W	0.60	0.79
7	Pacific	01°N, 155°E	0.86	0.83
8	Pacific	01°S, 167°E	0.87	0.83
9	Pacific	01°S, 090°W	0.80	0.90
10	Pacific	07°N, 134°E	0.76	0.92
11	Pacific	07°N, 171°E	0.63	0.93
12	Pacific	09°N, 168°E	0.49	0.72
13	Pacific	09°S, 158°W	0.55	0.73
14	Pacific	09°S, 179°E	0.65	0.93
15	Pacific	13°N, 145°E	0.80	0.77
16	Pacific	15°N, 146°E	0.59	0.73
17	Pacific	17°N, 170°W	0.28	0.60
18	Pacific	19°N, 167°E	-0.09	0.74
19	Pacific	21°S, 160°W	-0.06	0.40
20	Pacific	23°S, 135°W	-0.04	0.45
21	Pacific	24°N, 124°E	0.44	0.56
22	Pacific	24°N, 166°W	0.14	0.74
23	Pacific	26°N, 128°E	0.49	0.68
24	Pacific	28°N, 177°W	0.43	0.59
25	Pacific	32°N, 131°E	0.25	0.52
26	Pacific	33°N, 136°E	0.24	0.39
27	Pacific	34°N, 139°E	0.25	0.53
28	Pacific	35°N, 138°E	0.08	0.59
29	Pacific	35°N, 140°E	0.19	0.41
30	Indian	01°S, 073°E	0.38	0.59
31	Indian	06°S, 039°E	0.30	0.57
32	Indian	12°S, 097°E	0.59	0.78
33	Indian	20°S, 063°E	0.49	0.87
34	Indian	39°S, 078°E	0.34	0.17

known feature that can exist in this region (Hurlburt and Metzger 1998). In this case, there are actually two branches of the Kuroshio (a northern and southern branch) that bifurcate at ~163°E and join up again at ~173°E. If the analyst had the NLOM SSH nowcast and animations of past SSH nowcasts available, then an improved interpretation of the ocean mesoscale field and consequently an improved frontal analysis would be possible.

Another example of this is the frontal analysis of some of the fronts north of the Kuroshio. The analyst seems to see the edge of some eddies in the IR but due to clouds has a difficult time determining what the frontal feature is. This is especially evident with the eddies seen in NLOM at 143°E, 38°N and 147°E, 37°N. In this case, the analyst draws the front around the edge of both features. This gives the impression of a continuous front in these areas that are really eddies. Figure 15 shows two more examples for 6 November 2000 (Fig. 15(a)) and 20 November 2000 (Fig. 15(b)), and the conclusions are the basically the same. The 20 November WSC frontal analysis comparison to NLOM is even better from 130°E to 160°E, especially in the shape of the meander at 140°E. The frontal analysis even has a better representation of the northern branch of the Kuroshio bifurcation at the Shatsky Rise (near 165°E) discussed earlier.

Figures 16 and 17 show comparisons of the NLOM SSH field with the WSC frontal analysis for the Gulf Stream area. For 27 November 2000 (Fig. 16(a)) and 29 November 2000 (Fig. 16(b)), the Gulf Stream is in a fairly straight path mode from 75°W to 68°W and there is good agreement between the NLOM and WSC analysis frontal positions. East of 68°W, both products depict the meanders at 57°W and 51°W and the deep trough at 49°W. After this time, the Gulf Stream begins to change from the straight path and develops deep troughs at 68°W and 64°W, which are well represented by NLOM and the WSC analysis on 4 December 2000 (Fig. 17(a)) and 6 December 2000 (Fig. 17(b)). NLOM deepens the trough at 68°W more than the WSC analysis on 4 December, but this is verified on 6 December when the WSC analysis is updated in this area based on additional imagery data, showing the potential value of the NLOM SSH product to the WSC analyst. The WSC frontal analysis would have been improved on 4 December if NLOM data were available and used by the WSC.

Figures 18 and 19 are additional comparisons of the NLOM SSH field and WSC frontal analysis for the Loop Current in the Gulf of Mexico. The results for 11 November 2000 (Fig. 18(a)) and 15 November 2000 (Fig. 18(b)) show excellent agreement of frontal position on the east and west side of the Loop Current. There are some differences between NLOM and the WSC analysis on the northeast side of the Loop Current front. The discrepancy occurs because the WSC analyst observed warm surface water on IR imagery. The warm surface water is being advected around a cyclonic circulation north of the Loop Current that is seen in the NLOM SSH field near 87°W, 28°N. The circulation around the cyclonic feature acts to pull warm surface water to the north, but this is not accompanied by surface circulation or 3-D water mass changes and is therefore not the dynamic Loop Current front. The later WSC analyses on 20 November 2000 (Fig 19(a)) and 22 November 2000 (Fig 19(b)) no longer include this warm surface feature in the frontal analysis, and the agreement with the NLOM frontal position with SSH is much improved. If the WSC had access to the NLOM SSH field and had observed the cyclonic feature to the north, the analyst would have had more information on the source of the warm surface water seen on imagery and the frontal product could have been improved.

MODAS Synthetic Temperature Profiles from NLOM SSH and MODAS SSH vs XBT Data

NAVOCEANO currently uses the MODAS as their operational system for 3-D oceanographic analysis. The MODAS synthetic database climatology uses SSH and SST nowcasts to calculate 3-D temperature and salinity profiles as a first guess for a 3-D MODAS OI analysis. Real-time expendable bathythermograph

(XBT) data are assimilated to improve the analysis. However, the value of the MODAS synthetic profiles is that the first guess is closer to the observations, which improves the quality of the final analysis. The full-grid MODAS 3-D analysis is then used as input to acoustical Tactical Decision Aids (TDAs) and also is currently assimilated into the Global Navy Coastal Ocean Model (NCOM) to initialize the model for short-term upper-ocean forecasts. The current operational SSH analysis is obtained from a global 2-D SSH OI analysis using MODAS. This statistical analysis has some limitations because it lacks the dynamics to properly move features. Since NLOM is an ocean model, it has the needed dynamics to act as a dynamic interpolator of the satellite altimetry data and should provide an improved SSH field for the MODAS synthetics and a more dynamically correct initialization field for the global NCOM (scheduled for transition in FY03).

Figures 20-22 show comparisons of MODAS synthetic profiles derived from the MODAS SSH field and the NLOM SSH field for an air-dropped expendable bathythermograph (AXBT) cross section along 144°E in July 1999 for the Kuroshio. The location of the section is overlaid on the NLOM SSH anomaly relative to the NLOM mean (Fig. 20(a)) and the MODAS SSH anomaly relative to the MODAS mean (Fig. 20(b)) fields. Figure 20(c) shows the mean and RMS errors for NLOM-derived synthetics, MODAS-derived synthetics, and climatological temperature with the AXBT data as the ground truth. In this case, NLOM synthetics have lower RMS error for this set of AXBTs (especially between 100 and 300 meters) compared to MODAS synthetics or climatology. This means that the NLOM SSH is adding value to the synthetics.

Figures 21 and 22 show the actual temperature sections and the temperature difference sections. It is obvious that both NLOM (Figs. 21(b) and 22(b)) and MODAS (Figs. 21(c) and 22(c)) provide value over climatology (Figs. 21(d) and 22(d)). In this case, the AXBT section is located in a highly variable area as it crosses a warm Kuroshio meander between 35°N and 36°N and a warm eddy near 41°N. Although NLOM synthetics are too warm compared with MODAS at the southern part of the section (near 34°N), they have lower error throughout the rest of the section. In this highly variable mesoscale area, the location and shape of features is the dominant error source for SSH. In this case, NLOM does a better job with the location and slope of the Kuroshio front and the eddy to the north. This is indicated by the lower NLOM temperature errors north of 38°N and near 41°N. Overall, NLOM synthetics are slightly better than MODAS synthetics for this section.

Figures 23-25 show results from a similar AXBT section in September 1999 along 165°E. This is an area with less mesoscale variability than the previous section, but the section does cross the Kuroshio near 35°N. The RMS error (Fig. 23(c)) comparisons indicate that NLOM and MODAS synthetics are very similar for this section. Both products show good agreement with the AXBTs across the front and are much better than climatology. In fact, it is very easy to locate the position of the Kuroshio by looking at the climatology error (Fig. 25(d)), but the MODAS and NLOM errors are so small that it is difficult to detect where the front is located. NLOM has better agreement than MODAS with the AXBT north of 35°N because the NLOM SSH field correctly has a low height (colder) feature that is observed by the XBTs.

Figure 26 shows another comparison with an AXBT section for the Gulf Stream area in August 1999. This section is in the Sargasso Sea south of the Gulf Stream with no frontal crossing. In this case, climatology is tougher to beat with RMS errors lower than 1°C (Fig. 26(c)) for most depths down to 500 meters. NLOM and MODAS are superior near the surface because both are assimilating SST data, but all three products are performing about the same at depth for this section. The cross sections of temperature and temperature error (Figs. 27 and 28) confirm this with very low errors for NLOM, MODAS, and climatology. It is a very encouraging result to show that even in areas of low variability where the altimetry signals are small, the NLOM system is accurate and is not adding unwanted error.

Figures 29-31 shows a continuation of the previous section to the north as it crosses the Gulf Stream near 36.5°N. This is also a mixed result, with NLOM having smaller RMS error below 200 meters and larger RMS error between 50 and 100 meters (Fig. 29(c)). This is mainly due to the NLOM SSH field having too strong a cyclonic recirculation gyre north of the Gulf Stream (north of 37°N), which causes the NLOM synthetics to be much too cold near the surface. However, the NLOM synthetics have lower temperature errors than MODAS across the Gulf Stream front (Figs. 31(b) and (c)), which indicates that NLOM has a more realistic height change across the Gulf Stream than MODAS.

These results tend to indicate that the NLOM synthetics are an improvement over the MODAS synthetics, but the improvement is small at this time. The advantage that NLOM has over MODAS is a forecast capability, so if NLOM is only equal to MODAS in performance, NLOM is the preferred product. NRL continues research to improve the accuracy of the NLOM SSH field. One area of research is investigating the nonsteric contribution to the SSH (Shriver and Hurlburt 2000). The MODAS synthetic algorithms require information only on the steric SSH that contribute to the temperature and salinity changes in the water column. At the present time, no effort is made to separate the steric and nonsteric components in the SSH assimilation process. By treating the nonsteric contribution separately during assimilation, the steric part of the signal will be more accurate, and this should improve the quality of the synthetic profiles. NRL will continue to identify other sources of error and improve the quality of the NLOM steric height field.

NLOM SSH Forecast Statistics

The ability of NLOM to forecast SSH and the positions of major fronts and eddies represents a new Naval product that could be a powerful tool for future planning. The future positions of major ocean fronts would give the warfighter some guidance on how changes in the ocean environment could affect future missions. Figure 32 shows an example of a nowcast (Fig. 32(a)), a 14-day forecast (Fig. 32(b)), and a 30-day forecast (Fig. 32(c)) of SSH from NLOM for the Kuroshio. An accurate forecast of SSH would allow the Navy to predict changes in the 3-D temperature and salinity field by using the predicted SSH and SST to calculate MODAS synthetic profiles. Changes in the 3-D ocean environment would change acoustic conditions in the deep water and could be used as planning for future deployment of Fleet assets.

Figures 33-38 show the forecast errors for prediction of the positions of the Kuroshio and Gulf Stream vs climatology and persistence for twelve 30-day forecasts from the NLOM system in 1999. The mean axis error is that obtained by calculating the area between the two frontal paths represented by the NLOM prediction, persistence, or no change in the path and the climatological position of the front vs the nowcast position from the NLOM system, which is considered the verification. The area between the paths is then divided by the length of the nowcast front to obtain the mean axis error. The results indicate that for the Kuroshio, the NLOM system has skill over persistence and climatology for 30 days in 5 of the 12 monthly forecasts for 1999. January (Fig. 33(a)), April (Fig. 34(c)), May (Fig. 35(a)), September (Fig. 37(a)), and December (Fig. 38(c)) all show skill out to 30 days. The others months indicate a varying level of skill. The results for June (Fig. 35(c)) show skill out 20 days, while August (Fig. 36(c)) is basically equal to the persistence error throughout the length of the forecast. In all months for the Kuroshio, the NLOM system beats climatology as a predictor of the frontal path. The remaining months show NLOM skill over persistence for at least ~10 days. These results indicate that NLOM is a better predictor of the Kuroshio frontal position than persistence or climatology.

The Gulf Stream results are different than the Kuroshio results. Research at NRL (Hurlburt and Hogan 2000) has indicated that although 1/16° resolution produces realistic simulations of the Gulf Stream pathway, 1/32° resolution is required to produce a robust result for the mean pathway and variability of front.

The forecast statistics for the Gulf Stream seem to confirm this result. In each of the monthly cases, the NLOM system has skill for forecasting frontal positions, but the length of forecast skill is diminished for the Gulf Stream vs the Kuroshio. In most cases, NLOM indicates skill over persistence out past ~15 days, with a maximum of ~25 days for March (Fig. 34(b)), October (Fig. 37(d)), and December (Fig. 38(d)). Only in April (Fig. 34(d)), May (Fig. 35(b)), and July (Fig. 36(b)) is the length of forecast skill less than 15 days, but in every case, the model has skill for at least ~10 days.

Figures 39-50 show additional forecast verification statistics for the 12 monthly forecasts in 1999. Statistics for SSH anomaly correlation, a standard similar to that used in atmospheric forecast verification, and SSH RMS error vs forecast length are shown each month for the Gulf Stream, Kuroshio, and the entire Global domain. These statistics are calculated by comparing the model forecast SSH field vs the analysis SSH from NLOM valid on the day of the forecast. In all cases for both anomaly correlation and RMS error on the Global domain (panels (c) and (f)), the model is beating persistence and climatology. The anomaly correlation is showing useful model skill (anomaly correlation >0.6, Murphy and Epstein (1989)) for at least 30 days.

To investigate the model skill in regional areas dominated by flow instabilities and high SSH variability, verification statistics are also shown for the Kuroshio (panels (b) and (e)) and Gulf Stream (panels (a) and (c)) areas. For the Kuroshio, NLOM has predictive skill over persistence out to 30 days in all months except February (Fig. 40, panels (b) and (e)), July (Fig. 45, panels (b) and (e)), and October (Fig. 48, panels (b) and (e)), with February being the month with skill for the shortest forecast length (~10 days). However, in the Gulf Stream, like the axis error comparisons discussed above, NLOM shows forecast skill for a shorter length. The SSH anomaly correlations indicate that NLOM typically has skill for less than 20 days. In 5 of the 12 cases, NLOM beats persistence in the Gulf Stream out to 30 days. In all cases, however, the anomaly correlation shows that the model prediction has no skill (anomaly correlation <0.6) at 30 days and, in some months, climatology has the lowest error beyond 20 days.

The difference in model skill between the Kuroshio and Gulf Stream is due to the resolution of the NLOM system and the dynamics of the two strong western boundary currents. As stated earlier, the results shown here are consistent with other NRL research (Hurlburt and Hogan 2000), which indicates that at least 1/32° is required for proper simulation of the Gulf Stream. Results indicate that the Kuroshio dynamics are well-represented by the model and for most of the ocean, based on the forecast statistics for the Global domain, 1/16° resolution is enough to allow skillful forecasts of SSH. Even though the current system does not show 30-day skill for the Gulf Stream, the results indicate that the system has skill to at least 15 days. NRL is currently working on a 1/32° Global system that is a possible candidate for a later upgrade to the NLOM system, and this system should improve the Gulf Stream results.

4. SUMMARY AND CONCLUSIONS

This report has described components of the NLOM system and validation tests of the assimilative and non-assimilative model. The system consists of a 1/16° global version of NLOM that includes a mixed layer and assimilation based on OI deviation analysis using the model as a first guess, subsurface statistical inference, and slow data insertion. The model is forced by FNMOC wind and thermal fields and assimilates SST from the MODAS global SST analysis. The non-assimilative model can accurately depict the large-scale circulation and the mesoscale variability of the world ocean and also shows skill in nowcasting SST. This is an important test for the model if it is to have success as an accurate dynamic interpolator of satellite altimeter data for nowcasts and skill in forecasting the movements of major fronts and eddies.

The assimilative system was tested in the same mode that is running at NAVOCEANO using only operationally available data, and it was compared to independent observations. The SST nowcasts of NLOM were compared with observed buoy time series and the MODAS analysis, which was assimilated into NLOM. As expected, the NLOM SST field is almost identical to the MODAS SST analysis and both compare favorably to the independent buoy data. The NLOM SSH nowcasts (both non-assimilative and assimilative) are compared to observed tide-gauge sea-level data, and results indicate that NLOM has skill in nowcasting SSH in both cases. However, higher correlations are obtained in the assimilative case, which shows the value of the data assimilation.

The NLOM system was tested for its ability to nowcast locations of major ocean fronts and eddies. The system will be used to improve the quality of the NAVOCEANO frontal analysis products. The position of fronts from the NLOM SSH field was compared to independent NAVOCEANO frontal analyses for the Kuroshio, Gulf Stream, and Gulf of Mexico. In many areas, the two products compared very well, but the results indicated that in areas where there were differences, NLOM would have added value to the WSC analyst. The errors in the WSC analysis are mainly due to IR imagery that is difficult or impossible to interpret because of clouds. The NLOM provides a useful guidance product for the WSC analyst to improve the frontal analysis in areas where interpretation of IR imagery is difficult due to the clouds or during the warmer months when the fronts lose their surface SST signal. Comparisons of SSH and SST also help distinguish between shallow fronts (which have a signature in SST but little in SSH) and fronts that extend deeper and have an SSH signature.

MODAS synthetic temperature profiles calculated from NLOM SSH were compared with those calculated from MODAS analysis SSH. The comparisons with independent AXBT data showed that the NLOM-derived synthetic profiles were slightly better than the MODAS-derived profiles, especially between 100- and 300-m depth. For most cases, NLOM and MODAS synthetics were greatly superior to climatology, and NLOM SSH had a better representation of the temperature changes across fronts, but the results for NLOM and MODAS were very similar. Research is currently underway at NRL to improve the NLOM synthetics, and these upgrades will be available in future upgrades of the system. The fact that NLOM synthetics are as good or slightly better than MODAS synthetics gives NLOM the edge because unlike MODAS, NLOM has the ability to forecast SSH. This adds an operational capability to the Navy that did not previously exist.

The ability of NLOM to forecast the global SSH field and the positions of fronts and eddies was also tested. NLOM predictions were verified against later analyses for 30-day forecasts for the global domain and for the Kuroshio and Gulf Stream regional areas. Results indicated that for the Global and Kuroshio domains, NLOM showed skill over persistence and climatology for SSH prediction for at least 30 days and in the Gulf Stream region for ~20 days. This is consistent with previous NRL research that indicates that 1/16° resolution is adequate for the Kuroshio, but 1/32° resolution is required for more accurate representation of the Gulf Stream.

5. ACKNOWLEDGMENTS

This work was performed as part of the NRL 6.4 Large Scale Models project and the 6.4 Ocean Data Assimilation project, managed by the Space and Naval Warfare Systems Command under program element 0603207N. It is also a contribution to the 6.2 Basin-Scale Ocean Prediction System project, as part of the Naval Ocean Modeling and Prediction program under program element 0602435N at the Office of Naval Research. The 1/16° global ocean model was run on the NAVOCEANO Cray T3E using grants of computer time from the DoD High Performance Computing Modernization Office, much of this under an FY98-00

DoD Challenge Project entitled "Global and basin-scale ocean modeling and prediction." The authors thank Ms. Jan Dastugue for help with the graphics and Ms. Tammy Townsend for help with the algorithm for long-term wind forcing for the 30-day forecasts.

6. REFERENCES

Fratantoni, D.M., W.E. Johns, and T.L. Townsend, 1995: Rings of the North Brazil Current: Their structure and behavior inferred from observations and a numerical simulation. *J. Geophys. Res.* **100**, 10,633-10,654.

Hellerman, S. and M. Rosenstein, 1983: Normal monthly wind stress over the world ocean with error estimates. *J. Phys. Oceanogr.* **13**, 1093-1104.

Hurlburt, H.E. and A.J. Wallcraft, 2000a: Eddy-resolving global ocean modeling and prediction. 2000 Innovation Collection Case Study for the Smithsonian Institution's Permanent Research Collection at http://innovate.si.edu, 7 pp.

Hurlburt, H.E. and A.J. Wallcraft, 2000b: A real-time 1/16° global ocean nowcast/forecast system. *NAVO MSRC Navigator*, Naval Oceanographic Office Major Shared Resource Center, Stennis Space Center, MS, 3 pp.

Hurlburt, H.E., R.C. Rhodes, C.N. Barron, E.J. Metzger, O.M. Smedstad, and J.F. Cayula, 2000: A feasibility demonstration of ocean model eddy-resolving nowcast/forecast skill using satellite altimeter data. NRL/MR/7320—00-8235, Naval Research Laboratory, Stennis Space Center, MS, 23 pp.

Hurlburt, H.E., M.J. Bell, G. Evensen, C.N, Barron, A. Hines, O.M. Smedstad, and D. Storkey, 2002: Operational global ocean prediction systems. Proceedings of the *En route to GODAE International Symposium*, 13-15 June 2002, Biarritz, France, pp. 97-105.

Hurlburt, H.E., R.C. Rhodes, O.M. Smedstad, A.J. Wallcraft, E. J. Metzger, J.F. Shriver, and A.B. Kara, 2001: "A real-time, eddy-resolving 1/16° global ocean prediction system," in *Report of the NASA High-Resolution Ocean Topography Science Working Group*, D.B. Chelton, ed., College of Oceanic and Atmospheric Sciences, Oregon State U., Corvallis, OR, Ref. 2001-4, Oct. 2001, pp. 52-60.

Hurlburt, H.E. and E.J. Metzger, 1998: Bifurcation of the Kuroshio Extension at the Shatsky Rise. *J. Geophys. Res.* **103**, 7549-7566.

Hurlburt, H.E. and J.D. Thompson, 1980: A numerical study of Loop Current intrusions and eddy shedding. *J. Phys. Oceanogr.* **10**, 1611-1651.

Hurlburt, H.E. and P.J. Hogan, 2000: Impact of 1/8° to 1/64° resolution on Gulf Stream model-data comparisons in basin-scale subtropical Atlantic Ocean models. *Dyn. Atmos. Ocean.* **32**, 283-329.

Hurlburt, H.E., A.J. Wallcraft, W.J. Schmitz Jr., P.J. Hogan, and E.J. Metzger, 1996: Dynamics of the Kuroshio/Oyashio current system using eddy-resolving models of the North Pacific Ocean. *J. Geophys. Res.* **101**, 941-976.

Hurlburt, H.E., D.N. Fox, and E.J. Metzger, 1990: Statistical inference of weakly correlated subthermocline fields from satellite altimeter data. *J. Geophys. Res.-Oceans* **95**, 11,375-11,409.

Jacobs, G.A., H.E. Hurlburt, J.C. Kindle, E.J. Metzger, J.L. Mitchell, W.J. Teague, and A.J. Wallcraft, 1994: Decade-scale trans-Pacific propagation and warming effects of an El Niño anomaly. *Nature* **370**, 360-363.

Jacobs, G.A., C.N. Barron, M.R. Carnes, D.N. Fox, H.E. Hurlburt, P. Pistek, R.C. Rhodes, W.J. Teague, J.P. Blaha, R. Crout, and K.R. Whitmer, 1999: Navy altimeter requirements. NRL/FR/7320—99-9696. Naval Research Laboratory, Stennis Space Center, MS, 20 pp.

Jacobs, G.A., C.N. Barron, and R.C. Rhodes, 2001: Mesoscale characteristics. *J. Geophys. Res.-Oceans* **106**(C9), 19,581-19,595.

Jacobs, G.A. and J.L. Mitchell, 1997: Combining multiple altimeter missions. *J. Geophys. Res.-Oceans* **102**(C10): 23,187-23,206.

Metzger, E.J. and H.E. Hurlburt, 1996: Coupled dynamics of the South China Sea, the Sulu Sea, and the Pacific Ocean. *J. Geophys. Res.* **101**, 12,331-12,352.

Metzger, E.J., H.E. Hurlburt, G.A. Jacobs, and J.C. Kindle, 1994: Hindcasting wind-driven anomalies using reduced-gravity global models with 1/2° and 1/4° resolution. NRL/7323—93-9444, Naval Research Laboratory, Stennis Space Center, MS, 22 pp.

Metzger, E.J., H.E. Hurlburt, J.C. Kindle, Z. Sirkes, and J.M. Pringle, 1992: Hindcasting of wind-driven anomalies using a reduced-gravity global ocean model. *Mar. Technol. Soc. J.* **26**(2), 23-32.

Metzger, E.J., O.M. Smedstad, H.E. Hurlburt, A.J. Wallcraft, and R.C. Rhodes, 2001: Nowcasting and forecasting the global ocean. Backscatter, AMRS Association, Winter 2001, pp. 25-30.

Moore, D.R. and A.J. Wallcraft, 1998: Formulation of the NRL Layered Ocean Model in spherical coordinates. NRL/7323—96-0005, Naval Research Laboratory, Stennis Space Center, MS, 24 pp.

Murphy, A.H., and E.S. Epstein, 1989: Skill scores and correlation coefficients in model verification. *Mon. Wea. Rev.* **117**, 572-581.

Rhodes, R.C., H.E. Hurlburt, A.J. Wallcraft, C.N. Barron, P.J. Martin, O.M. Smedstad, S.L. Cross, E.J. Metzger, J.F. Shriver, A.B. Kara, and D.S. Ko, 2002: Navy real-time global modeling system. *Oceanogr.* **15**(1), 29-43.

Shriver, J.F. and H.E. Hurlburt, 2000: The effect of upper ocean eddies on the non-steric contribution to the barotropic mode. *Geophys. Res. Lett.* **27**, 2713-2716.

Shriver, J.F. and H.E. Hurlburt, 1997: The contribution of the global thermohaline circulation to the Pacific to Indian Ocean throughflow via Indonesia. *J. Geophys. Res.*, **102**, 5491-5511.

Smedstad, O.M. and D.N. Fox, 1994: Assimilation of altimeter data in a two-layer primitive equation model of the Gulf Stream. *J. Phys. Oceanogr.* **24**, 305-325.

Smedstad, O.M., H.E. Hurlburt, E.J. Metzger, R.C. Rhodes, J.F. Shriver, A.J. Wallcraft, and A.B. Kara, 2002: A real-time 1/16º global ocean nowcast/forecast system. *J. Mar. Sys.* (in press).

Tilburg, C.E., H.E. Hurlburt, J.J. O'Brien, and J.F. Shriver, 2001: The dynamics of the East Australian current system: the Tasman front, the East Auckland current and the East Cape current. *J. Phys. Oceanogr.* **31**, 2917-2943.

Tilburg, C.E., H.E. Hurlburt, J.J. O'Brien, and J.F. Shriver, 2002: Remote topographic forcing of a baroclinic western boundary current: An explanation for the Southland Current and the pathway of the subtropical front east of New Zealand. *J. Phys. Oceanog.* **32**(11), 3216-3232.

Wallcraft, A.J., 1991: The Navy Layered Ocean Model users guide. NOARL Report 35, Naval Research Laboratory, Stennis Space Center, MS, 21 pp.

Wallcraft, A.J. and D.R. Moore, 1997: The NRL Layered Ocean Model. *Parallel Comput.* **23**, 2227-2242.

Wallcraft, A.J., H.E. Hurlburt, E.J. Metzger, R.C. Rhodes, J.F. Shriver, and O.M. Smedstad, 2002a: Real-time ocean modeling systems. in *Computing in Science and Engineering*, IEEE Computer Society and American Institute of Physics, Vol. 4, No. 2, pp, 50-57.

Wallcraft, A.J., A.B. Kara, H.E. Hurlburt, and P.A. Rochford, 2002b: The NRL Layered Ocean Model (NLOM) with an embedded mixed layer sub-model: formulation and tuning. *J. Atmos. Oceanic Technol.* (submitted).

Zamudio, L., H.E. Hurlburt, E.J. Metzger, and O.M. Smedstad, 2002: On the evolution of coastally trapped waves generated by Hurricane Juliette along the Mexican west coast. *Geophys. Res. Lett.* **29**(23), 2141, doi:10.1029/2002GL014769.

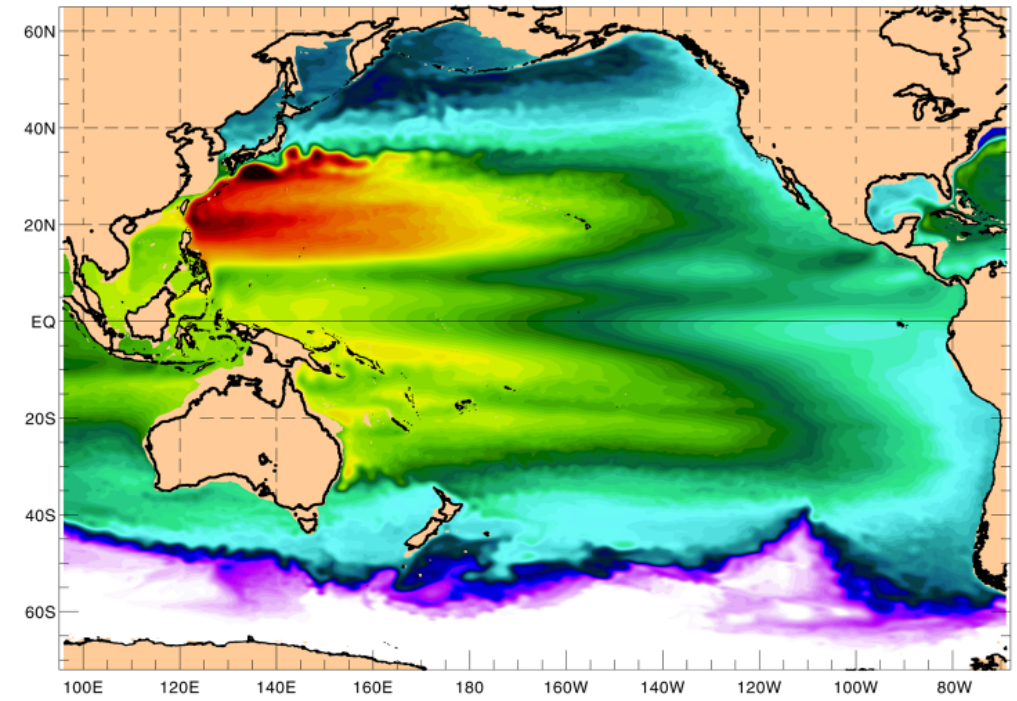

(a)

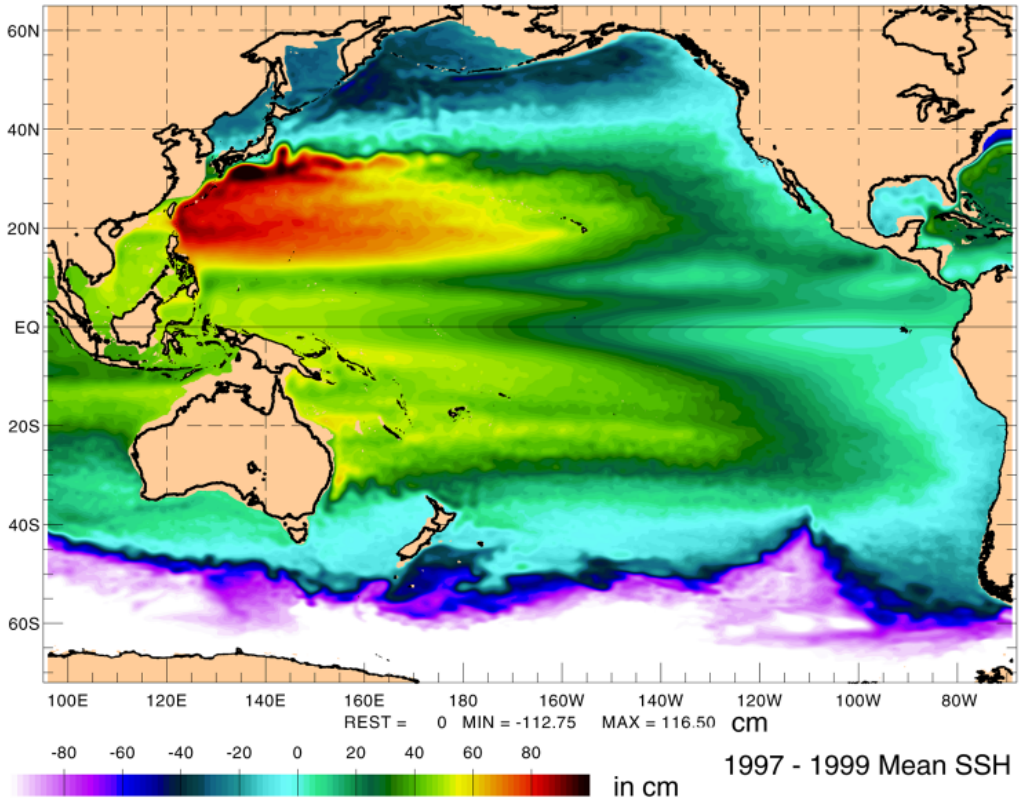

(b)

Fig. 1 — The 1997-1999 mean Pacific hemispheric SSH for (a) the non-assimilative 1/16° global NLOM and (b) the data assimilative 1/16° global NLOMl. NLOM is forced with NOGAPS wind and thermal fields.

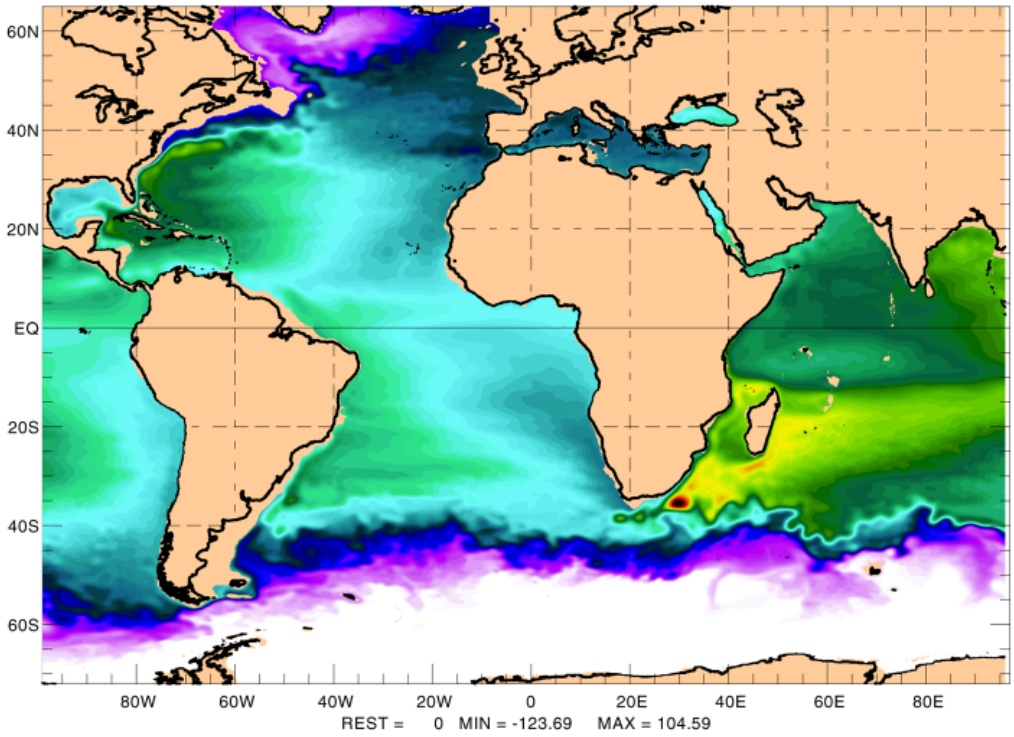

(a)

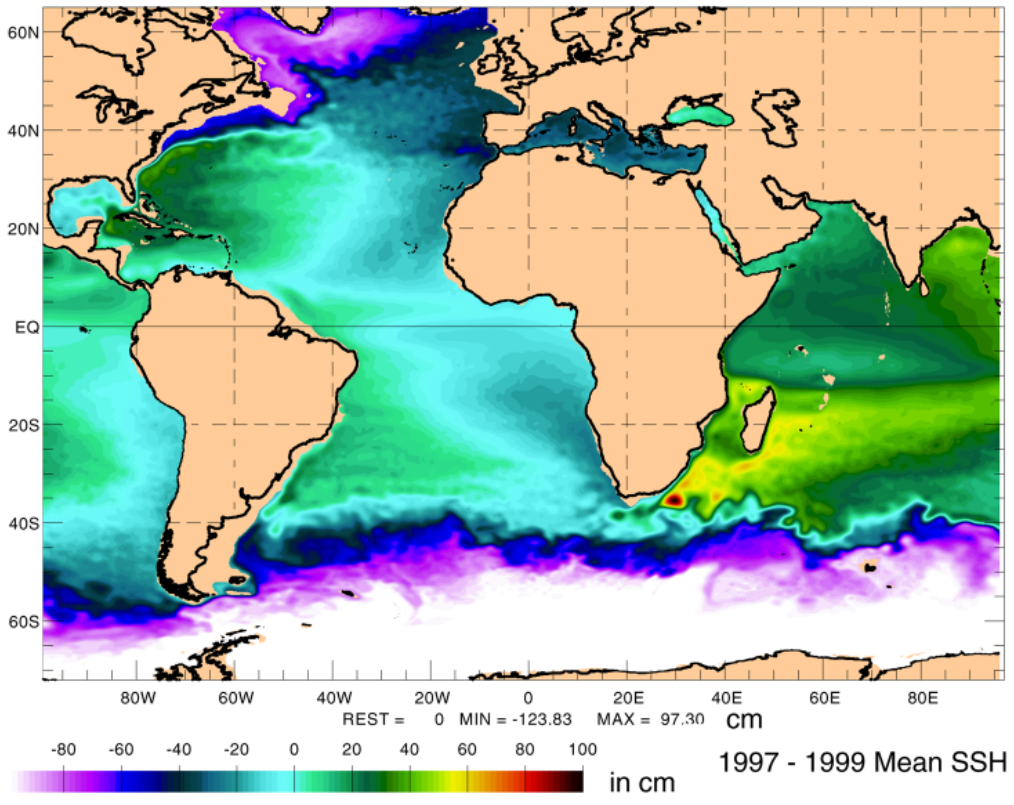

(b)

Fig. 2 — The 1997-1999 mean Atlantic/Indian hemispheric SSH for (a) the non-assimilative 1/16° global NLOM and (b) the data assimilative 1/16° global NLOM. NLOM is forced with NOGAPS wind and thermal fields.

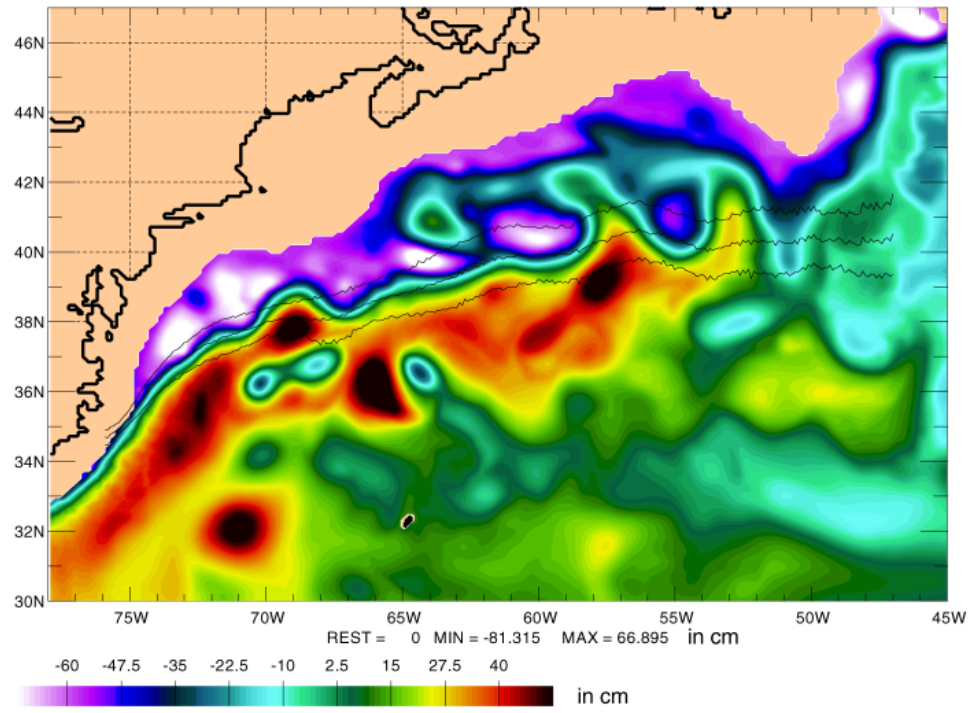

(a)

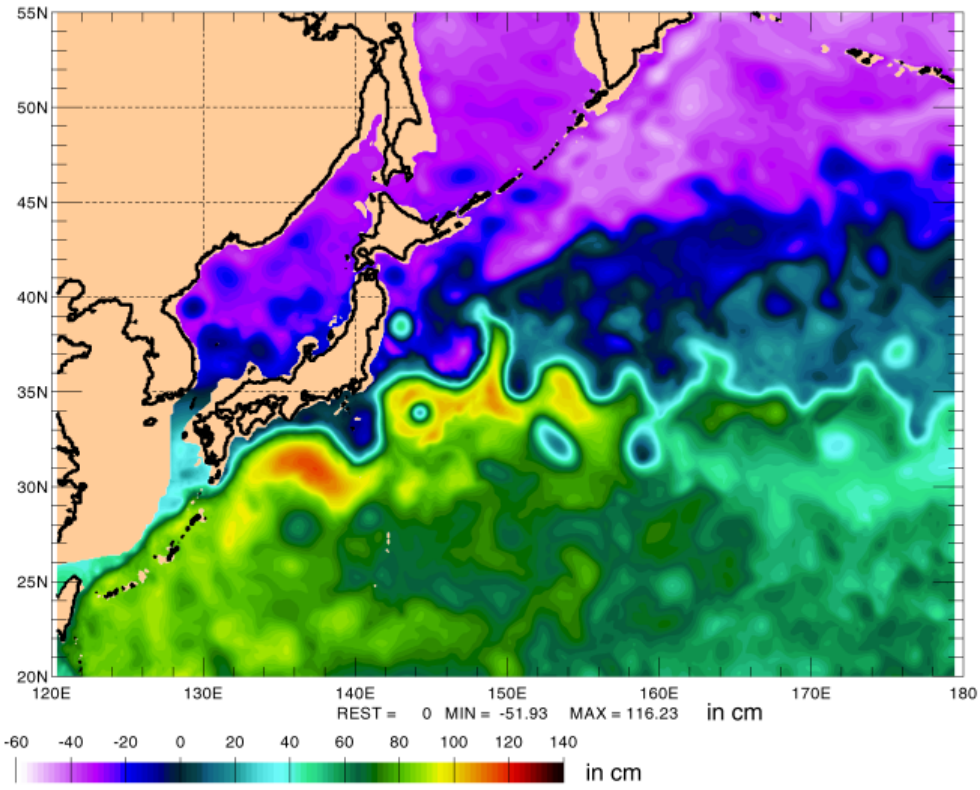

(b)

Fig. 3 — Snapshots of SSH from the non-assimilative 1/16° global NLOM forced by FNMOC wind and thermal fields for (a) the Gulf Stream region and (b) the Kuroshio Extension region. Superimposed on the Gulf Stream plot is the mean Gulf Stream northwall ±1 standard deviation calculated from satellite IR data.

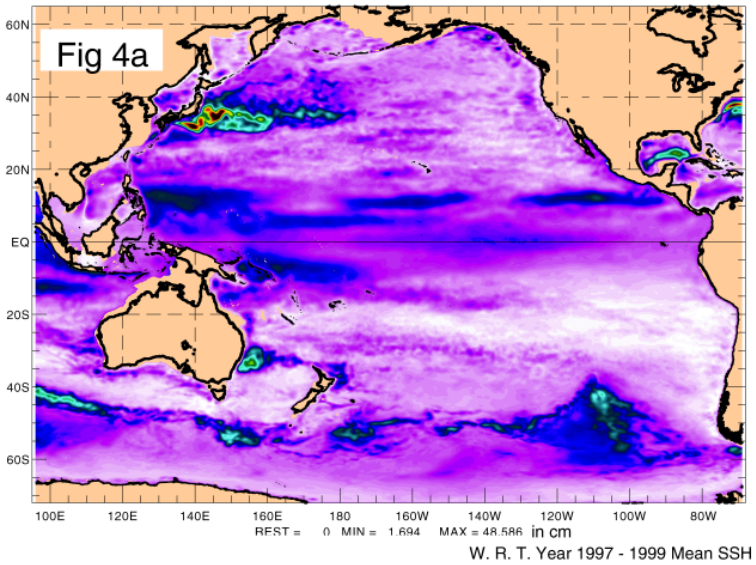

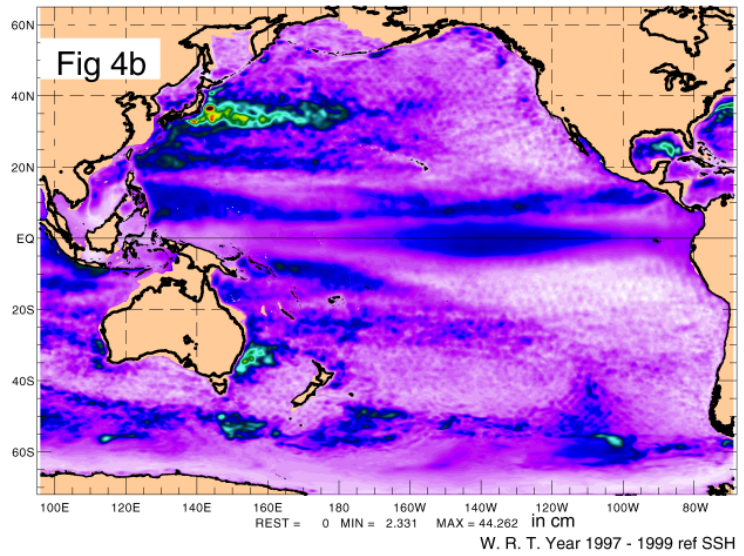

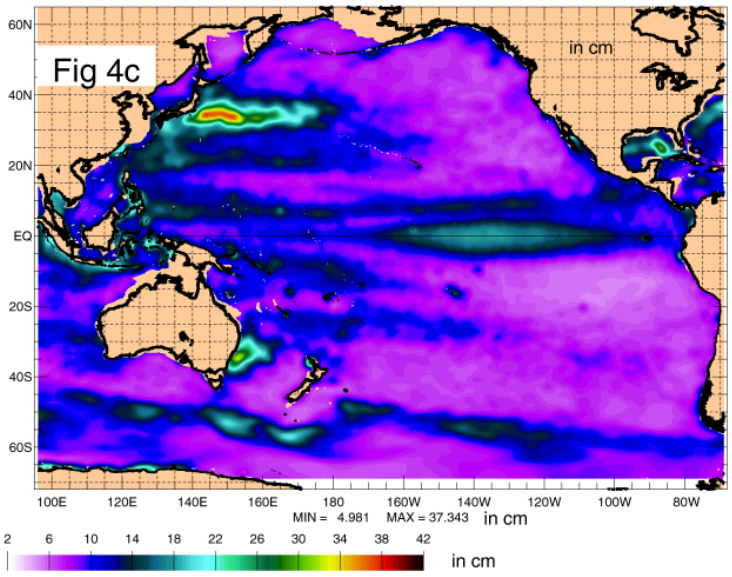

Fig. 4 — The 1997-1999 SSH variability in the Pacific hemisphere for (a) the non-assimilative 1/16° global NLOM, (b) the assimilative 1/16° global NLOM, and (c) TOPEX/Poseidon altimetry. NLOM is forced with NOGAPS wind and thermal fields.

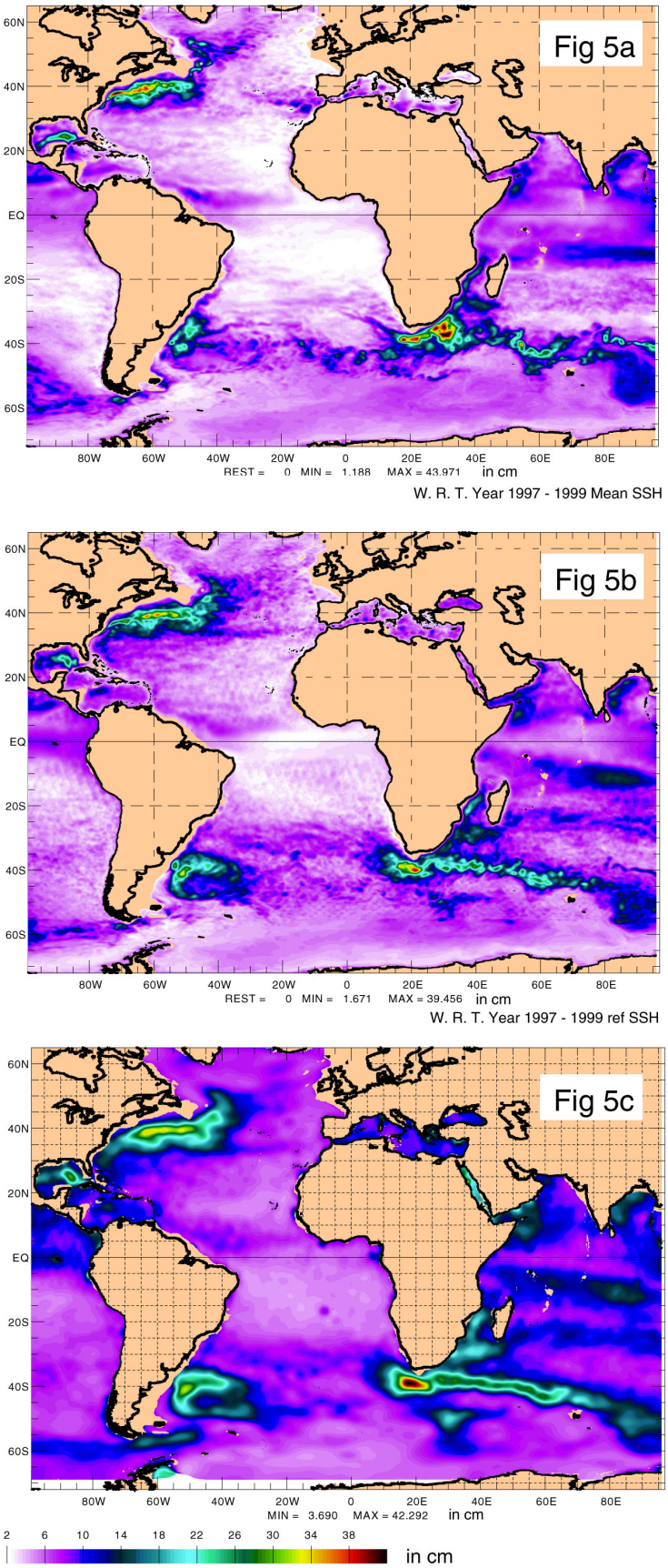

Fig. 5 — The 1997-1999 SSH variability in the Atlantic/Indian hemisphere for (a) the non-assimilative 1/16° global NLOM, (b) the assimilative 1/16° global NLOM, and (c) TOPEX/Poseidon altimetry. NLOM is forced with NOGAPS wind and thermal fields.

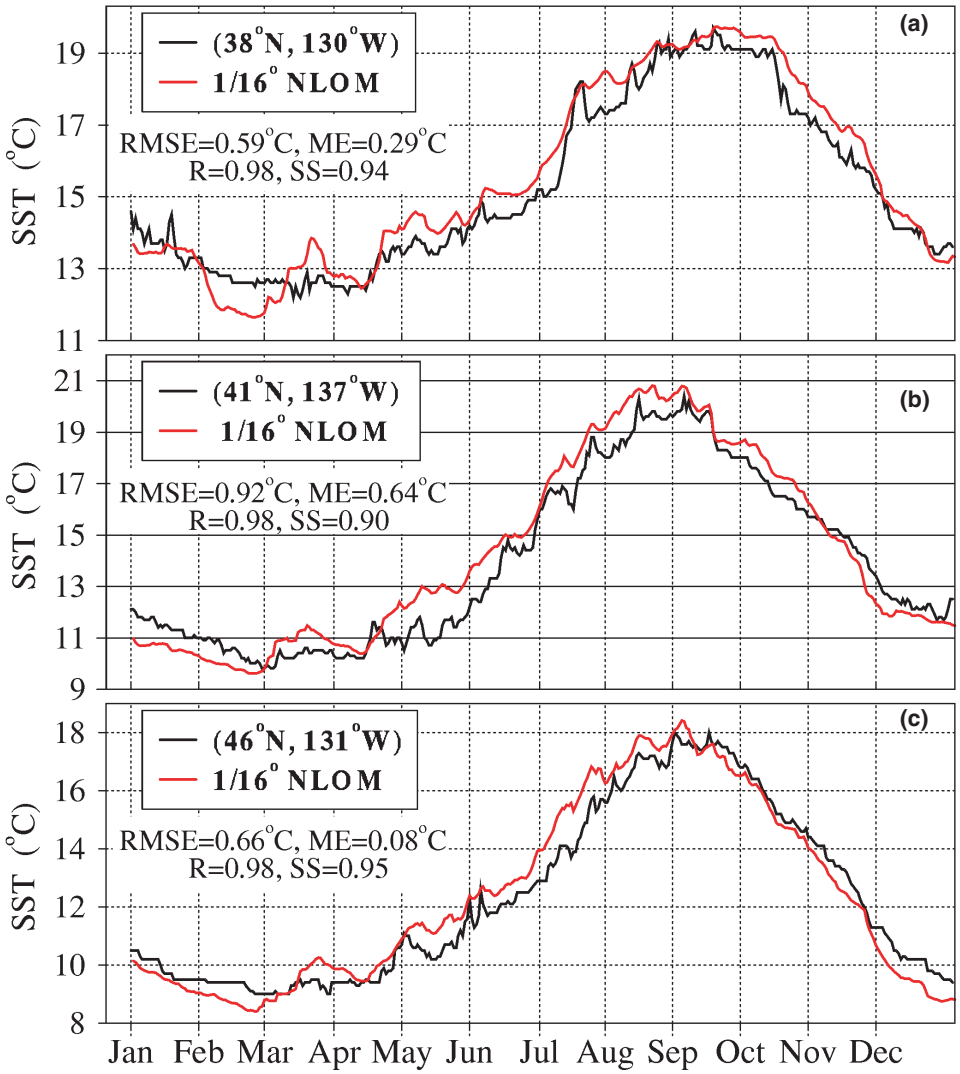

Fig. 6 — Daily observed SST from NOAA buoys (black) and model SST from the non-assimilative 1/16° global NLOM (red) forced with ECMWF wind and thermal fields for 1998 at (a) buoy at 38°N, 130°W; (b) buoy at 41°N, 137°W; and (c) buoy at 46°N, 131°W. NLOM included no assimilation of SST data. Statistics include root-mean-square error (RMSE), mean error (ME), correlation R, and skill score (SS).

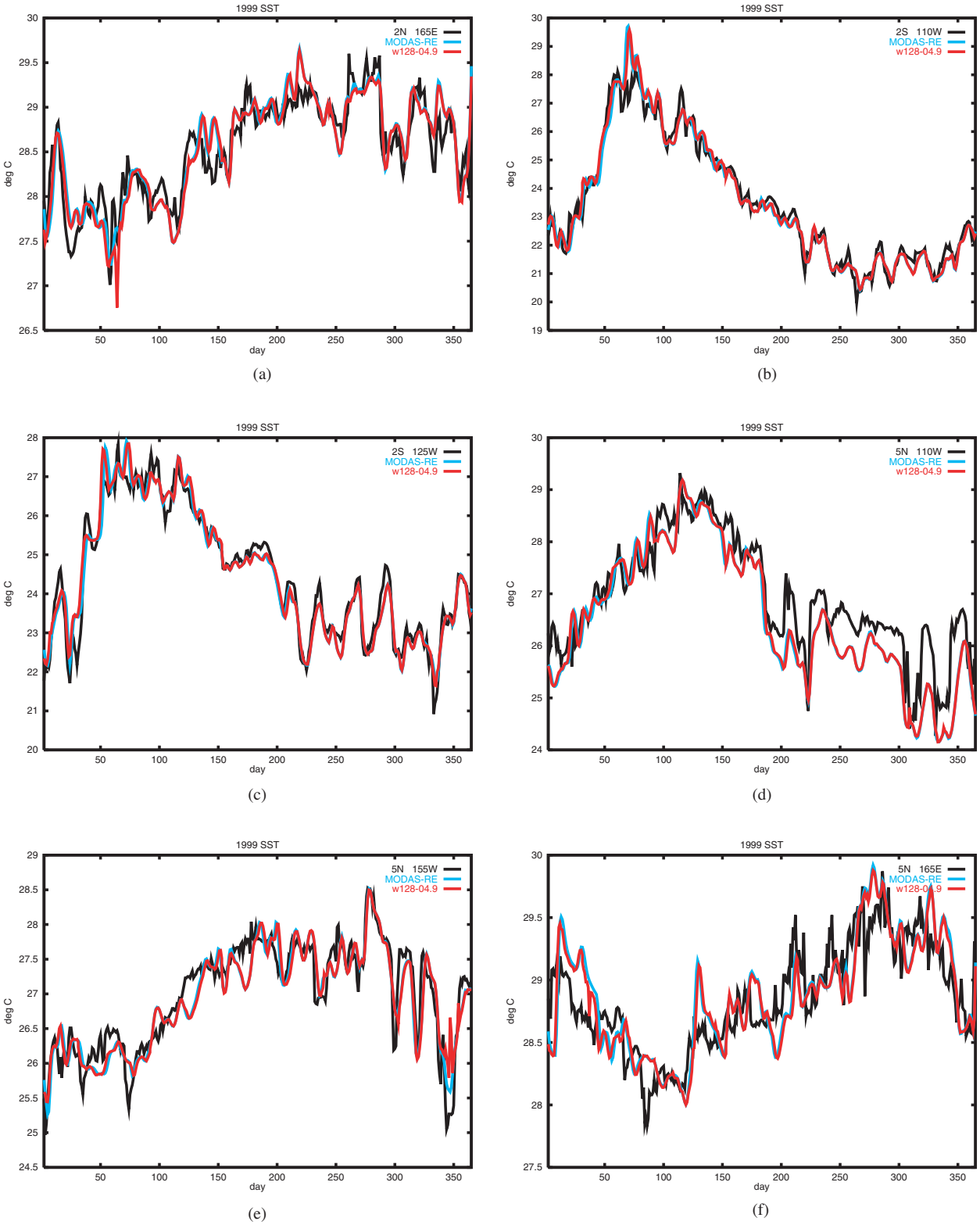

Fig. 7 — Observed SST from NOAA buoys (black), MODAS analysis SST (blue), and model SST from–assimilative 1/16° global NLOM (red) forced with FNMOC wind and thermal fields for 1999 at (a) buoy at 2°N, 165°E; (b) buoy at 2°S, 110°W; (c) buoy at 2°S, 125°W; (d) buoy at 5°N, 110°W; (e) buoy at 5°N, 155°W; and (f) buoy at 5°N, 165°E. NLOM is relaxed to MODAS analysis for assimilation.

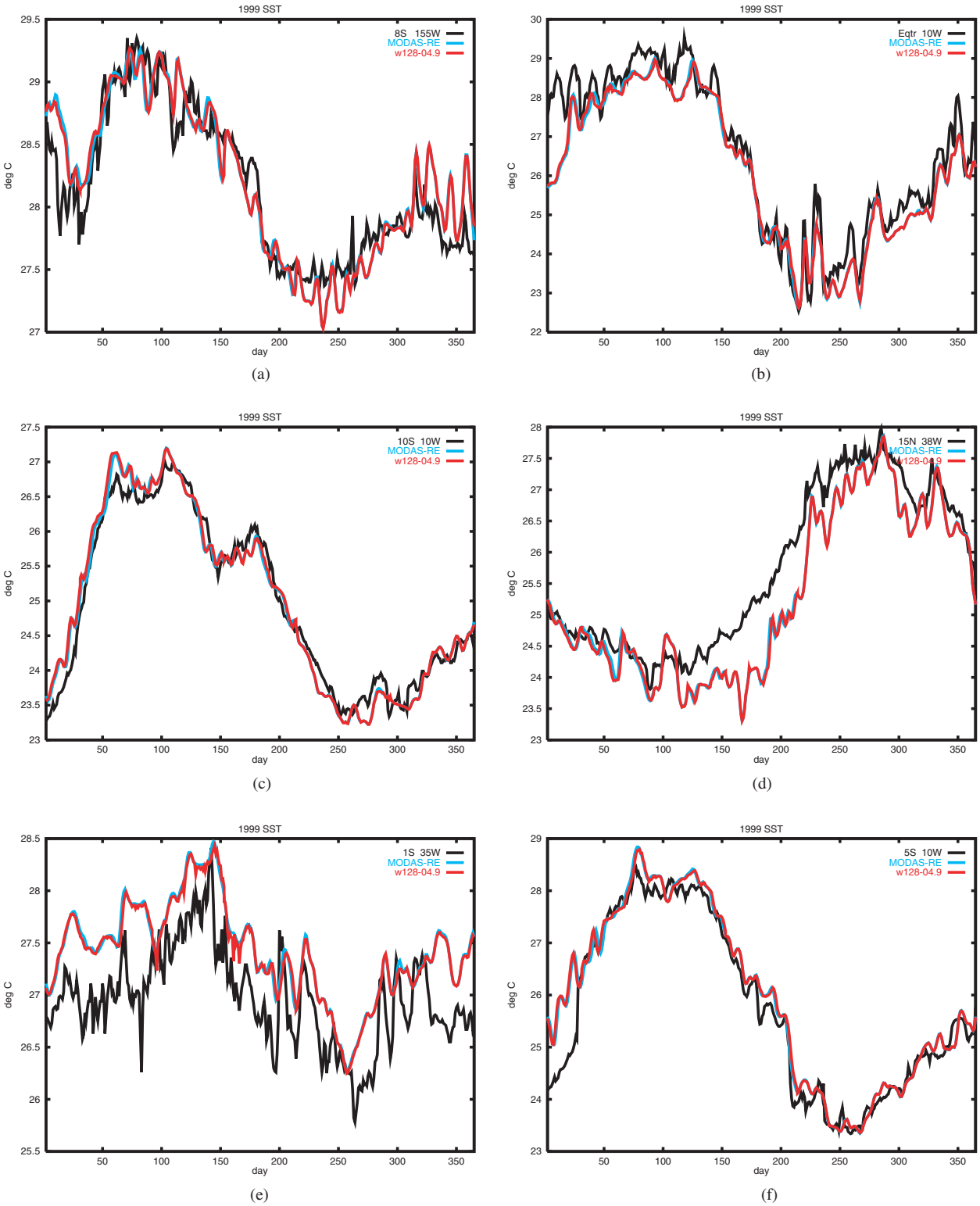

Fig. 8 — Same as Fig. 7 except for (a) buoy at 8°S, 155°W; (b) buoy at 0°N, 10°W; (c) buoy at 10°S, 10°W; (d) buoy at 15°N, 38°W; (e) buoy at 1°S, 35°W; and (f) buoy at 5°S, 10°W.

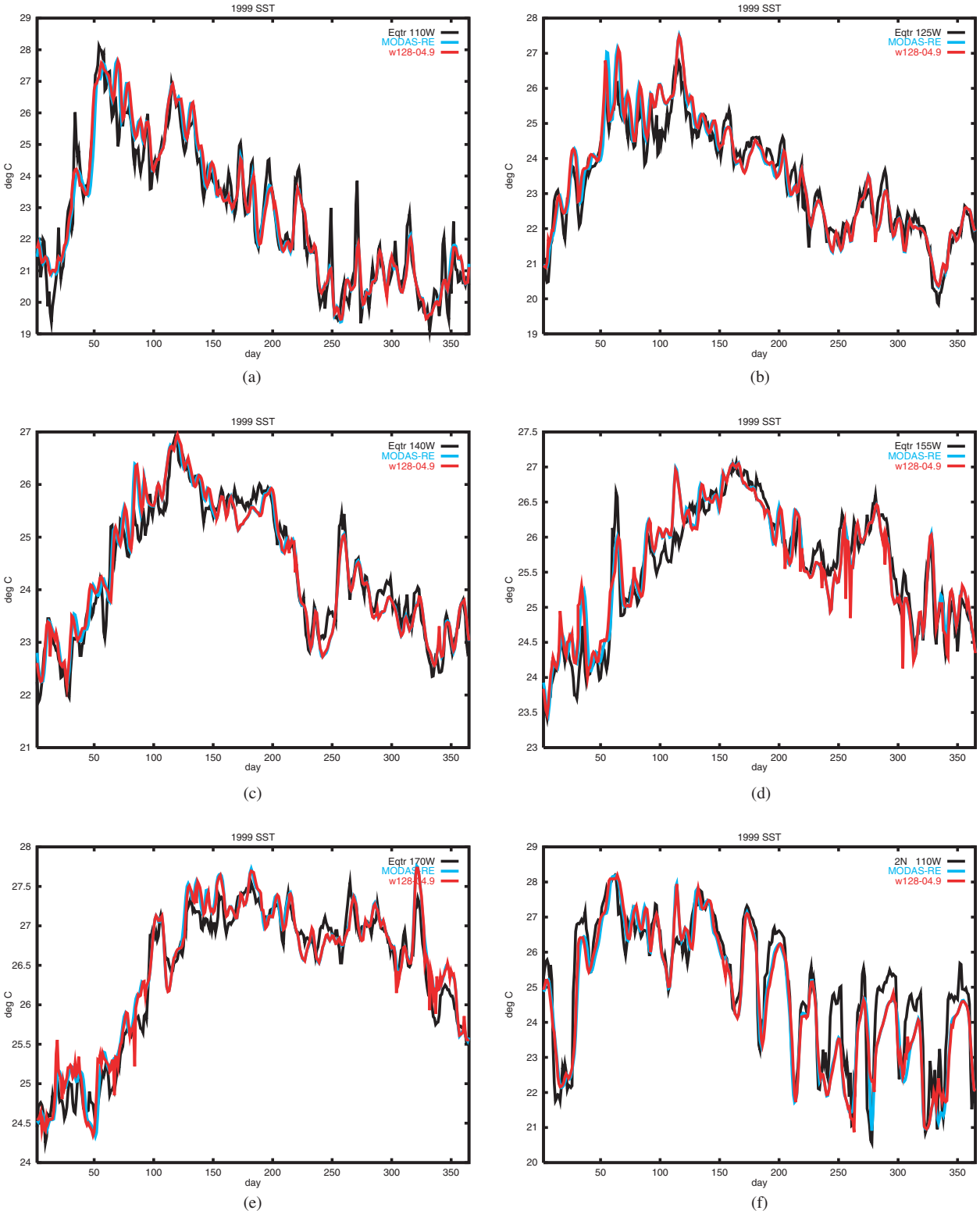

Fig. 9 — Same as Fig. 7 except for (a) buoy at 0°N, 110°W; (b) buoy at 0°N, 125°W; (c) buoy at 0°N, 140°W; (d) buoy at 0°N, 155°W; (e) buoy at 0°N, 170°W; and (f) buoy at 2°N, 110°W.

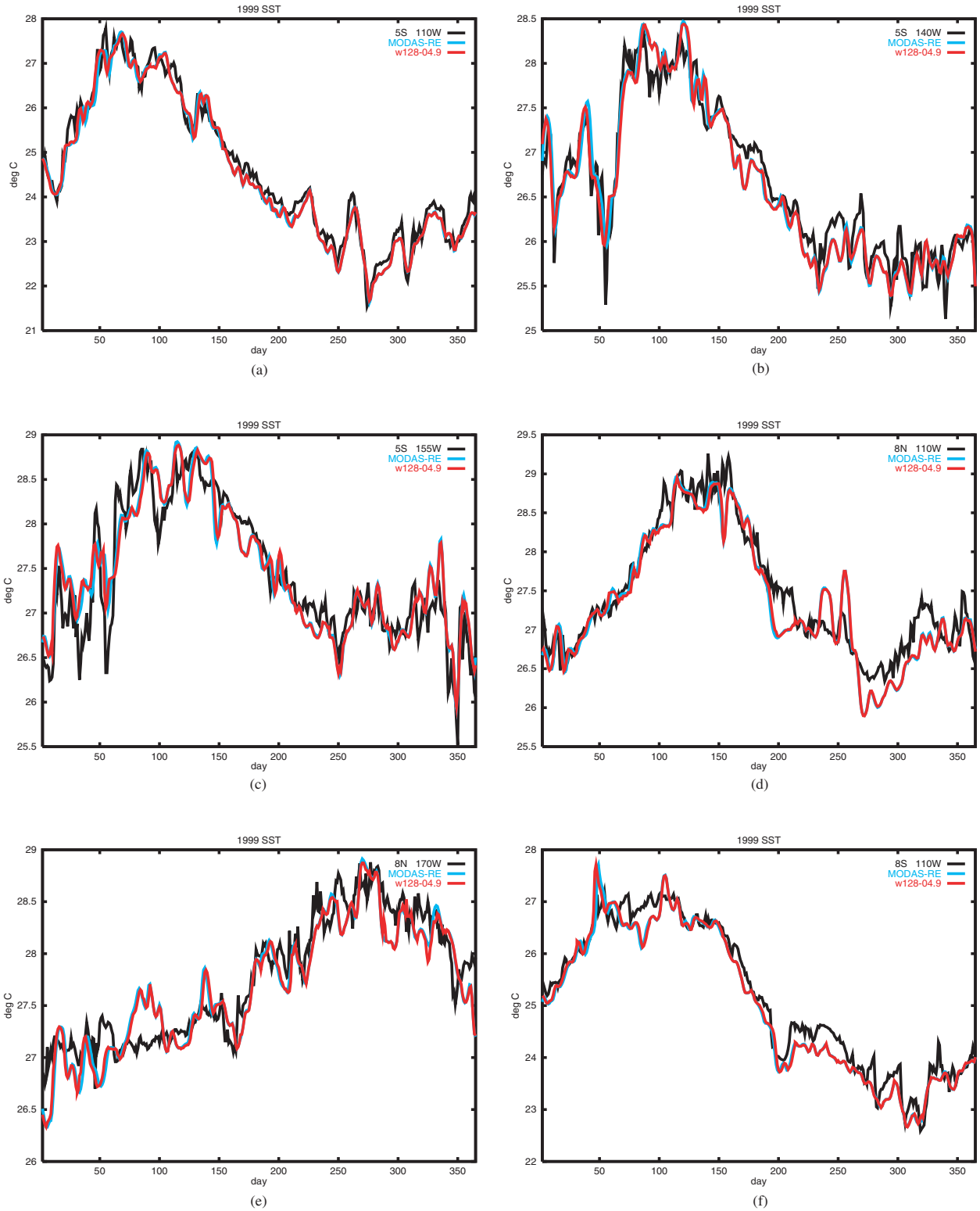

Fig. 10 — Same as Fig. 7 except for (a) buoy at 5°S, 110°W; (b) buoy at 5°S, 140°W; (c) buoy at 5°S, 155°W; (d) buoy at 8°N, 110°W; (e) buoy at 8°N, 170°W; and (f) buoy at 8°S, 110°W.

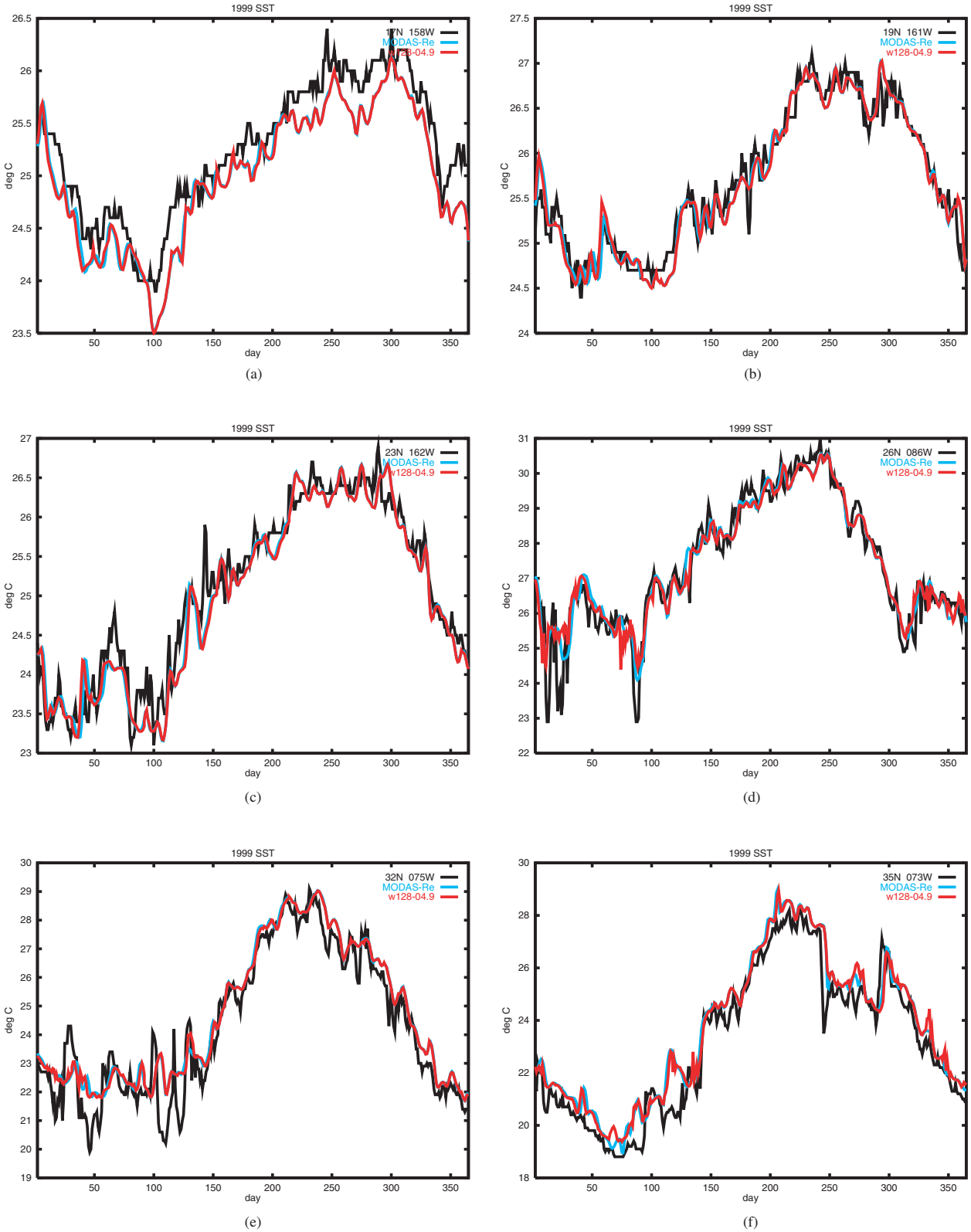

Fig. 11 — Same as Fig. 7 except for (a) buoy at 17°N, 158°W; (b) buoy at 19°N, 161°W; (c) buoy at 23°N, 162°W; (d) buoy at 26°N, 86°W; (e) buoy at 32°N, 75°W; and (f) buoy at 32°N, 73°W.

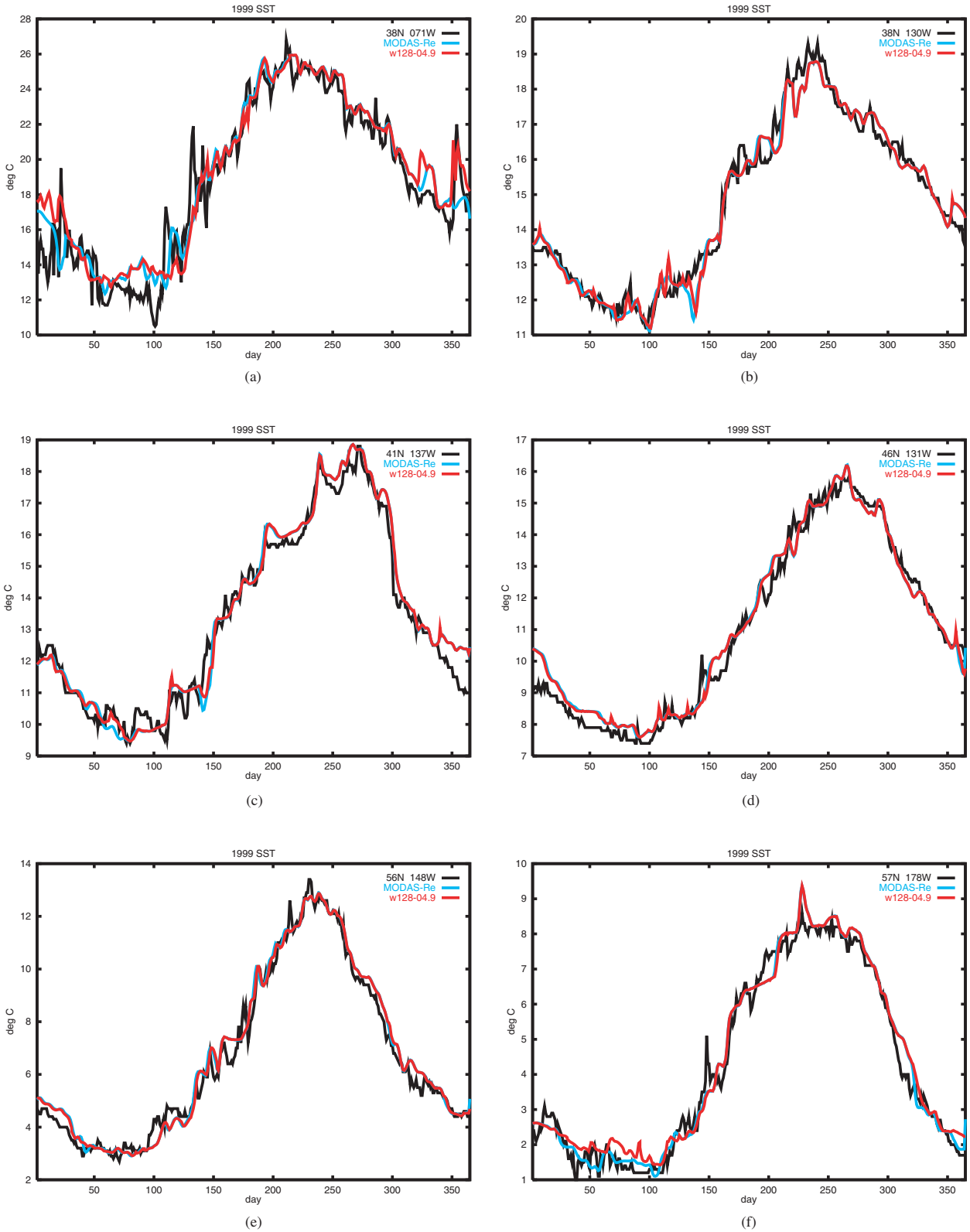

Fig. 12 — Same as Fig. 7 except for (a) buoy at 38°N, 71°W; (b) buoy at 38°N, 130°W; (c) buoy at 41°N, 137°W; (d) buoy at 46°N, 131°W; (e) buoy at 56°N, 148°W; and (f) buoy at 57°N, 178°W.

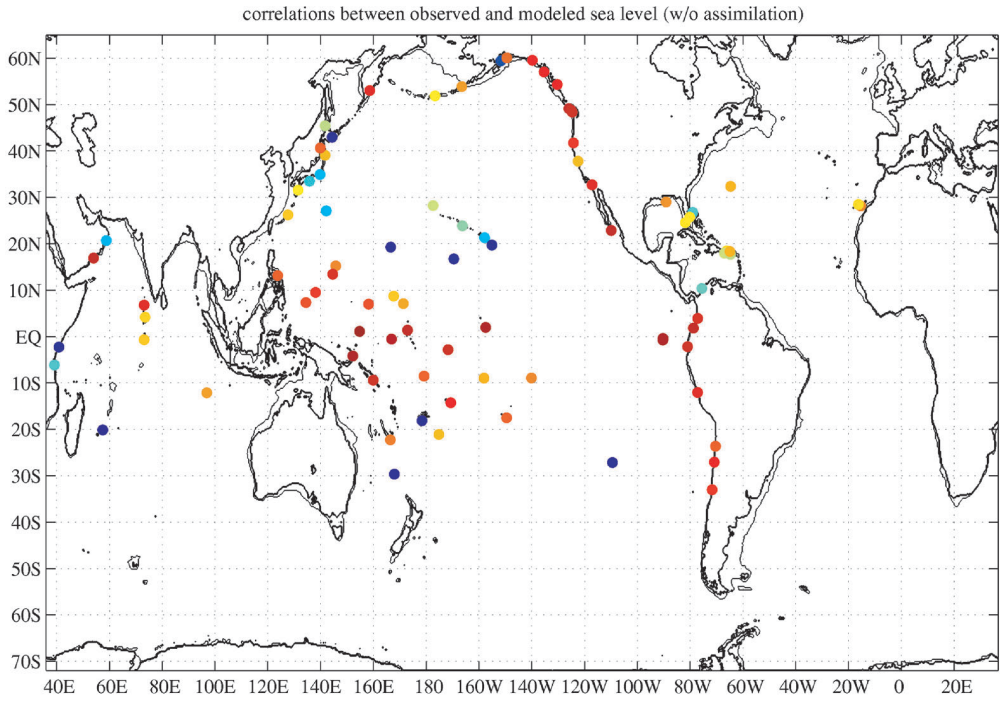

(a)

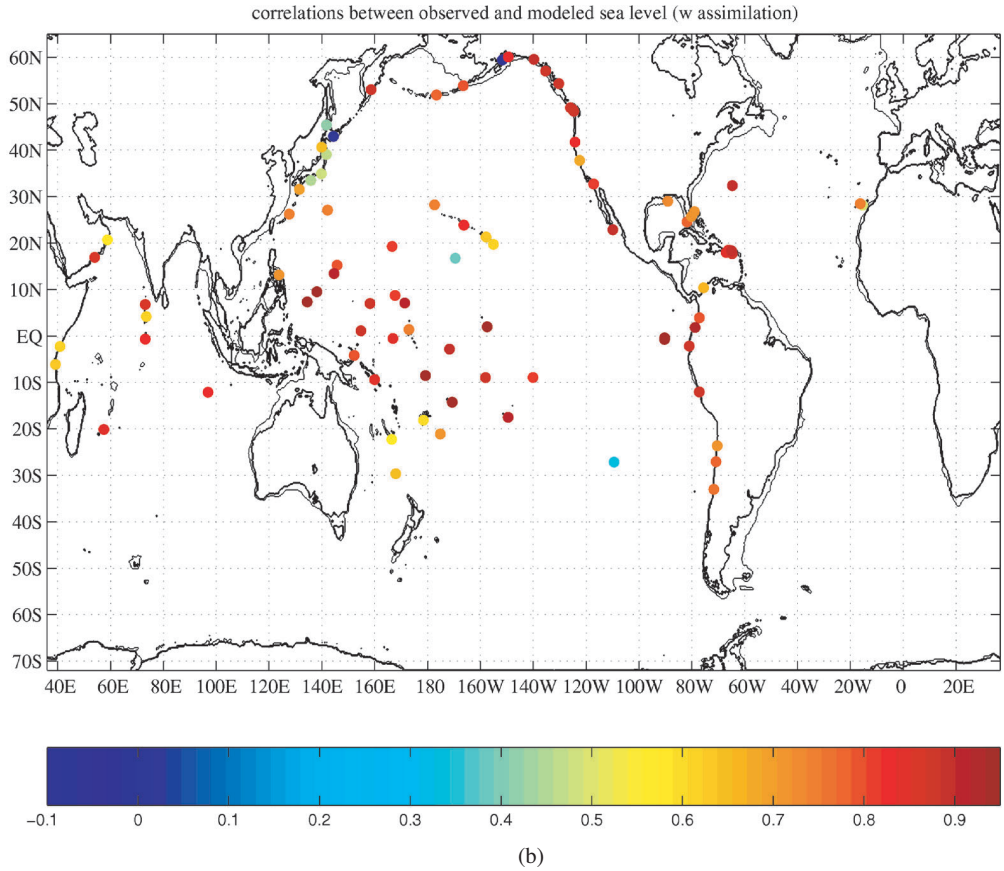

(b)

Fig. 13 — The 1997-1999 correlations coefficients for the IGOSS stations in Table 1 plotted by their location and color coded by the magnitude of the correlation coefficient with lower correlations in blue, increasing correlations in yellow and orange, and the higher correlations in red for (a) the non-assimilative 1/16° global NLOM and (b) the assimilative 1/16° global NLOM.

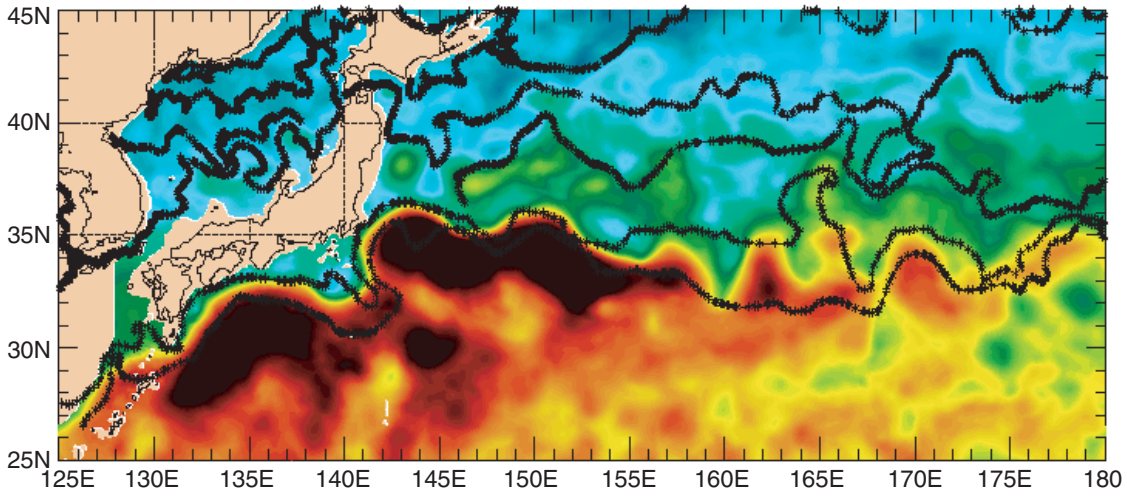

(a)

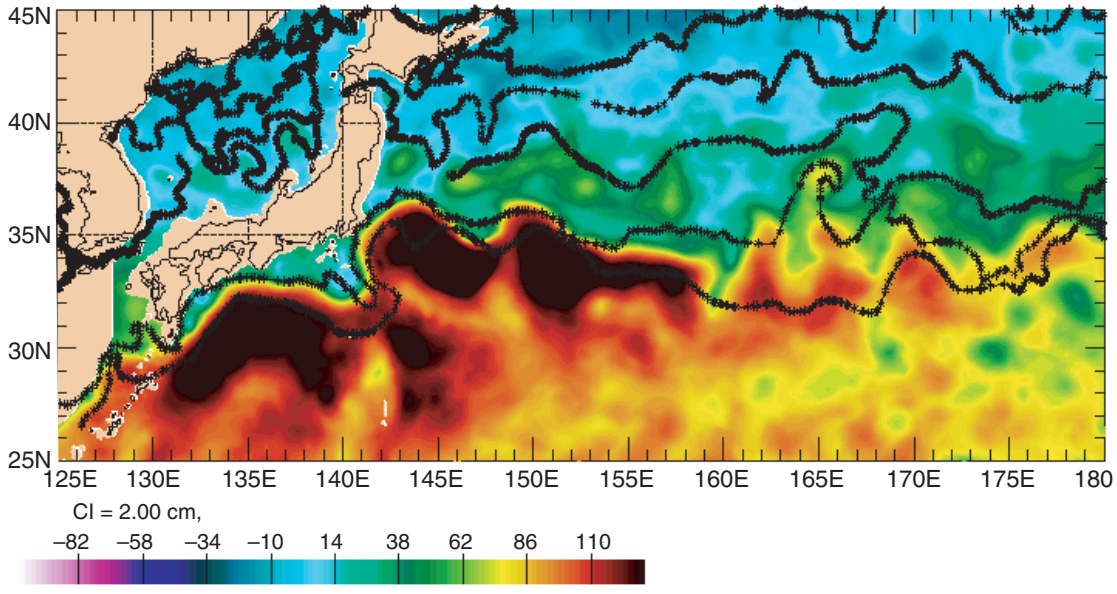

(b)

Fig. 14 — SSH analysis (nowcast) in the Kuroshio region from the assimilative 1/16° global NLOM for (a) 20 October 2000 and (b) 30 October 2000. Superimposed on each is the frontal analysis determined from satellite IR imagery (black lines) from the Naval Oceanographic Office for the same day.

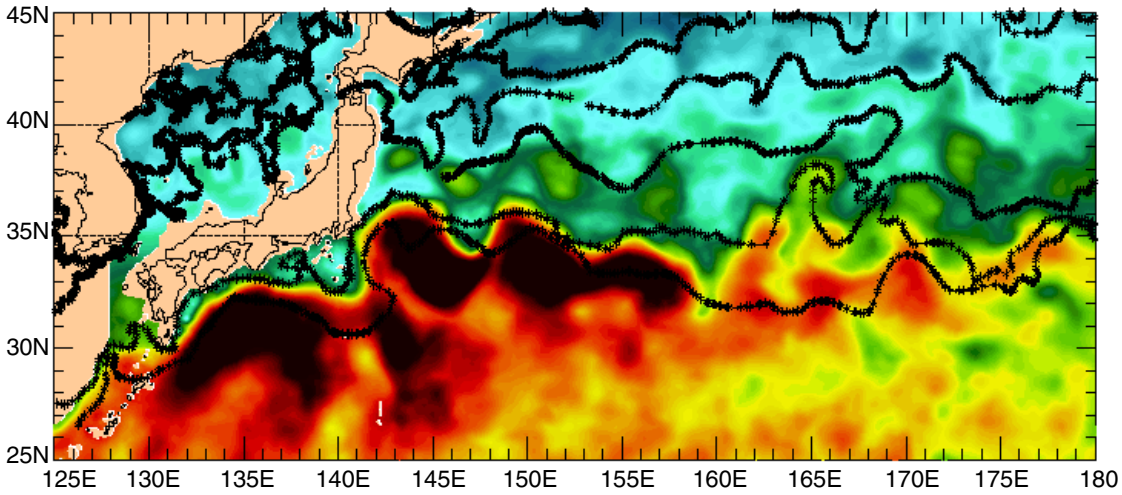

(a)

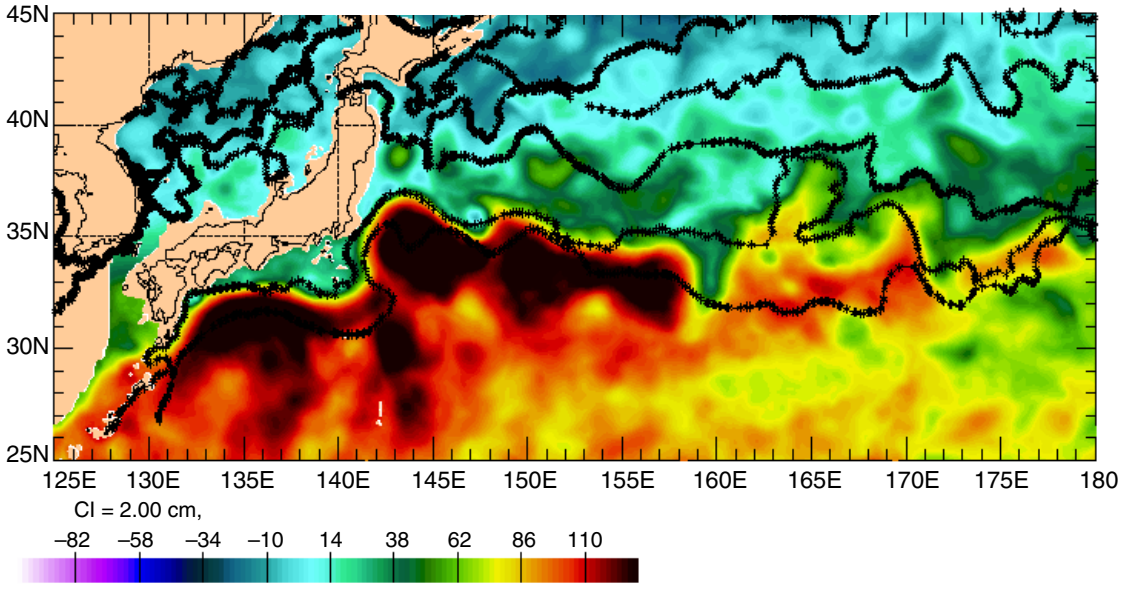

(b)

Fig. 15 — SSH analysis (nowcast) in the Kuroshio region from the assimilative 1/16° global NLOM for (a) 6 November 2000 and (b) 20 November 2000. Superimposed on each is the frontal analysis determined from satellite IR imagery (black lines) from the Naval Oceanographic Office for the same day.

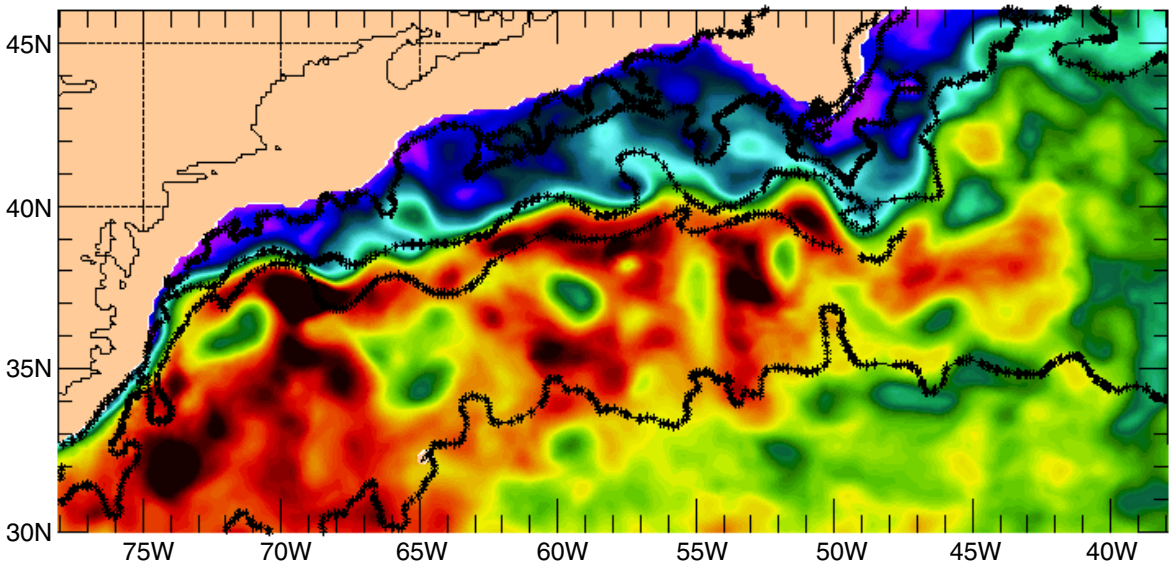

(a)

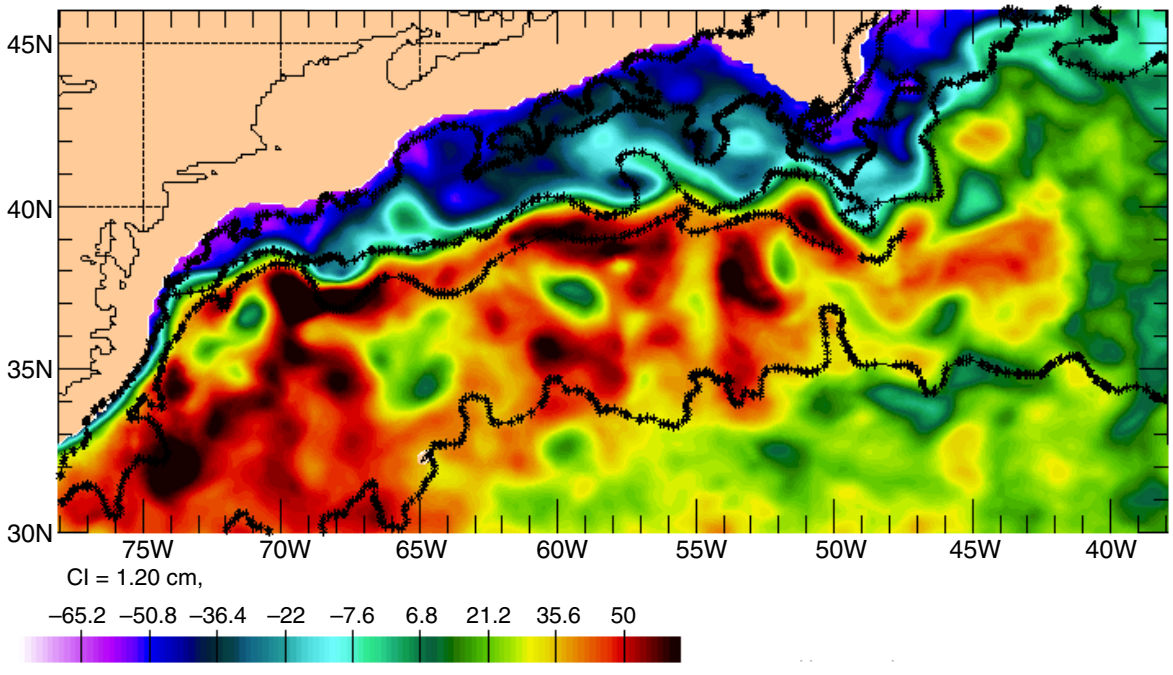

(b)

Fig. 16 — SSH analysis (nowcast) in the Gulf Stream region from the assimilative 1/16° global NLOM for (a) 27 November 2000 and (b) 29 November 2000. Superimposed on each is the frontal analysis determined from satellite IR imagery (black lines) from the Naval Oceanographic Office for the same day.

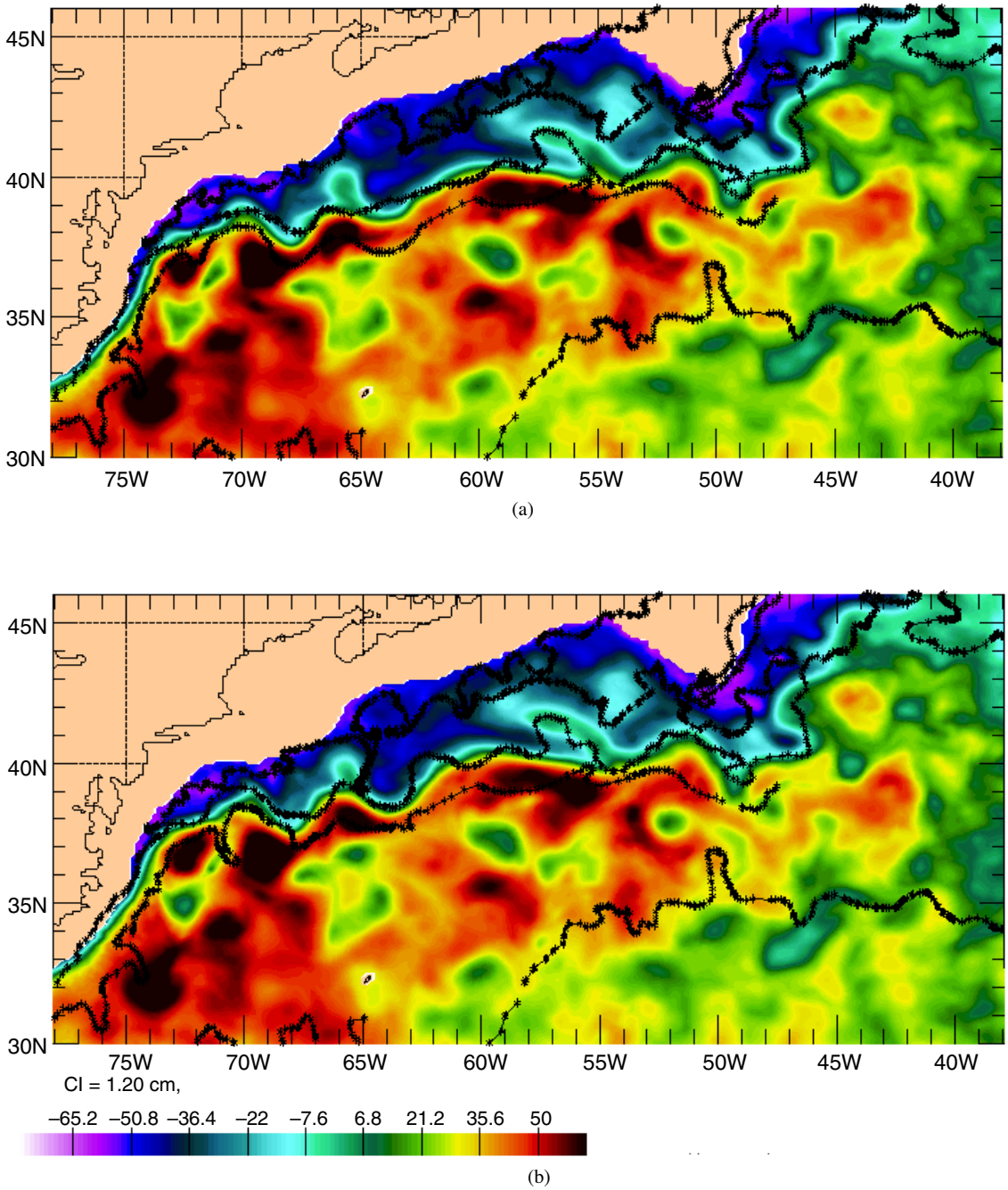

Fig. 17 — SSH analysis (nowcast) in the Gulf Stream region from the assimilative 1/16° global NLOM for (a) 4 December 2000 and (b) 6 December 2000. Superimposed on each is the frontal analysis determined from satellite IR imagery (black lines) from the Naval Oceanographic Office for the same day.

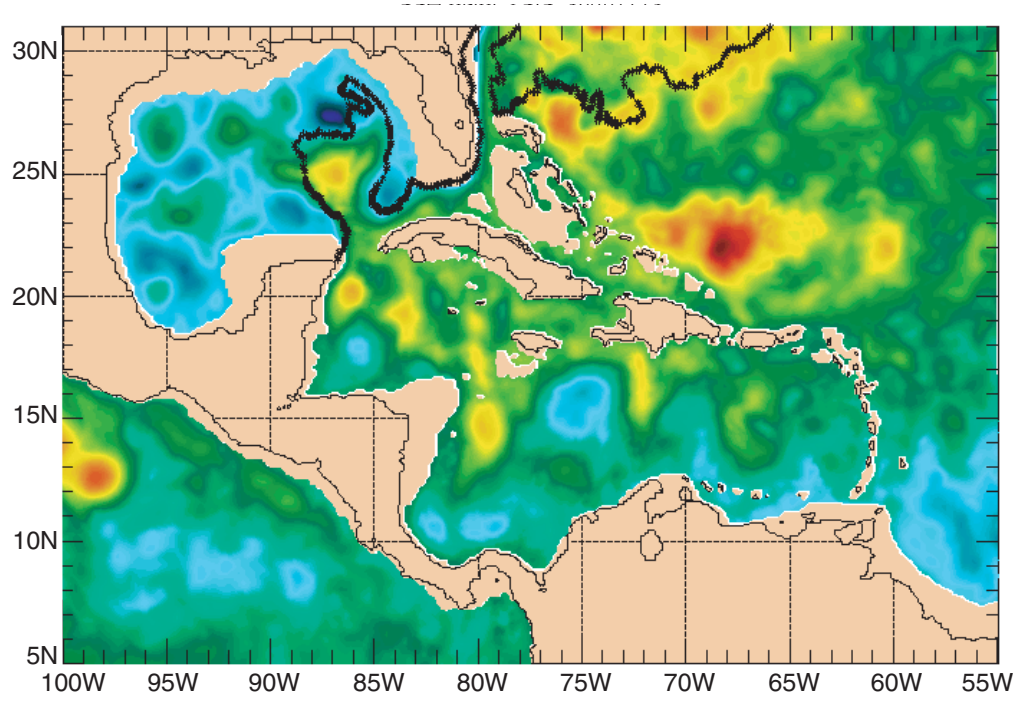

(a)

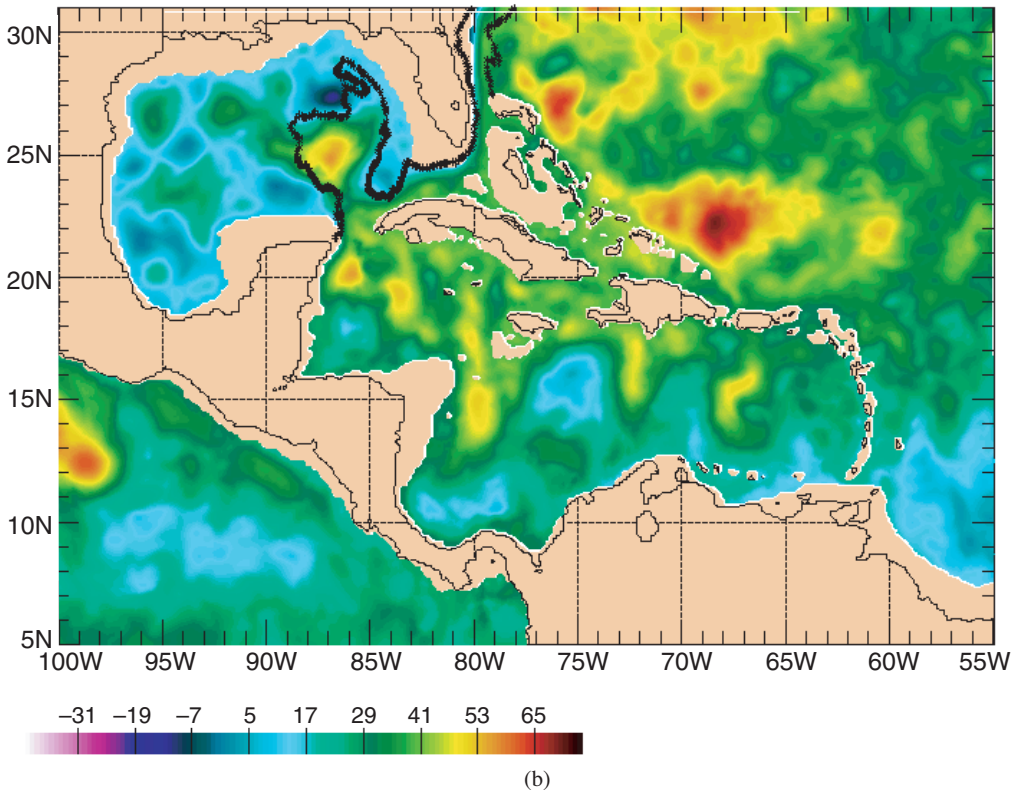

(b)

Fig. 18 — SSH analysis (nowcast) in the Intra-America Seas region from the assimilative 1/16° global NLOM for (a) 13 November 2000 and (b) 15 November 2000. Superimposed on each is the frontal analysis determined from satellite IR imagery (black lines) from the Naval Oceanographic Office for the same day.

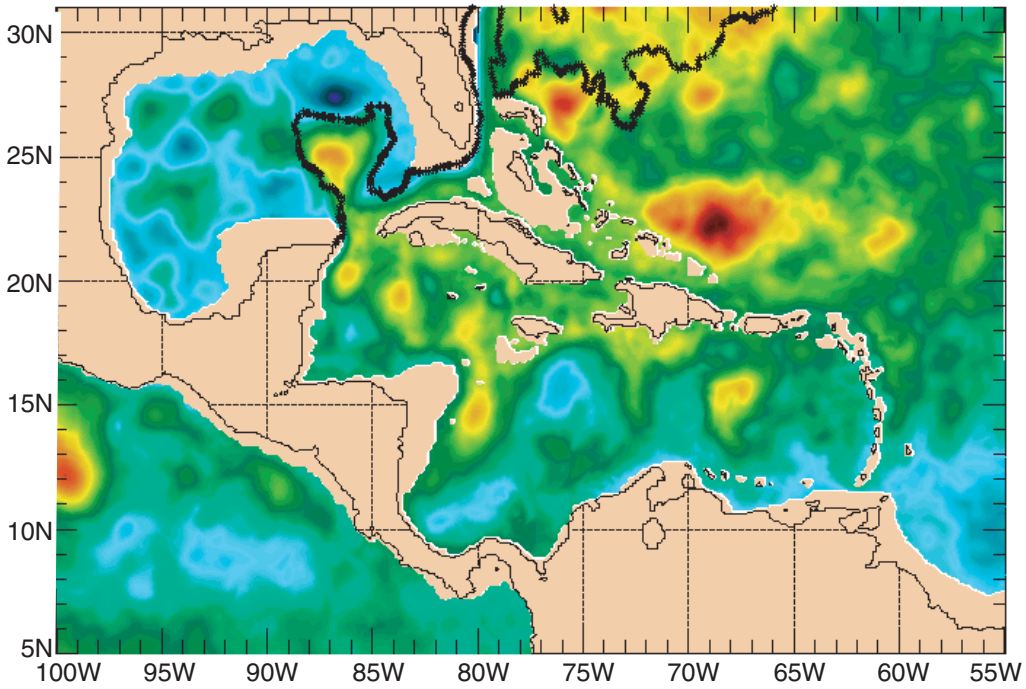

(a)

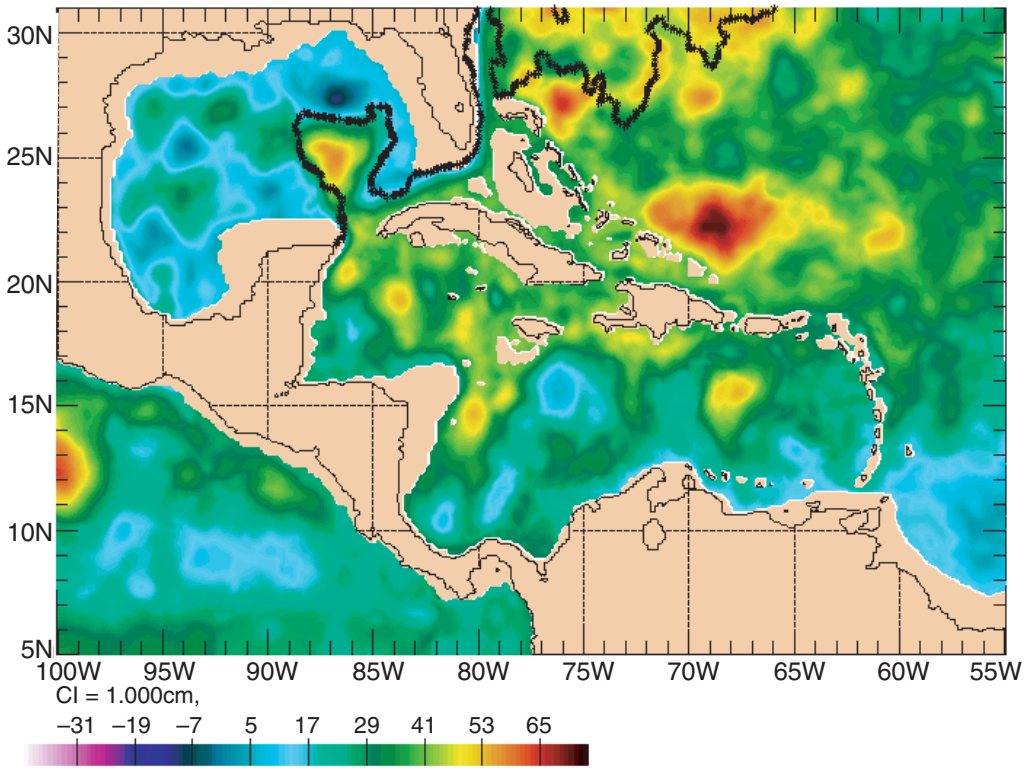

(b)

Fig. 19 — SSH analysis (nowcast) in the Intra-America Seas region from the assimilative 1/16° global NLOM for (a) 20 November 2000 and (b) 22 November 2000. Superimposed on each is the frontal analysis determined from satellite IR imagery (black lines) from the Naval Oceanographic Office for the same day.

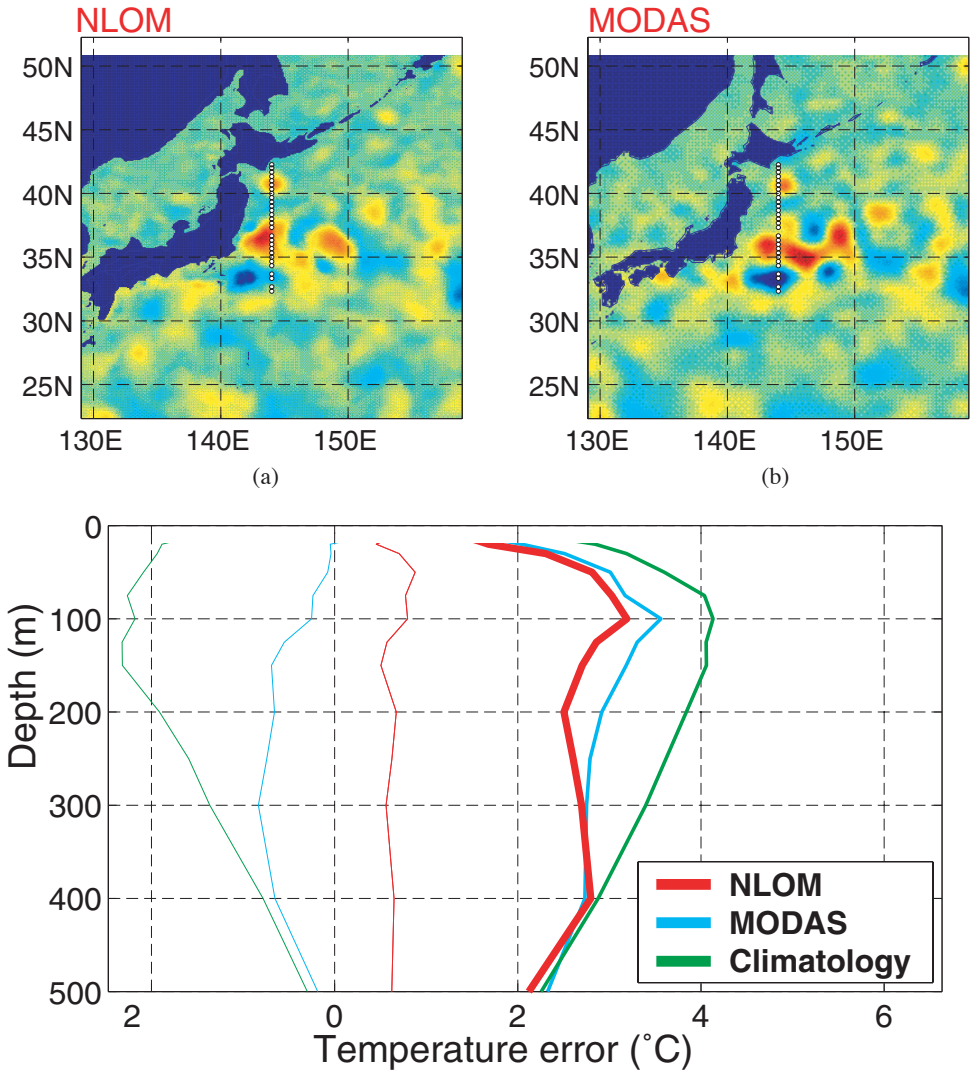

Fig. 20 — SSH anomalies with respect to a long term mean for (a) assimilative 1/16° global NLOM and (b) 1/8° global MODAS OI analysis from the Naval Oceanographic Office for 20 July 1999. Superimposed on with mean (thin lines) and RMS (thick lines) temperature error statistics for synthetic profiles as function of depth from NLOM-derived synthetics (red lines), MODAS-derived synthetics (blue lines), and MODAS climatological temperature (green lines).

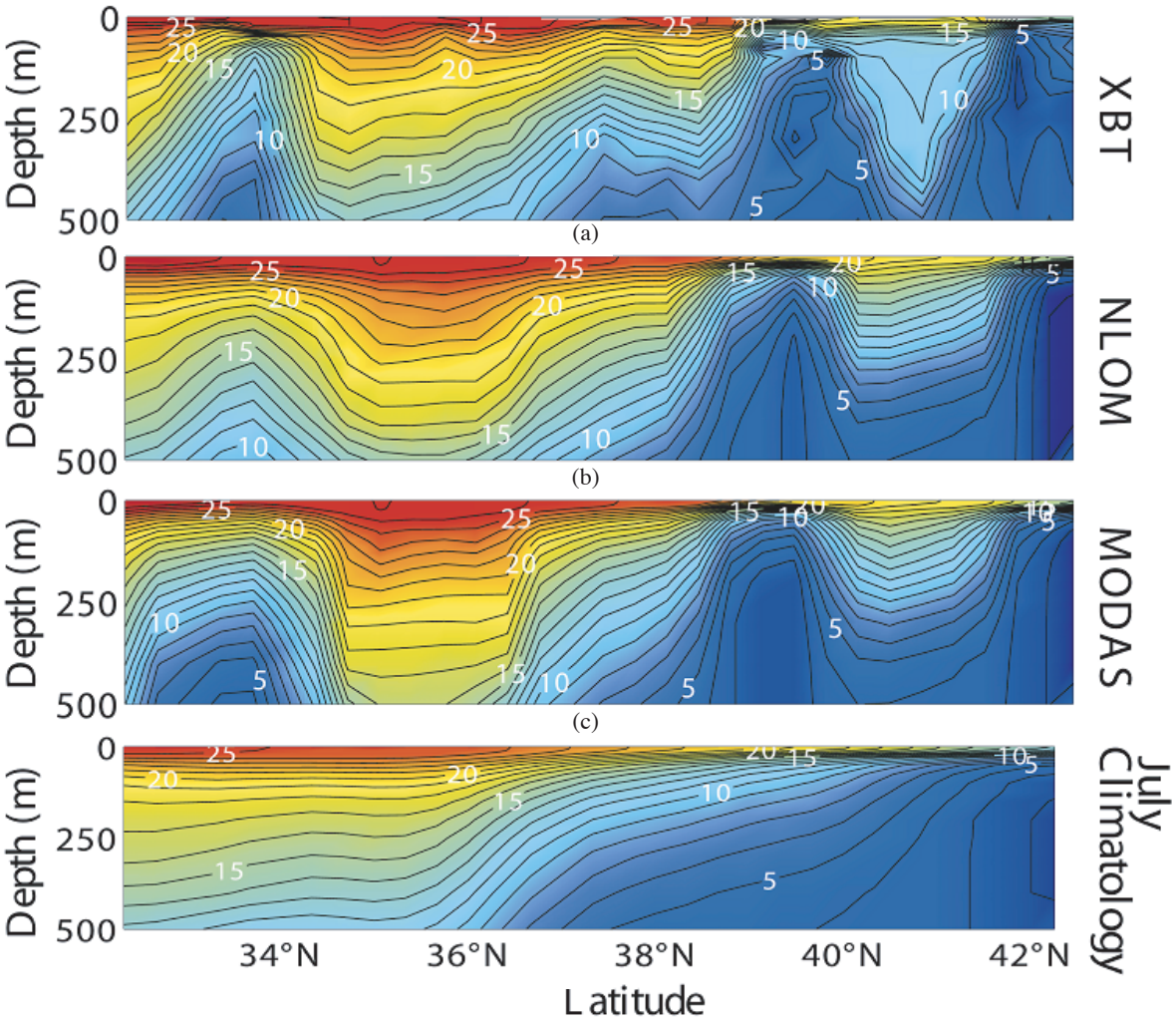

Fig. 21 — Temperature cross-sections along an XBT section at 144°E on 16-22 July 1999 from the surface to 500-m depth for (a) observed XBT data, (b) MODAS synthetic profiles derived from 1/16° global NLOM SSH field, (c) MODAS synthetic profiles derived from 1/8° global MODAS SSH field, and (d) July climatological temperature from MODAS.

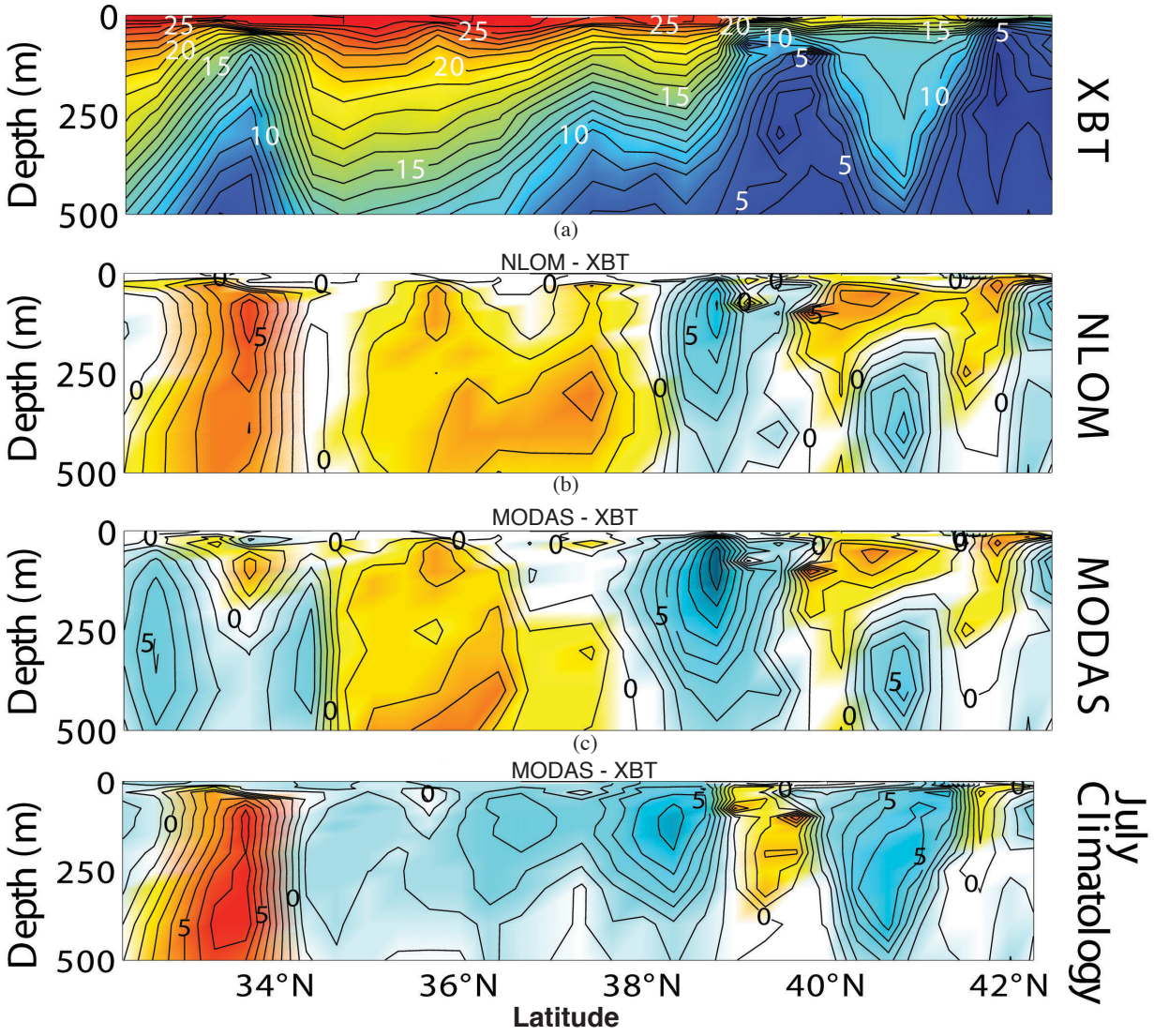

Fig. 22 — Observed XBT data (a) along a section at 144° E on 16-22 July1999 from the surface to 500-m depth and temperature error cross-sections for (b) MODAS synthetic profiles derived from 1/16° global NLOM SSH field-XBT data, (c) MODAS synthetic profiles derived from 1/8° global MODAS SSH field-XBT data, and (d) July climatological temperature from MODAS-XBT data.

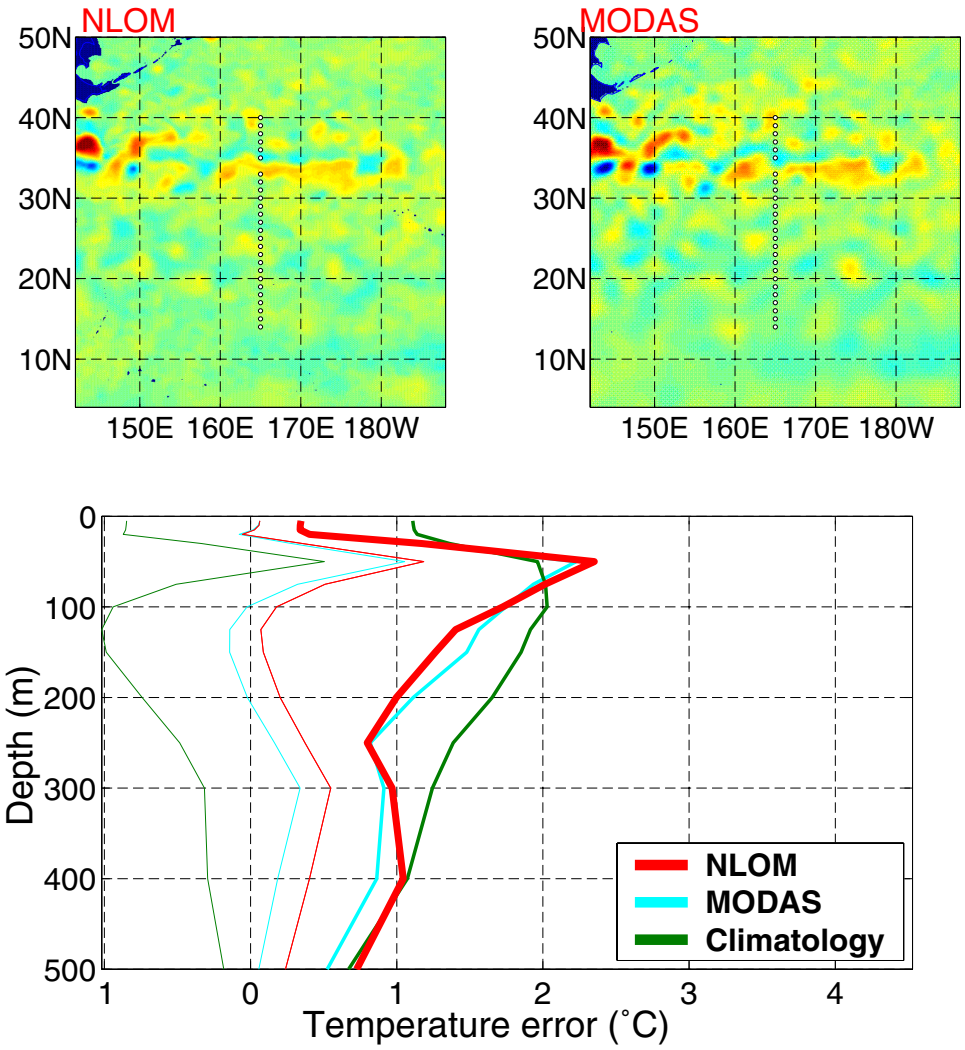

Fig. 23 — SSH anomalies from long-term means for (a) assimilative 1/16° global NLOM and (b) 1/8° global MODAS OI analysis from the Naval Oceanographic Office for 25 September 1999. Superimposed on each is the location of XBTs (white dots) used for statistical comparison c) of MODAS synthetic temperature profiles calculated from the NLOM and MODAS SSH fields with mean (thin lines) and RMS (thick lines) temperature error statistics for synthetic profiles as function of depth from NLOM-derived synthetics (red lines), MODAS-derived synthetics (blue lines), and MODAS climatological temperature (green lines).

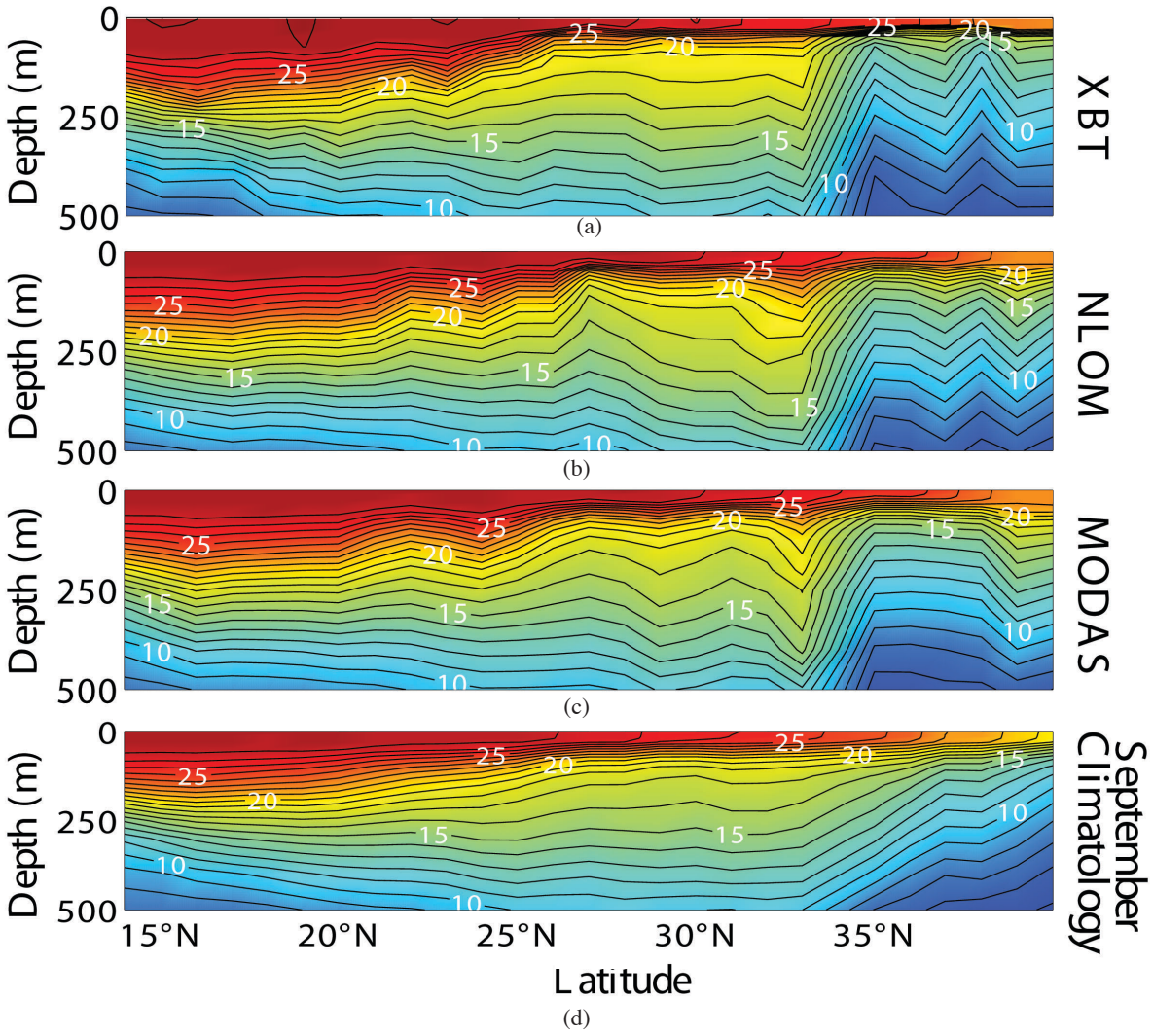

Fig. 24 —Temperature cross-sections along XBT section at 165°E on 21-28 September 1999 from the surface to 500-m depth for (a) observed XBT data, (b) MODAS synthetic profiles derived from 1/16° global NLOM SSH field, (c) MODAS synthetic profiles derived from 1/8° global MODAS SSH field, and (d) September climatological temperature from MODAS.

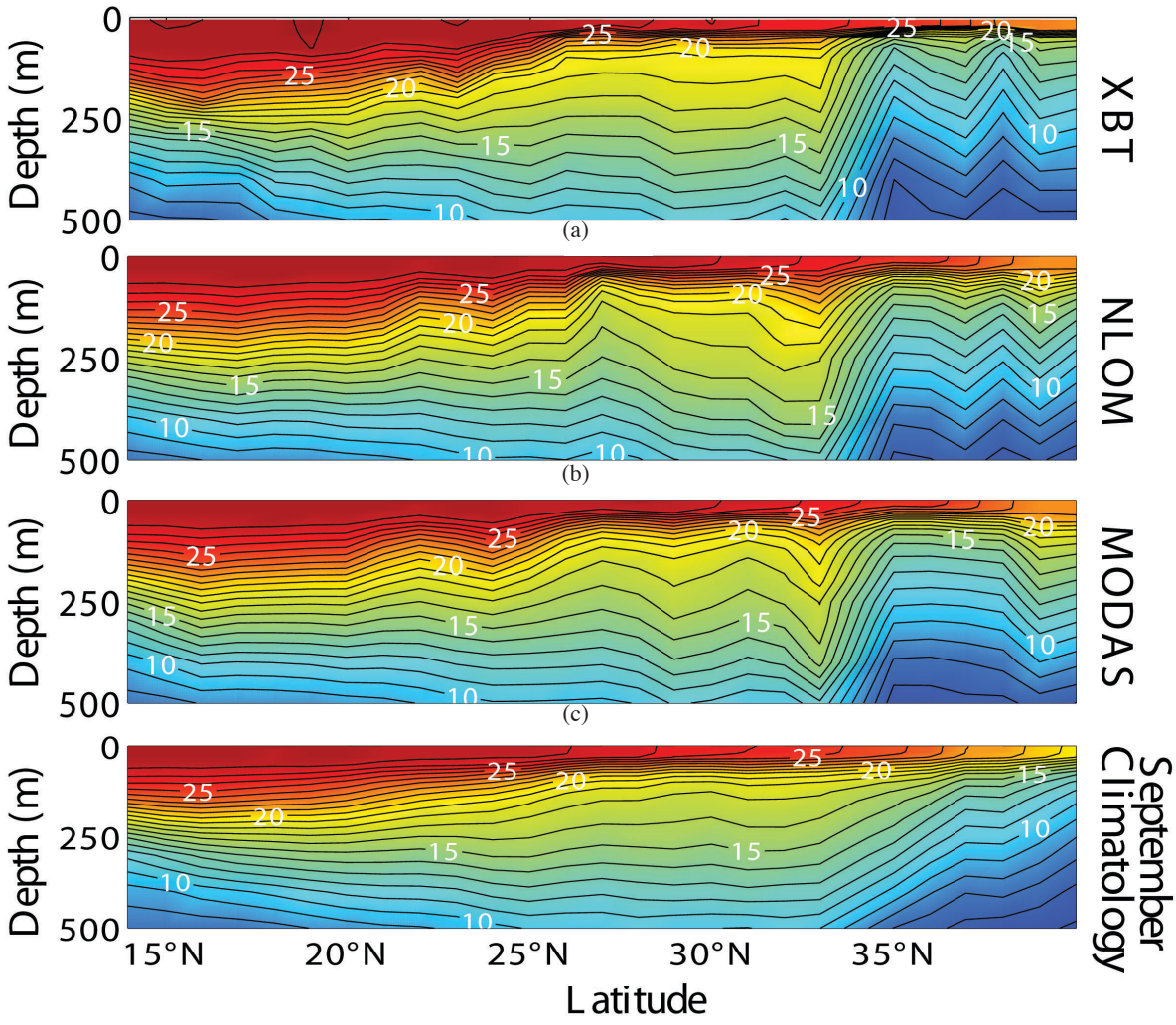

Fig. 25 — Observed XBT data (a) along section at 165° E on 21-28 September 1999 from the surface to 500-m depth and temperature error cross-sections for (b) MODAS synthetic profiles derived from 1/16° global NLOM SSH field-XBT data, (c) MODAS synthetic profiles derived from 1/8° global MODAS SSH field-XBT data, and (d) September climatological temperature from MODAS-XBT data.

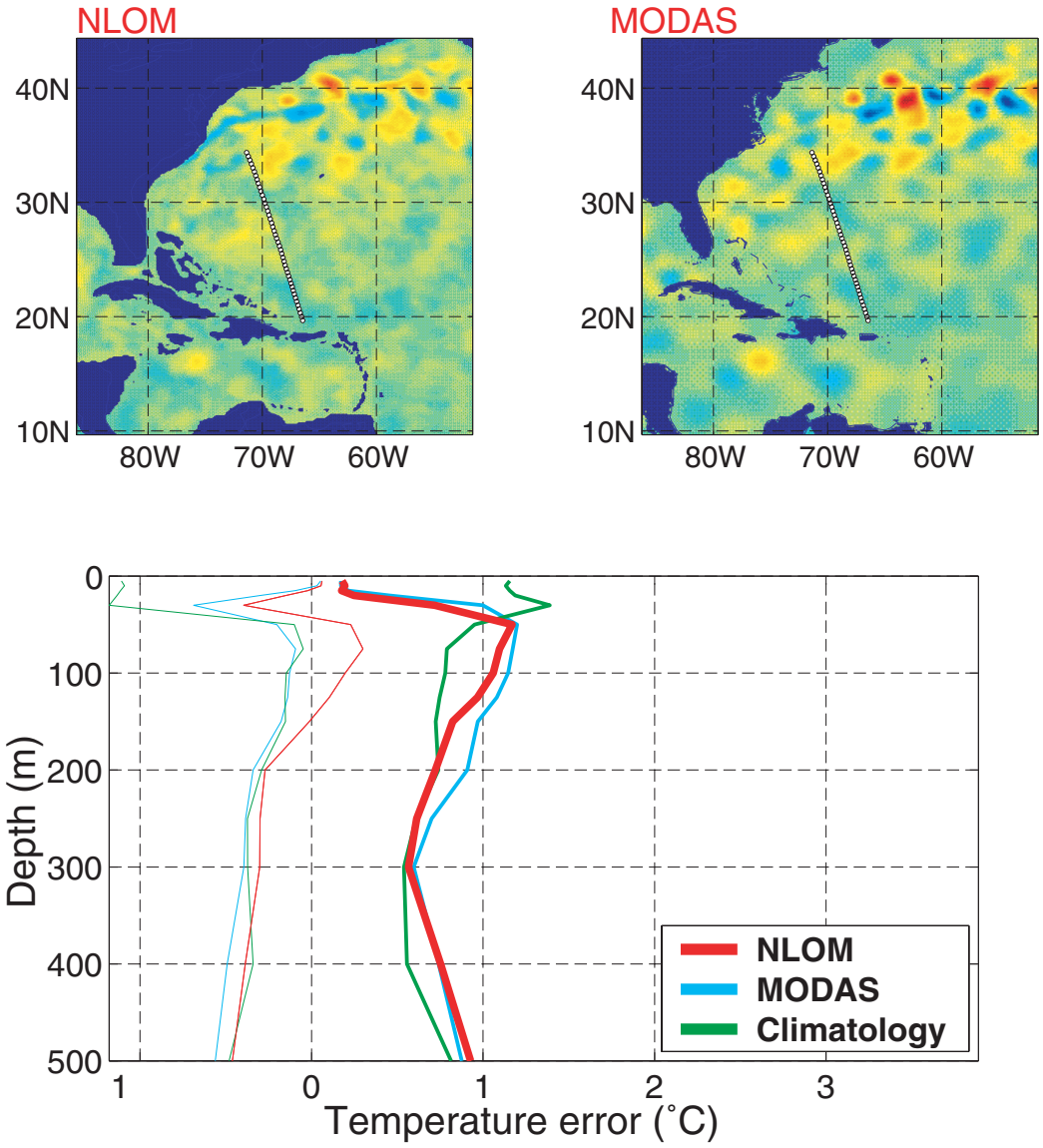

Fig. 26 — SSH anomalies from long-term means for (a) assimilative 1/16° global NLOM and (b) 1/8° global MODAS OI analysis from the Naval Oceanographic Office for 23 August 1999. Superimposed on each is the location of XBTs (white dots) used for statistical comparison (c) of MODAS synthetic temperature profiles calculated from the NLOM and MODAS SSH fields with mean (thin lines) and RMS (thick lines) temperature error statistics for synthetic profiles as function of depth from NLOM-derived synthetics (red lines), MODAS-derived synthetics (blue lines), and MODAS climatological temperature (green lines).

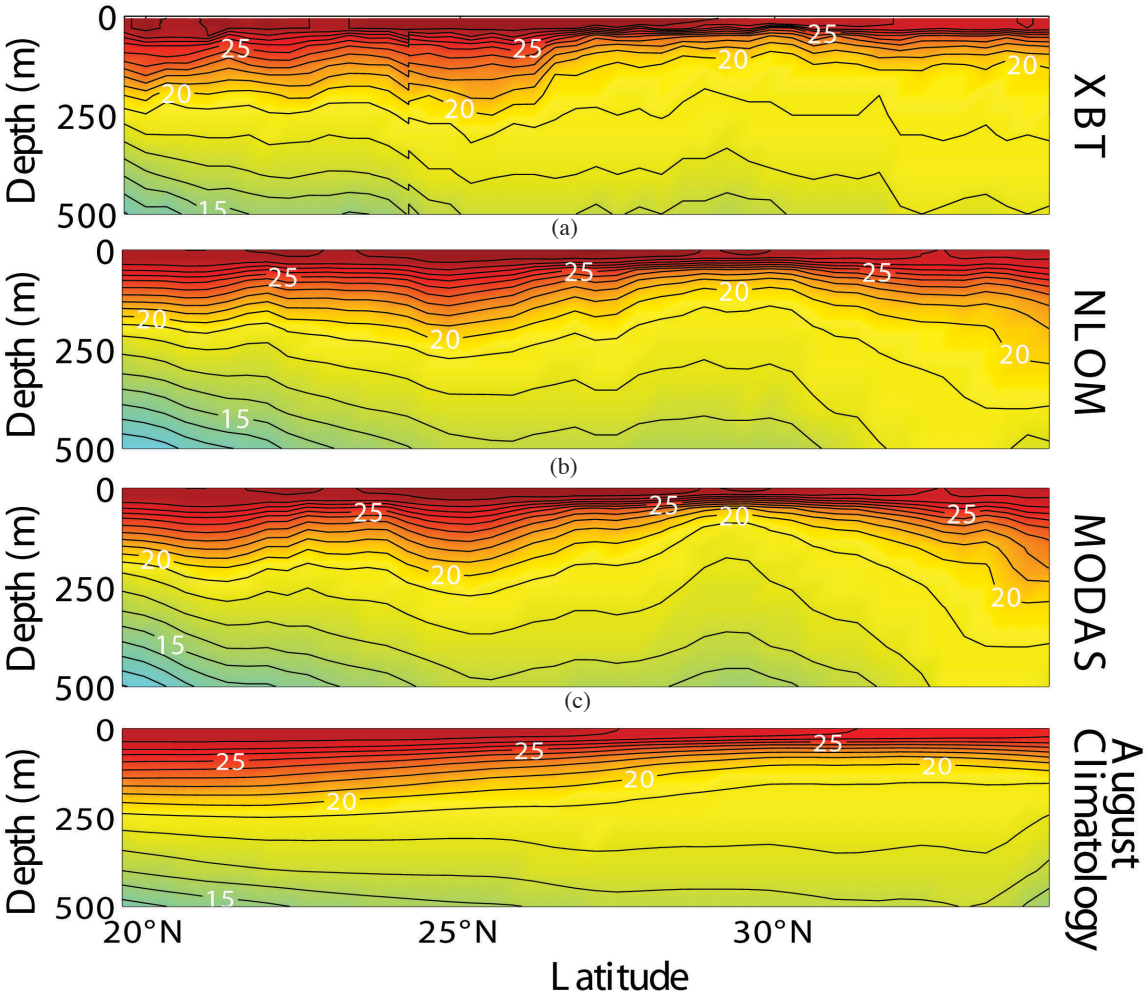

Fig. 27 — Temperature cross-sections along XBT section at 69° W on 22-24 August 1999 from the surface to 500-m depth for (a) observed XBT data, (b) MODAS synthetic profiles derived from 1/16° global NLOM SSH field, (c) MODAS synthetic profiles derived from 1/8° global MODAS SSH field and (d) August climatological temperature from MODAS.

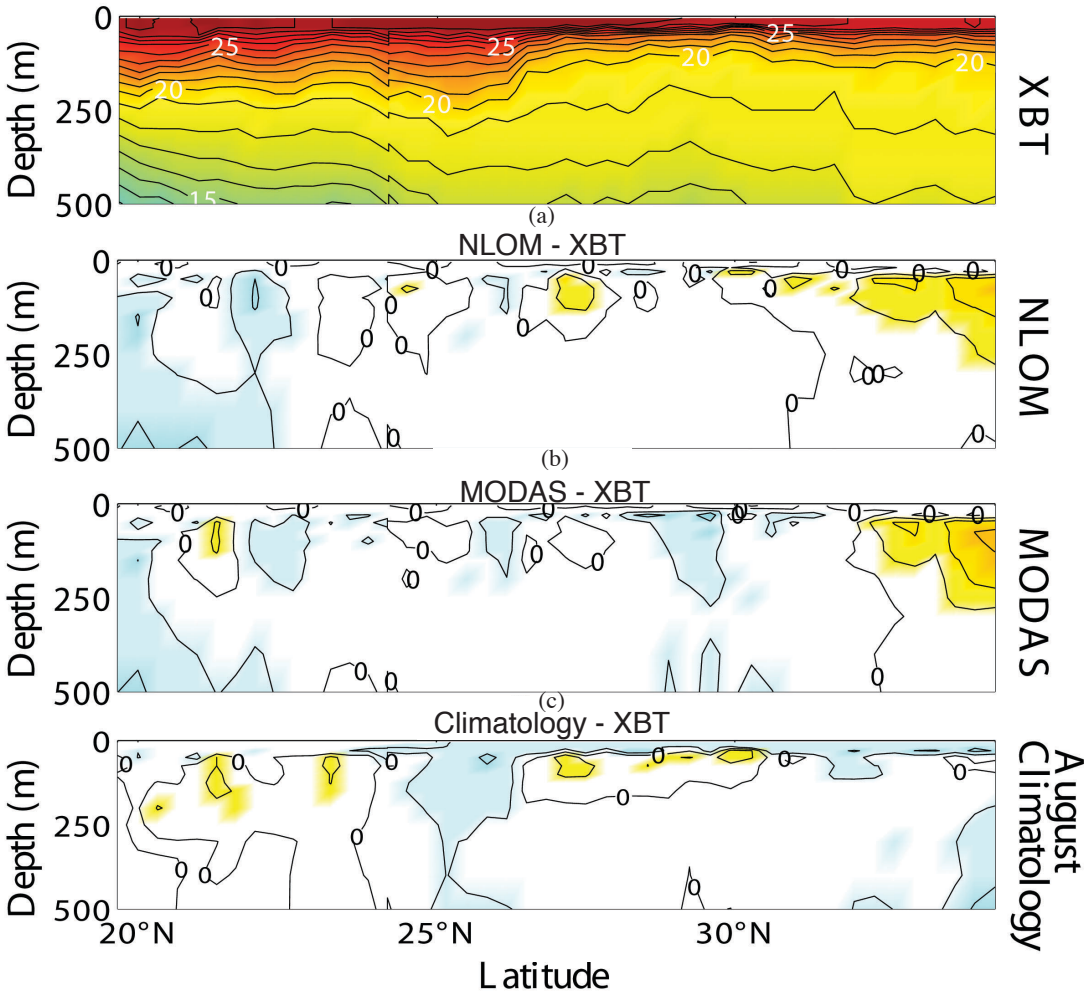

Fig. 28 — Observed XBT data (a) along section at 69°W on 22-24 August 1999 from the surface to 500-m depth and temperature error cross-sections for (b) MODAS synthetic profiles derived from 1/16° global NLOM SSH field-XBT data, (c) MODAS synthetic profiles derived from 1/8° global MODAS SSH field-XBT data, and (d) August climatological temperature from MODAS-XBT data.

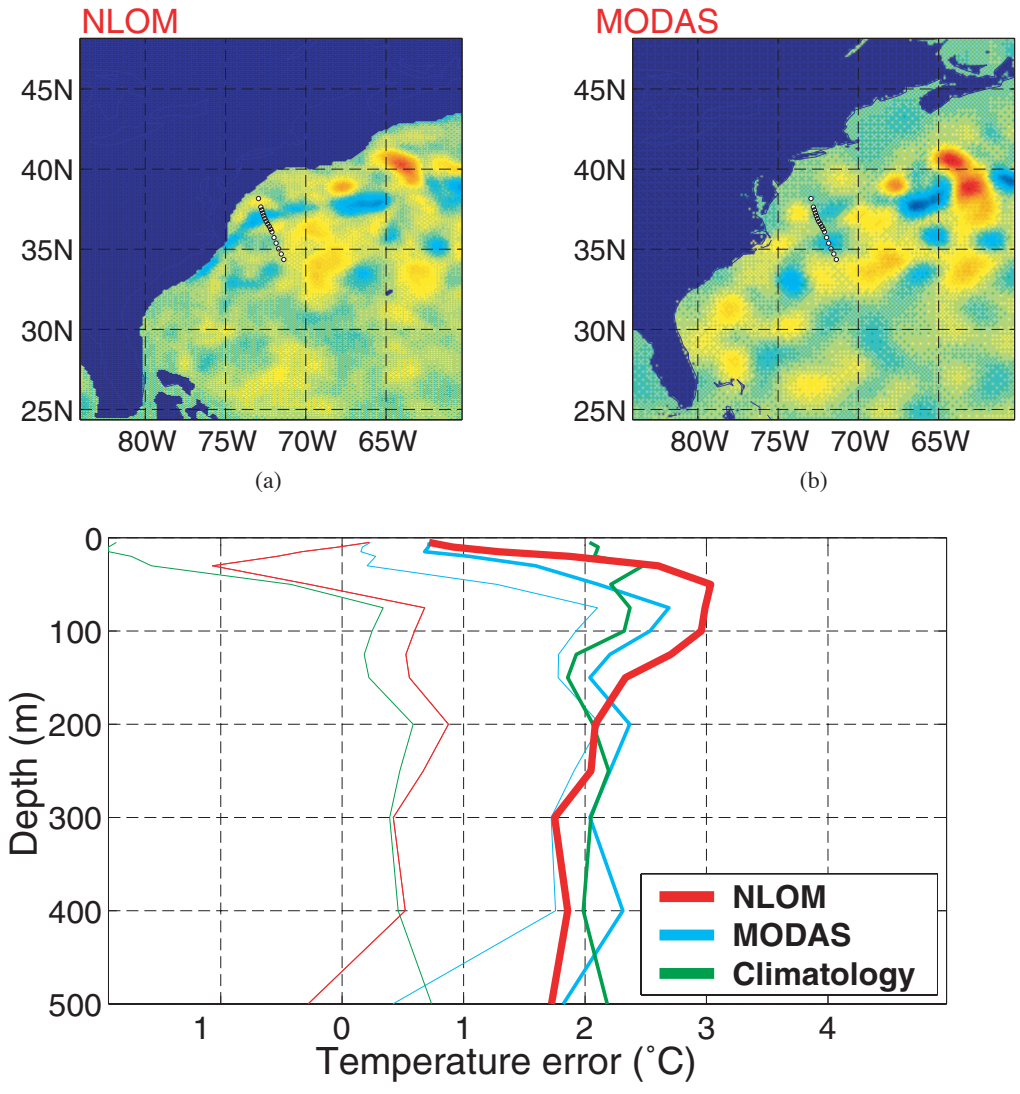

Fig. 29 — SSH anomalies from long-term means for (a) assimilative 1/16° global NLOM and (b) 1/8° global MODAS OI analysis from the Naval Oceanographic Office for 23 August 1999. Superimposed on each is the location of XBTs (white dots) used for statistical comparison (c) of MODAS synthetic temperature profiles calculated from the NLOM and MODAS SSH fields with mean (thin lines) and RMS (thick lines) temperature error statistics for synthetic profiles as function of depth from NLOM-derived synthetics (red lines), MODAS-derived synthetics (blue lines), and MODAS climatological temperature (green lines).

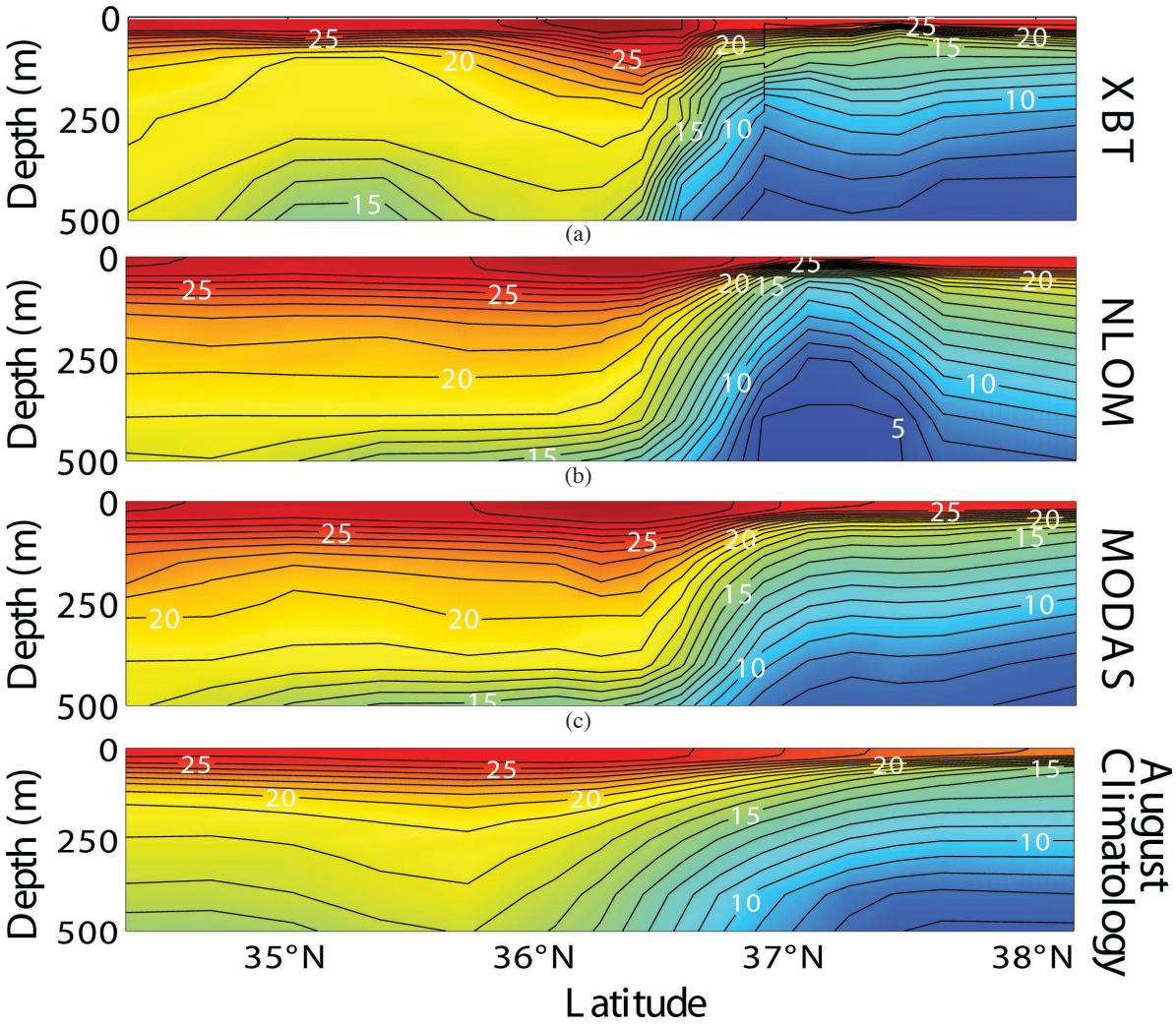

Fig. 30 — Temperature cross-sections along an XBT section at 73° W on 22-24 August 1999 from the surface to 500-m depth for (a) observed XBT data, (b) MODAS synthetic profiles derived from 1/16° global NLOM SSH field, (c) MODAS synthetic profiles derived from 1/8° global MODAS SSH field, and (d) August climatological temperature from MODAS.

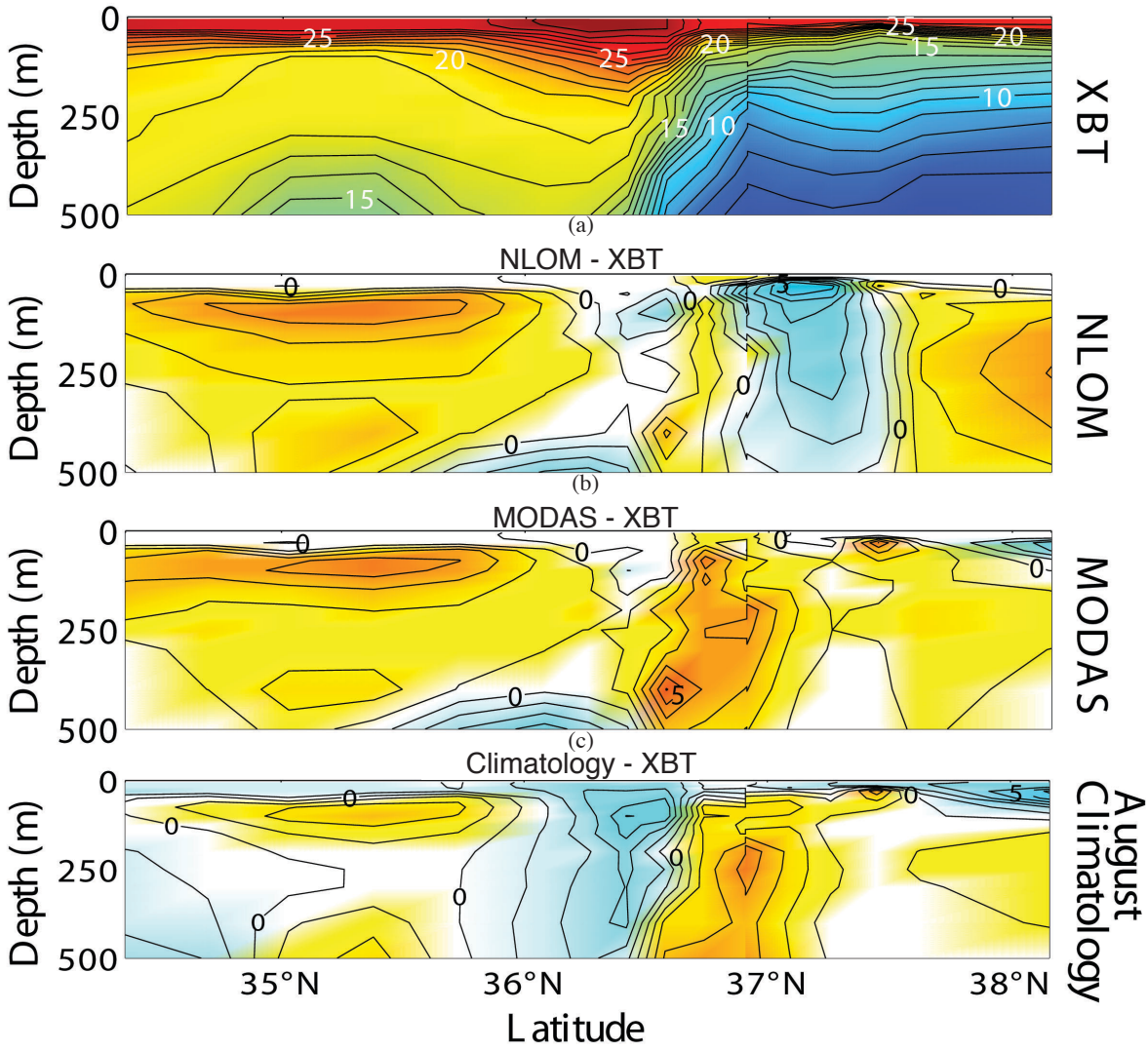

(a)

(b)

(c)

(d)

Fig. 31 — Observed XBT data (a) along section at 73° W on 22-24 August 1999 from the surface to 500-m depth and temperature error cross-sections for (b) MODAS synthetic profiles derived from 1/16° global NLOM SSH field-XBT data, (c) MODAS synthetic profiles derived from 1/8° global MODAS SSH field-XBT data, and (d) August climatological temperature from MODAS-XBT data.

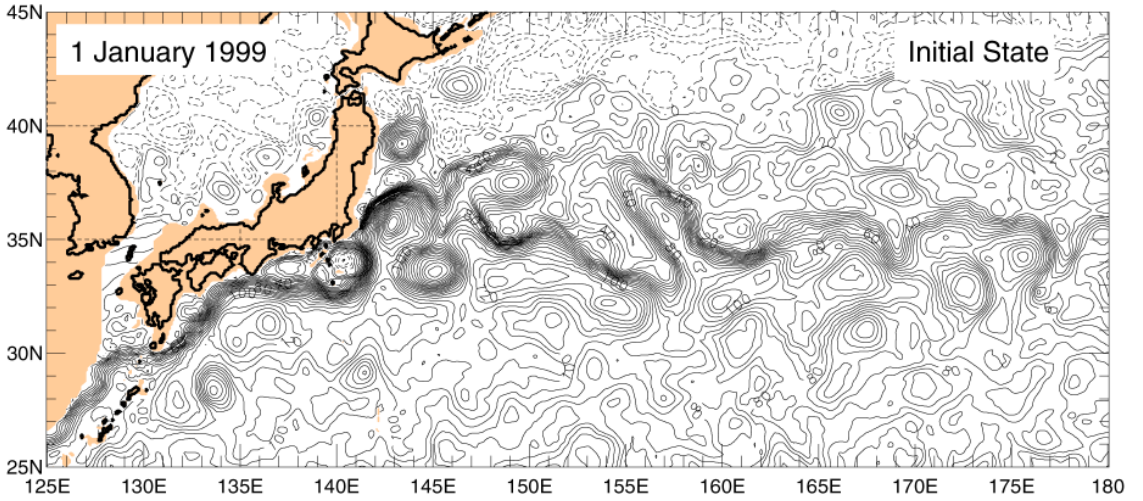

(a)

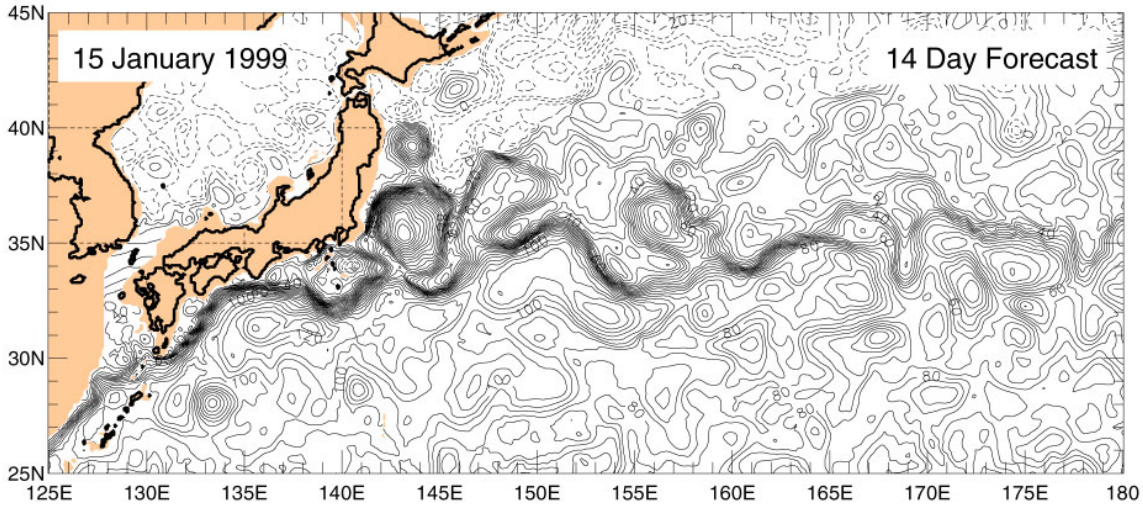

(b)

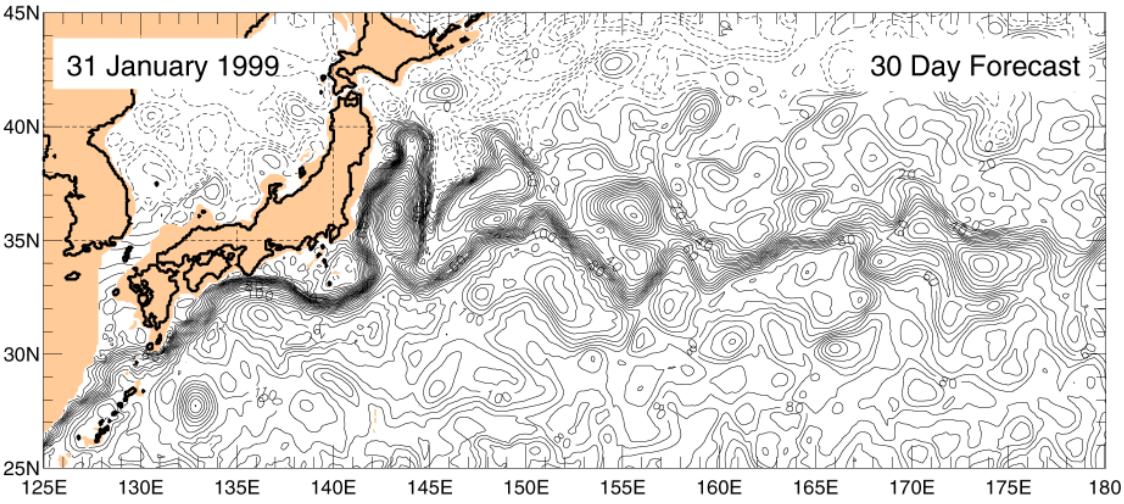

(c)

Fig. 32 — SSH for the Kuroshio region from the 1/16° global NLOM running in forecast mode for a 30-day forecast. The model forecast was initialized on 1 January 1999 (a) and forecasts are shown for (b) 15 January 1999 and (c) 31 January 1999. The model was forced with FNMOC wind and thermal fields gradually interpolating to climatological forcing for the long-term forecast.

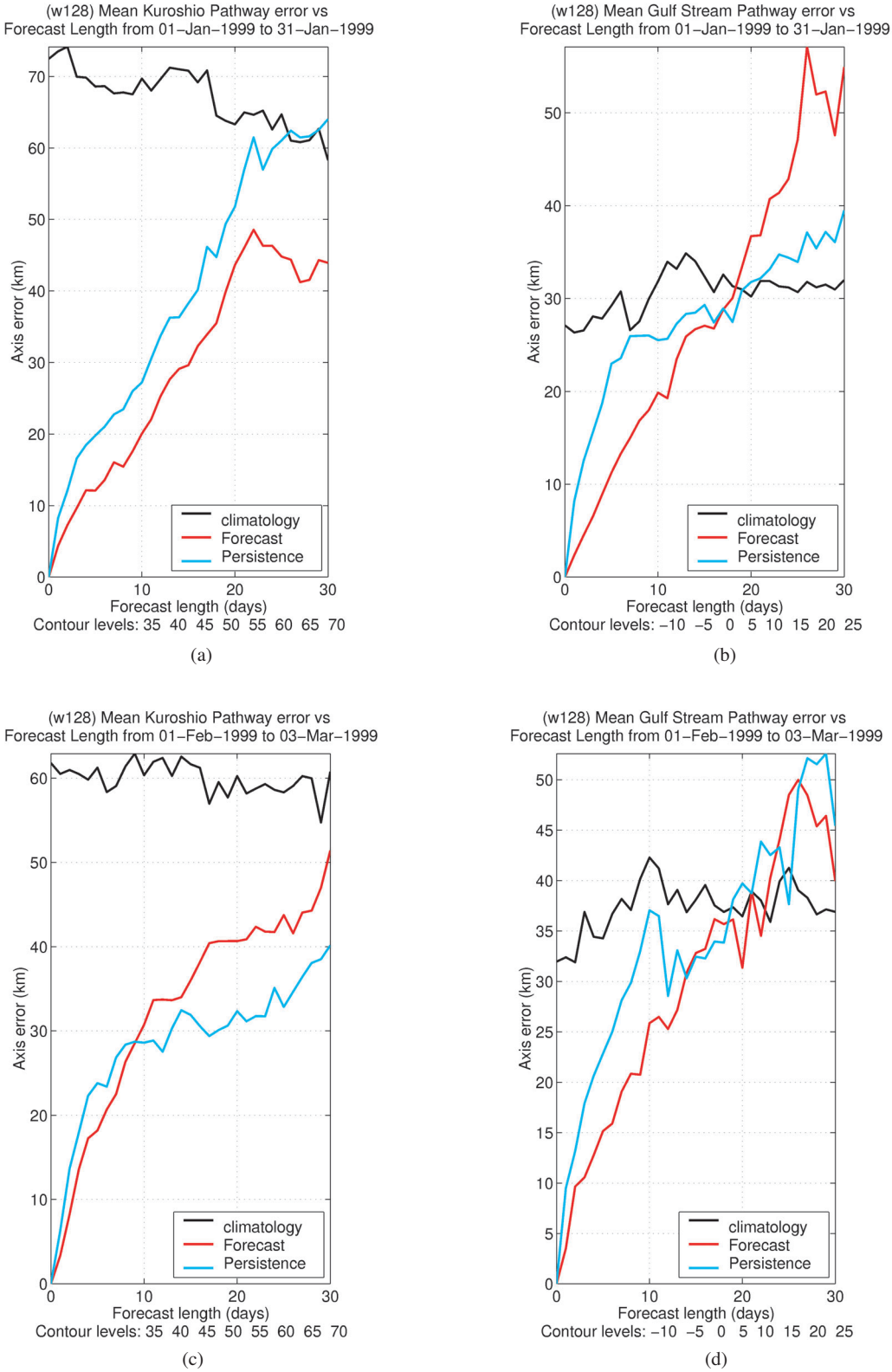

Fig. 33 — Mean pathway axis forecast error (km) vs forecast length (days) for 1/16° global NLOM forecast (red lines), climatology forecast (black lines), and persistence (blue lines) for (a) Kuroshio pathway in January 1999, (b) Gulf Stream pathway in January 1999, (c) Kuroshio pathway in February 1999, and (d) Gulf Stream pathway in February 1999.

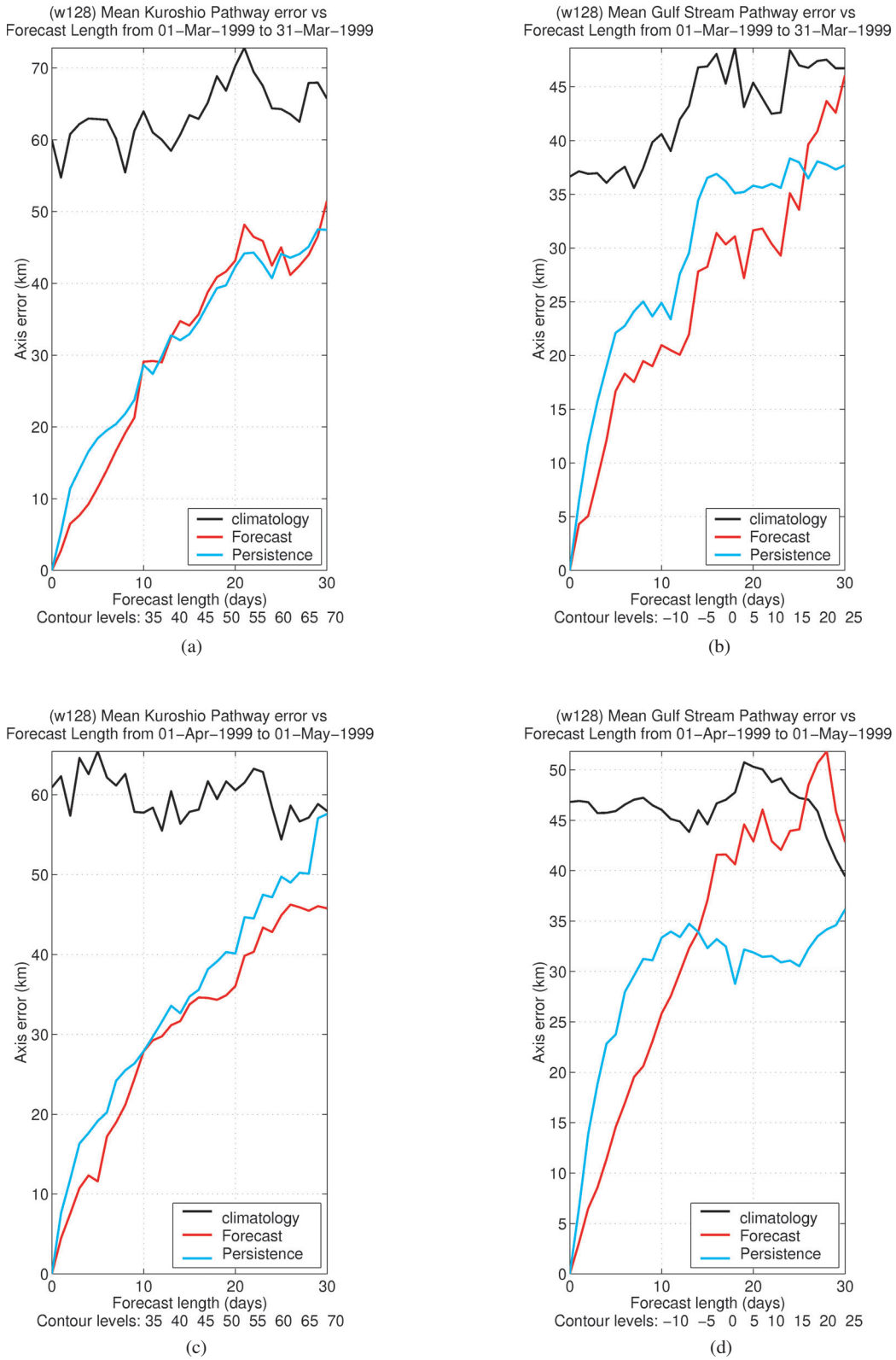

Fig. 34 — Mean pathway axis forecast error (km) vs forecast length (days) for 1/16° global NLOM forecast (red lines), climatology forecast (black lines), and persistence (blue lines) for (a) Kuroshio pathway in March 1999, (b) Gulf Stream pathway in March 1999, (c) Kuroshio pathway in April 1999, and (d) Gulf Stream pathway in April 1999.

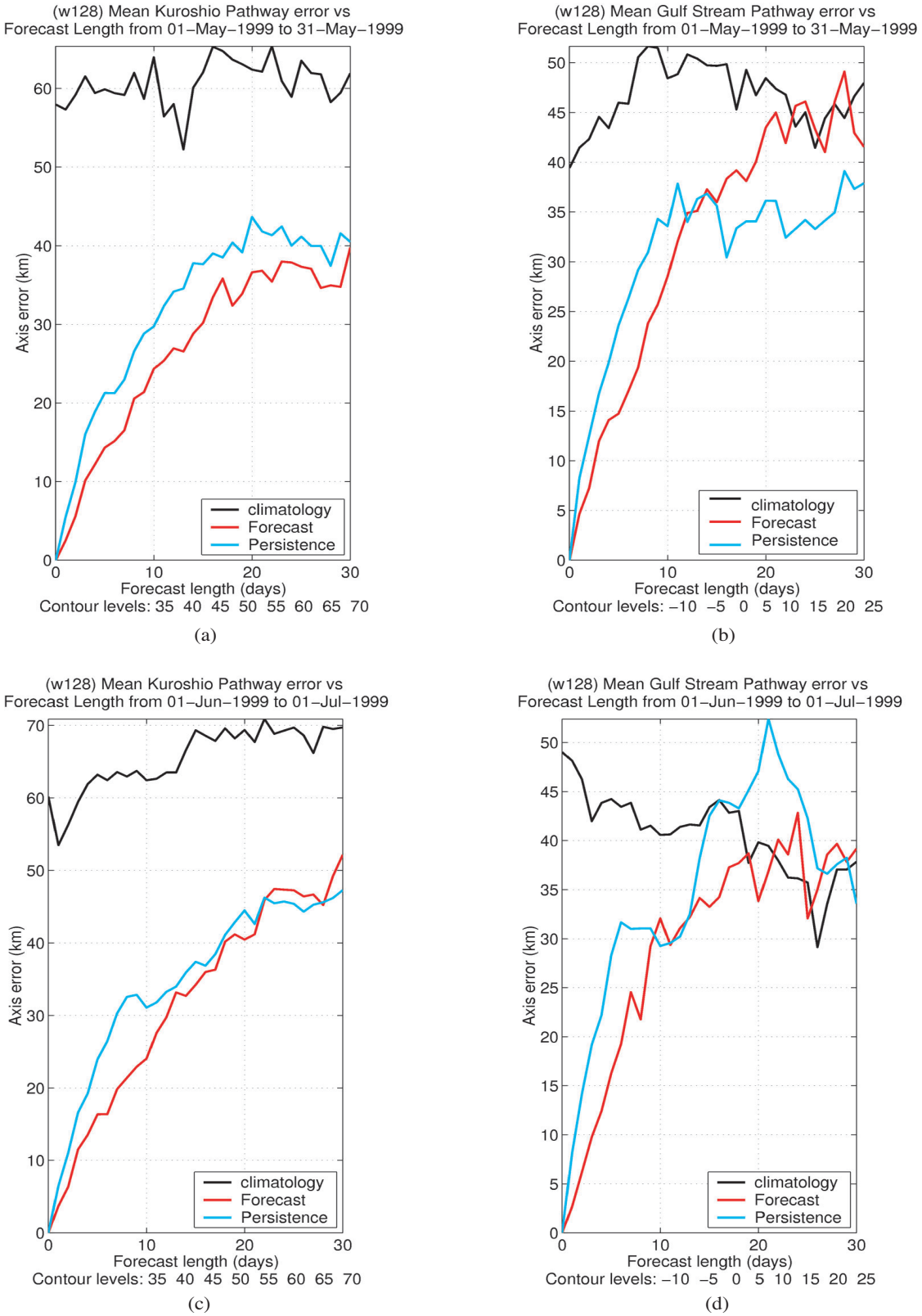

Fig. 35 — Mean pathway axis forecast error (km) vs forecast length (days) for 1/16° global NLOM forecast (red lines), climatology forecast (black lines), and persistence (blue lines) for (a) Kuroshio pathway in May 1999, (b) Gulf Stream pathway in May 1999, (c) Kuroshio pathway in June 1999, and (d) Gulf Stream pathway in June 1999.

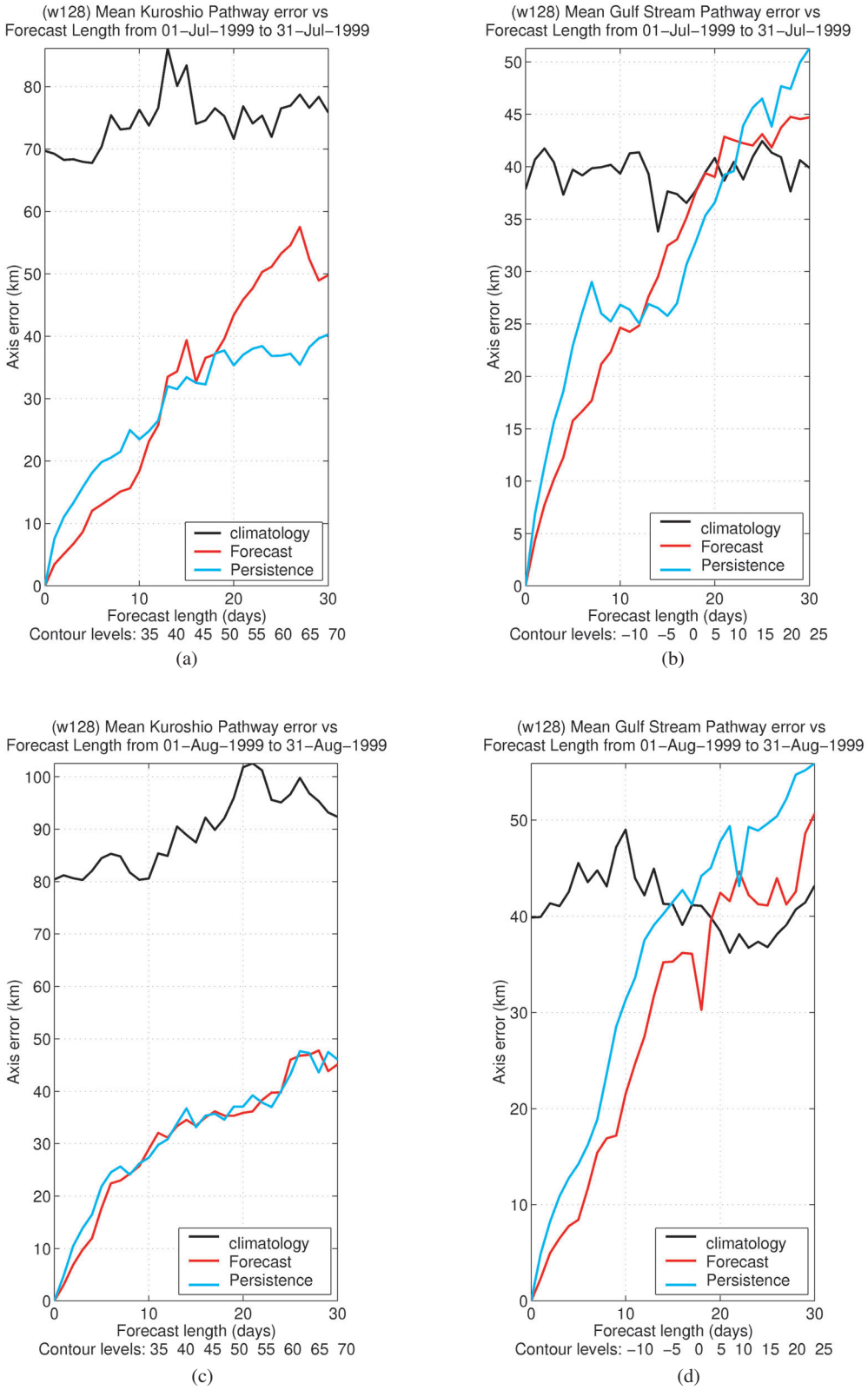

Fig. 36 — Mean pathway axis forecast error (km) vs forecast length (days) for 1/16° global NLOM forecast (red lines), climatology forecast (black lines), and persistence (blue lines) for (a) Kuroshio pathway in July 1999, (b) Gulf Stream pathway in July 1999, (c) Kuroshio pathway in August 1999, and (d) Gulf Stream pathway in August 1999.

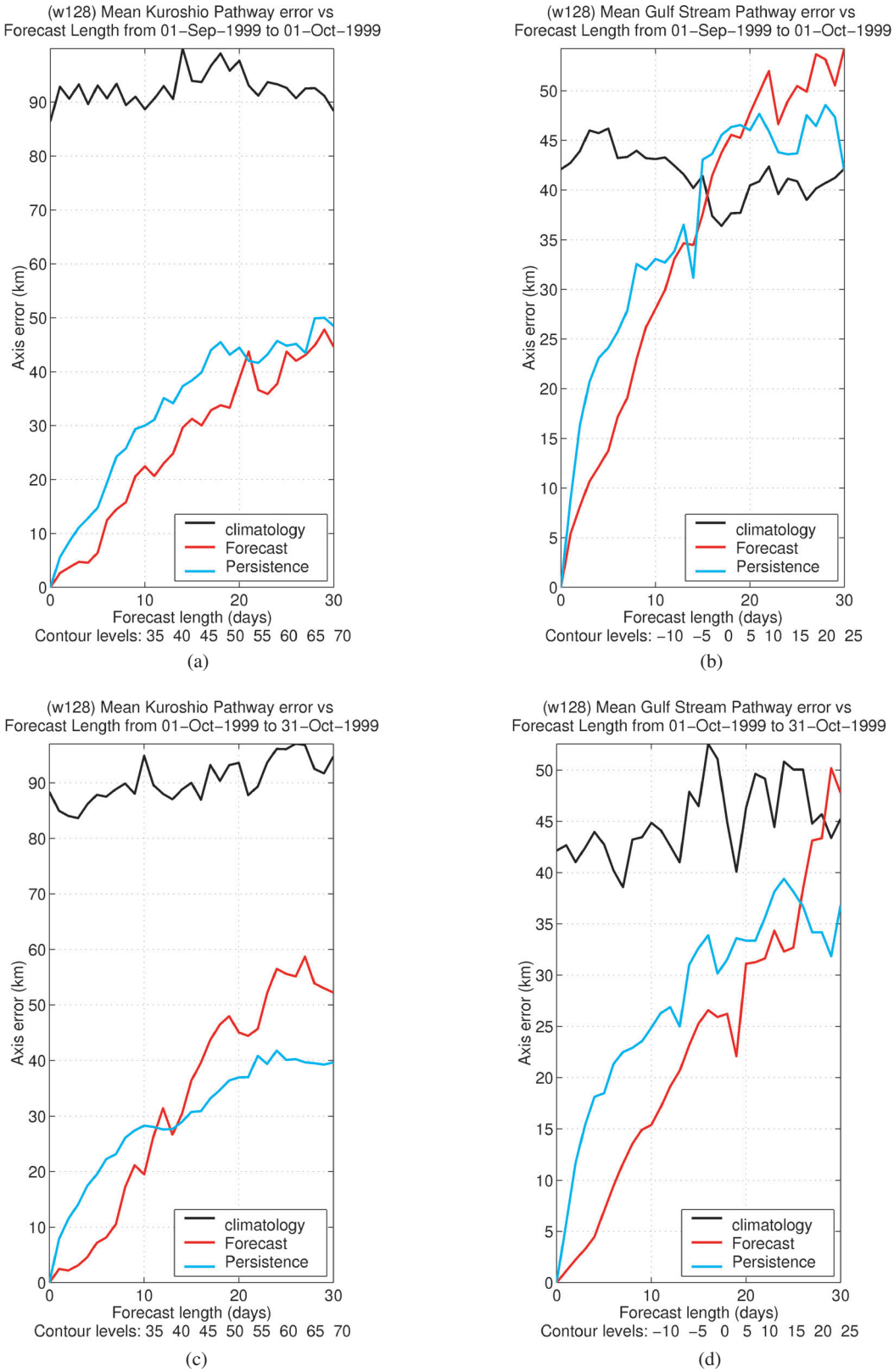

Fig. 37 — Mean pathway axis forecast error (km) vs forecast length (days) for 1/16° global NLOM forecast (red lines), climatology forecast (black lines), and persistence (blue lines) for (a) Kuroshio pathway in September 1999, (b) Gulf Stream pathway in September 1999, (c) Kuroshio pathway in October 1999, and (d) Gulf Stream pathway in October 1999.

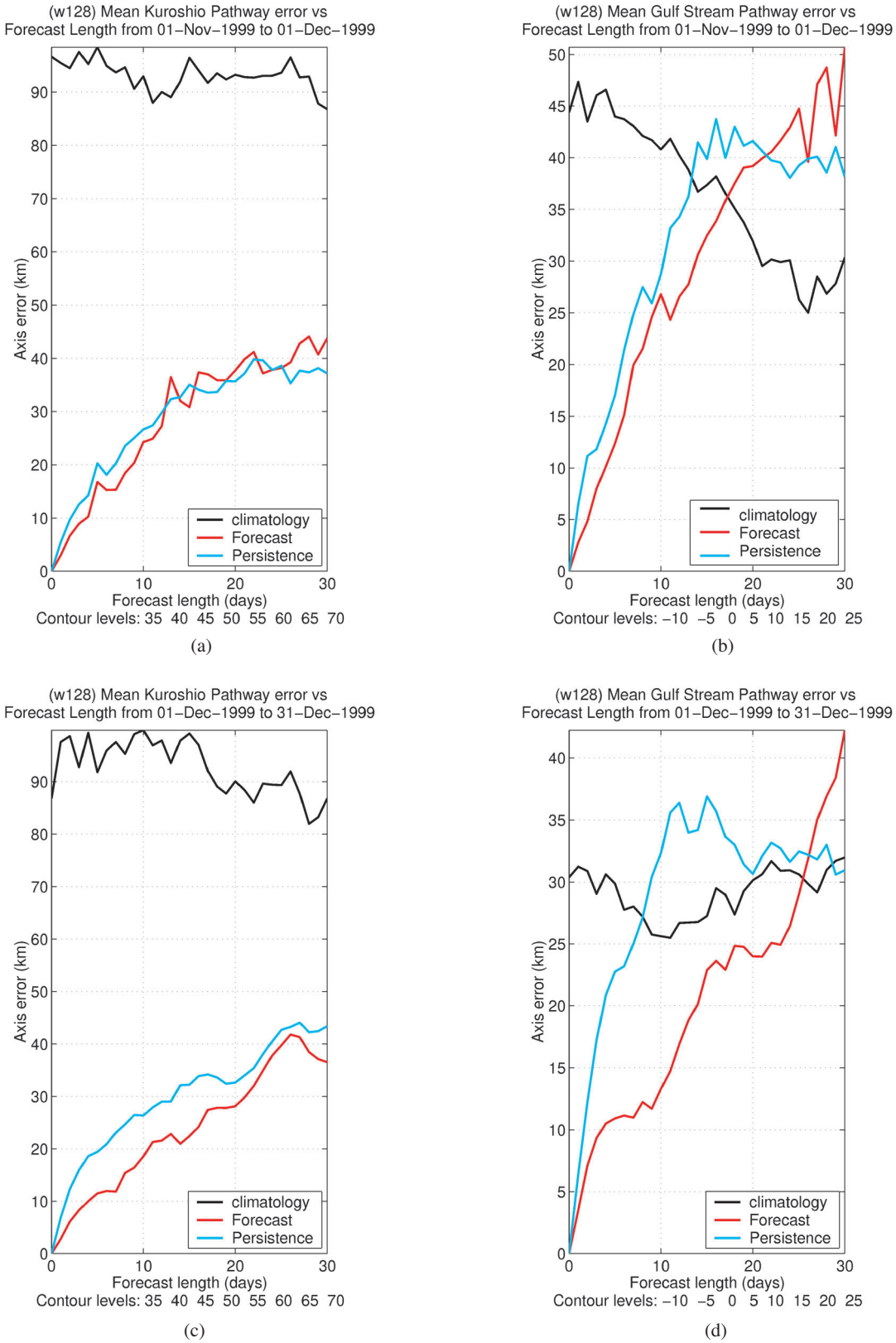

Fig. 38 — Mean pathway axis forecast error (km) vs forecast length (days) for 1/16° global NLOM forecast (red lines), climatology forecast (black lines), and persistence (blue lines) for (a) Kuroshio pathway in November 1999, (b) Gulf Stream pathway in November 1999, (c) Kuroshio pathway in December 1999, and (d) Gulf Stream pathway in December 1999.

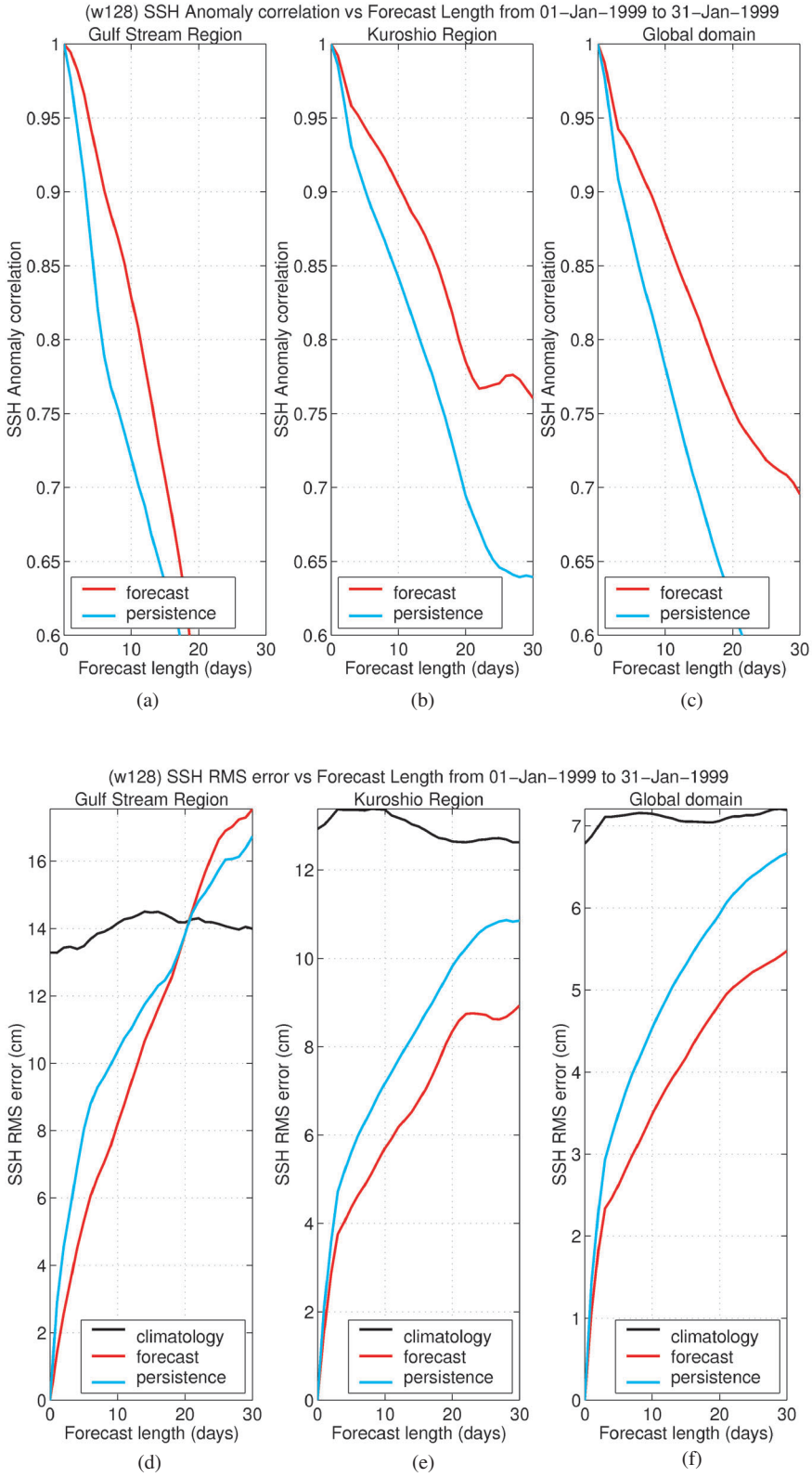

Fig. 39 — Forecast verification statistics for January 1999 from the 1/16° global NLOM SSH forecasts. SSH anomaly correlation vs forecast length (days) for NLOM forecast (red curve) and persistence forecast (blue curve) in (a) the Gulf Stream region, (b) the Kuroshio region, and (c) the entire Global domain; and SSH RMS error (cm) vs forecast length (days) for NLOM forecast (red curve), persistence forecast (blue curve), and climatology forecast (black curve) in (d) the Gulf Stream region, (e) the Kuroshio region, and (f) the entire Global domain.

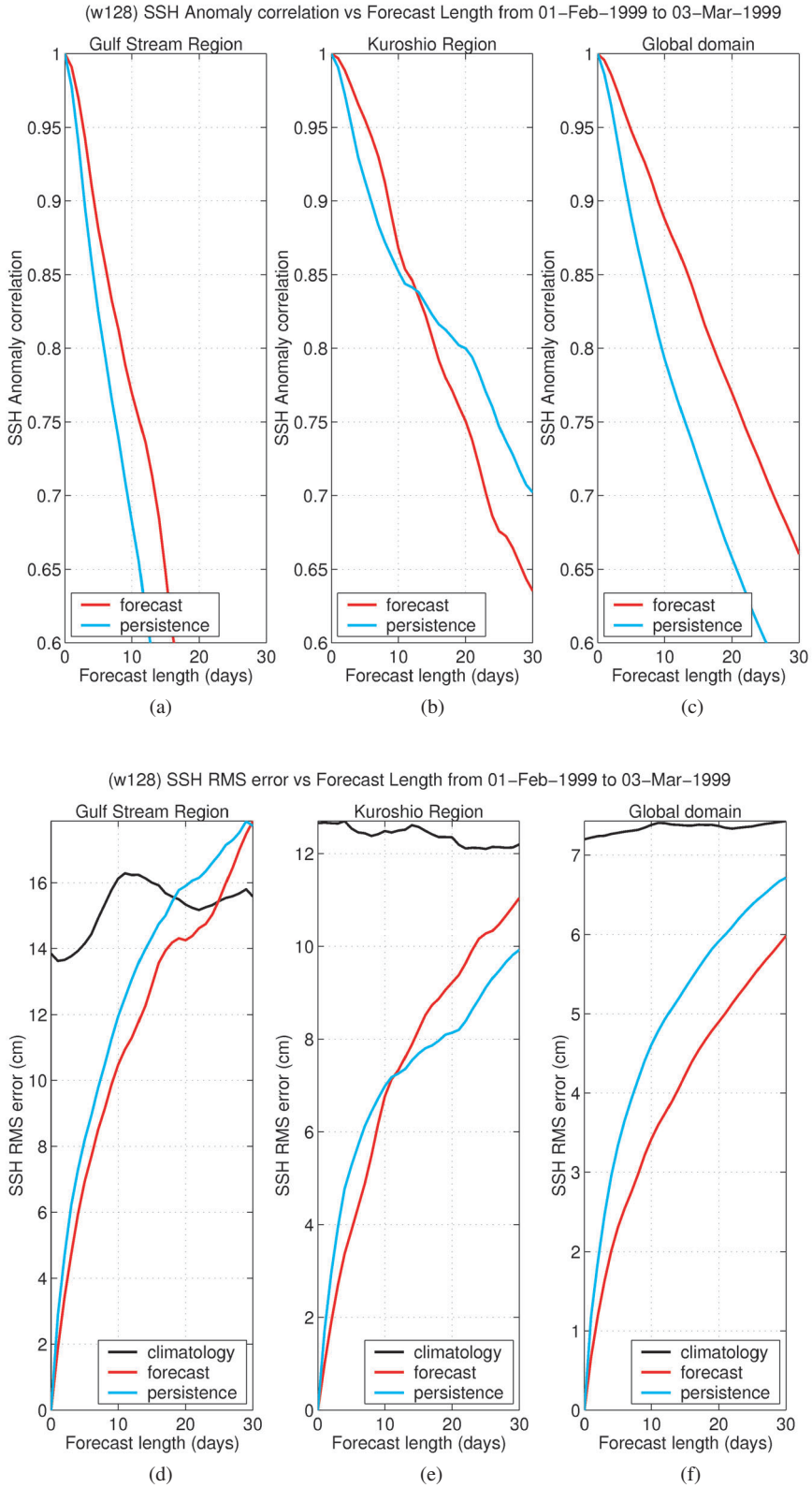

Fig. 40 — Forecast verification statistics for February 1999 from the 1/16° global NLOM SSH forecasts. SSH anomaly correlation vs forecast length (days) for NLOM forecast (red curve) and persistence forecast (blue curve) in (a) the Gulf Stream region, (b) the Kuroshio region, and (c) the entire Global domain; and SSH RMS error (cm) vs forecast length (days) for NLOM forecast (red curve), persistence forecast (blue curve), and climatology forecast (black curve) in (d) the Gulf Stream region, (e) the Kuroshio region, and (f) the entire Global domain.

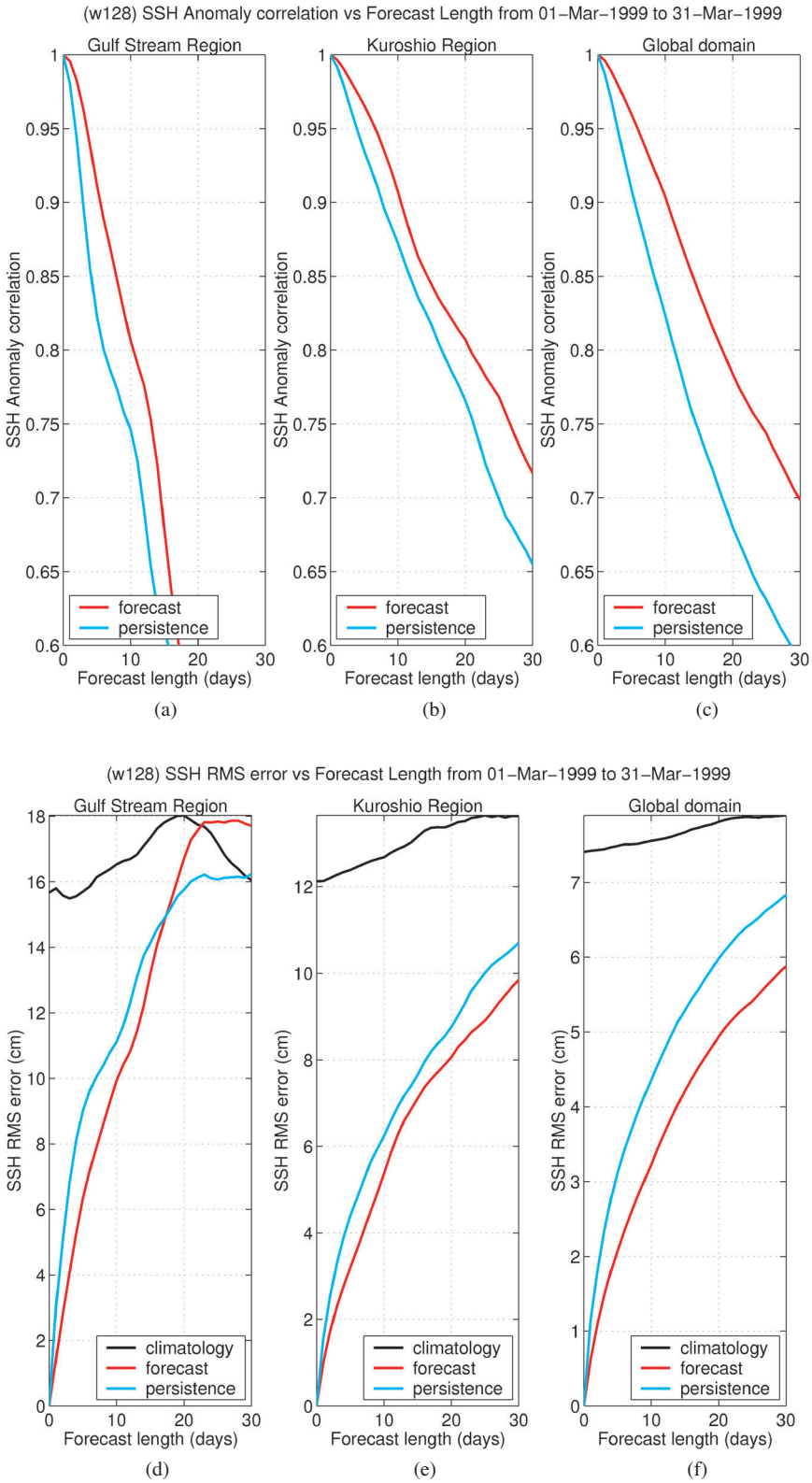

Fig. 41 — Forecast verification statistics for March 1999 from the 1/16° global NLOM SSH forecasts. SSH anomaly correlation vs forecast length (days) for NLOM forecast (red curve) and persistence forecast (blue curve) in (a) the Gulf Stream region, (b) the Kuroshio region, and (c) the entire Global domain; and SSH RMS error (cm) vs forecast length (days) for NLOM forecast (red curve), persistence forecast (blue curve), and climatology forecast (black curve) in (d) the Gulf Stream region, (e) the Kuroshio region, and (f) the entire Global domain.

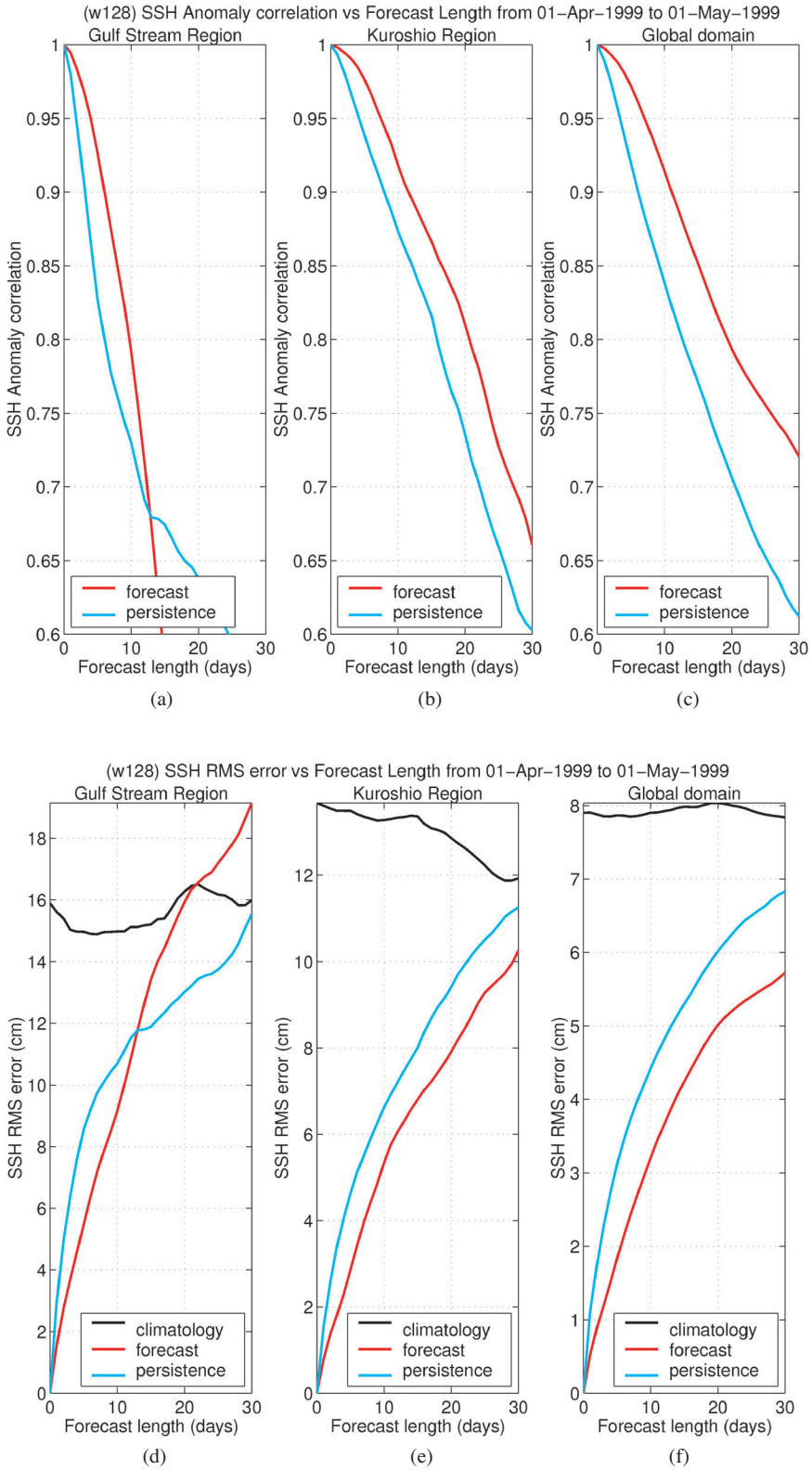

Fig. 42 — Forecast verification statistics for April 1999 from the 1/16° global NLOM SSH forecasts. SSH anomaly correlation vs forecast length (days) for NLOM forecast (red curve) and persistence forecast (blue curve) in (a) the Gulf Stream region, (b) the Kuroshio region and (c) the entire Global domain; and SSH RMS error (cm) vs forecast length (days) for NLOM forecast (red curve), persistence forecast (blue curve), and climatology forecast (black curve) in (d) the Gulf Stream region, (e) the Kuroshio region, and (f) the entire Global domain.

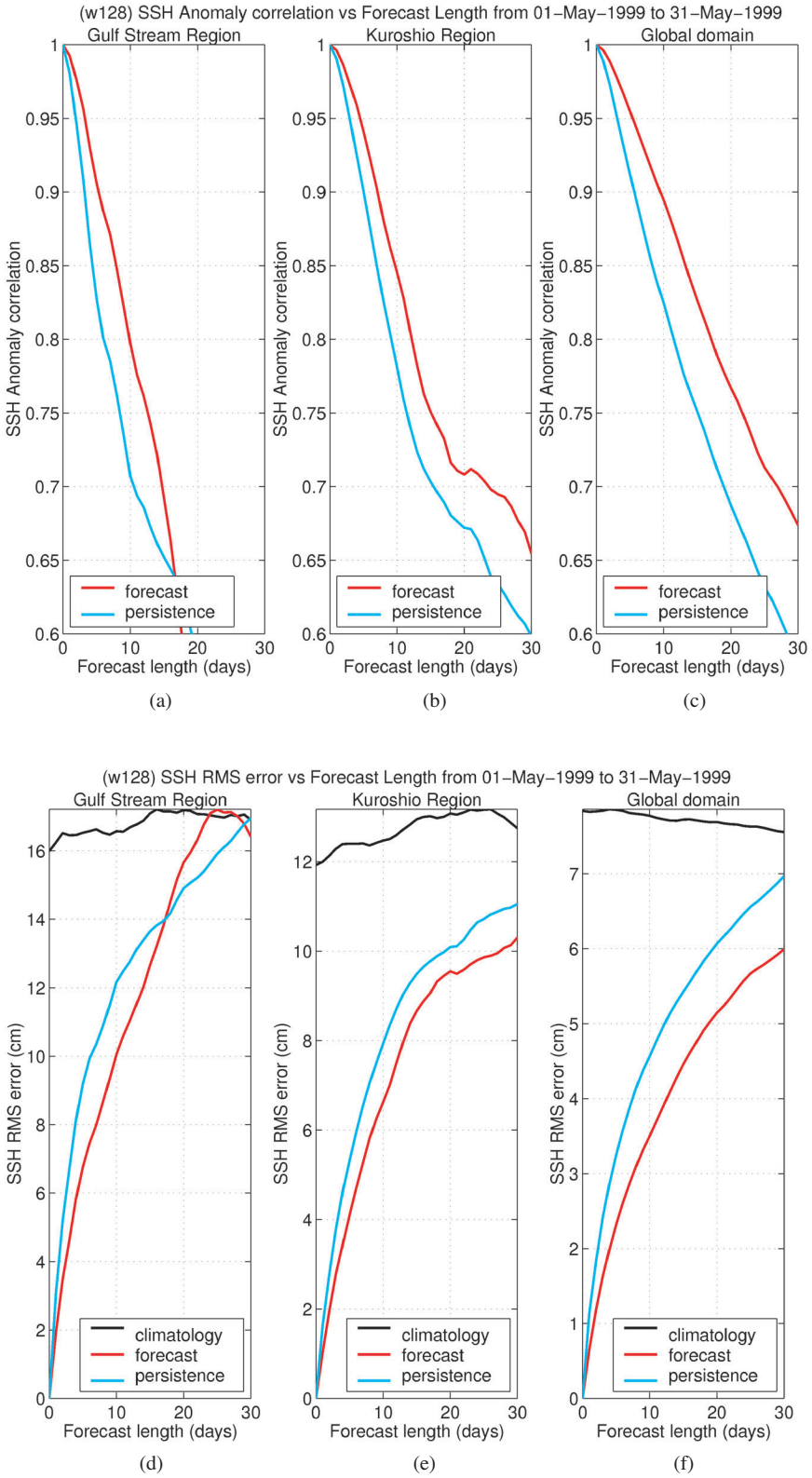

Fig. 43 — Forecast verification statistics for May 1999 from the 1/16° global NLOM SSH forecasts. SSH anomaly correlation vs forecast length (days) for NLOM forecast (red curve) and persistence forecast (blue curve) in (a) the Gulf Stream region, (b) the Kuroshio region, and (c) the entire Global domain; and SSH RMS error (cm) vs forecast length (days) for NLOM forecast (red curve), persistence forecast (blue curve), and climatology forecast (black curve) in (d) the Gulf Stream region, (e) the Kuroshio region, and (f) the entire Global domain.

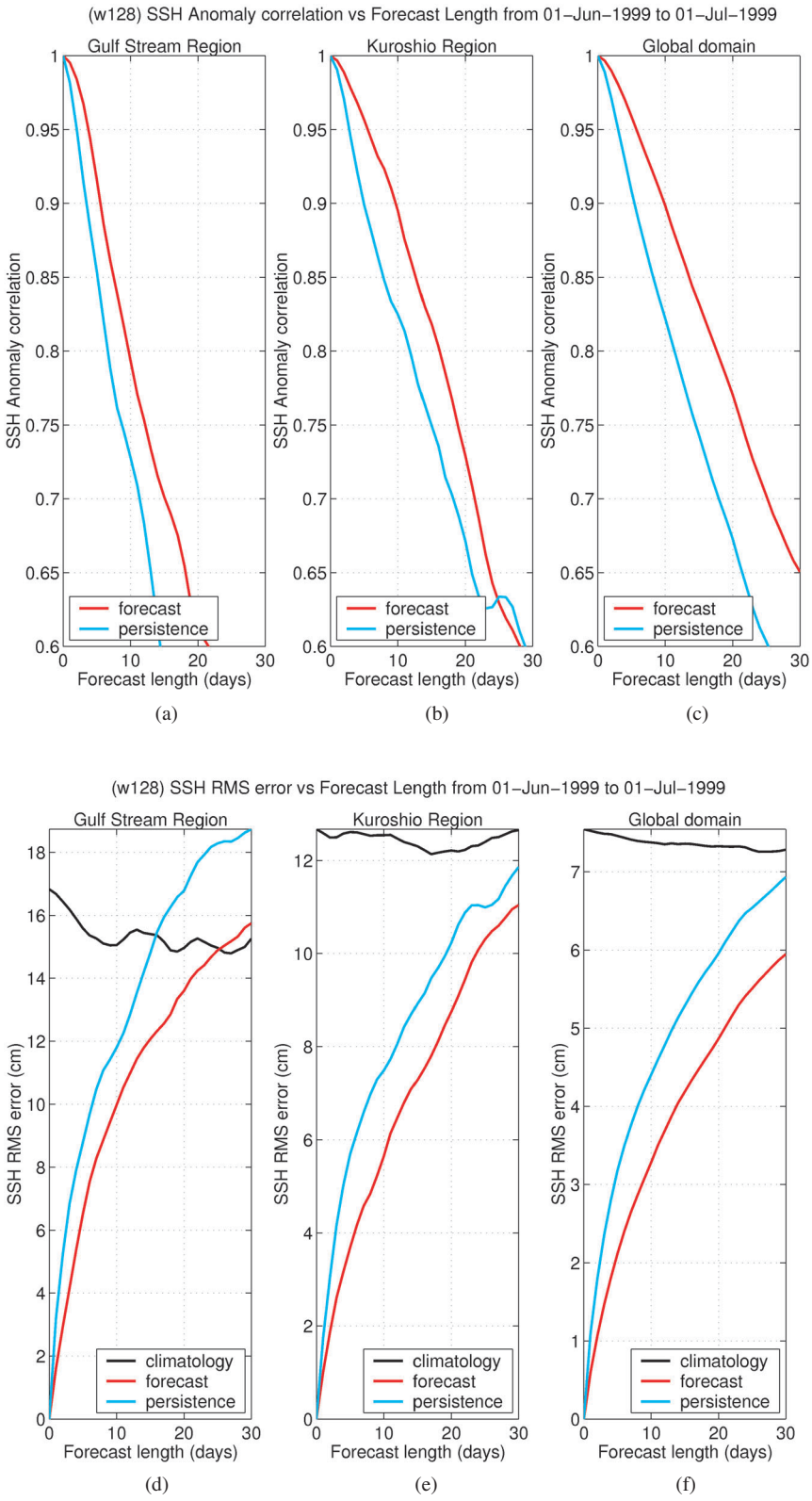

Fig. 44 — Forecast verification statistics for June 1999 from the 1/16° global NLOM SSH forecasts. SSH anomaly correlation vs forecast length (days) for NLOM forecast (red curve) and persistence forecast (blue curve) in (a) the Gulf Stream region, (b) the Kuroshio region, and (c) the entire Global domain; and SSH RMS error (cm) vs forecast length (days) for NLOM forecast (red curve), persistence forecast (blue curve), and climatology forecast (black curve) in (d) the Gulf Stream region, (e) the Kuroshio region, and (f) the entire Global domain.

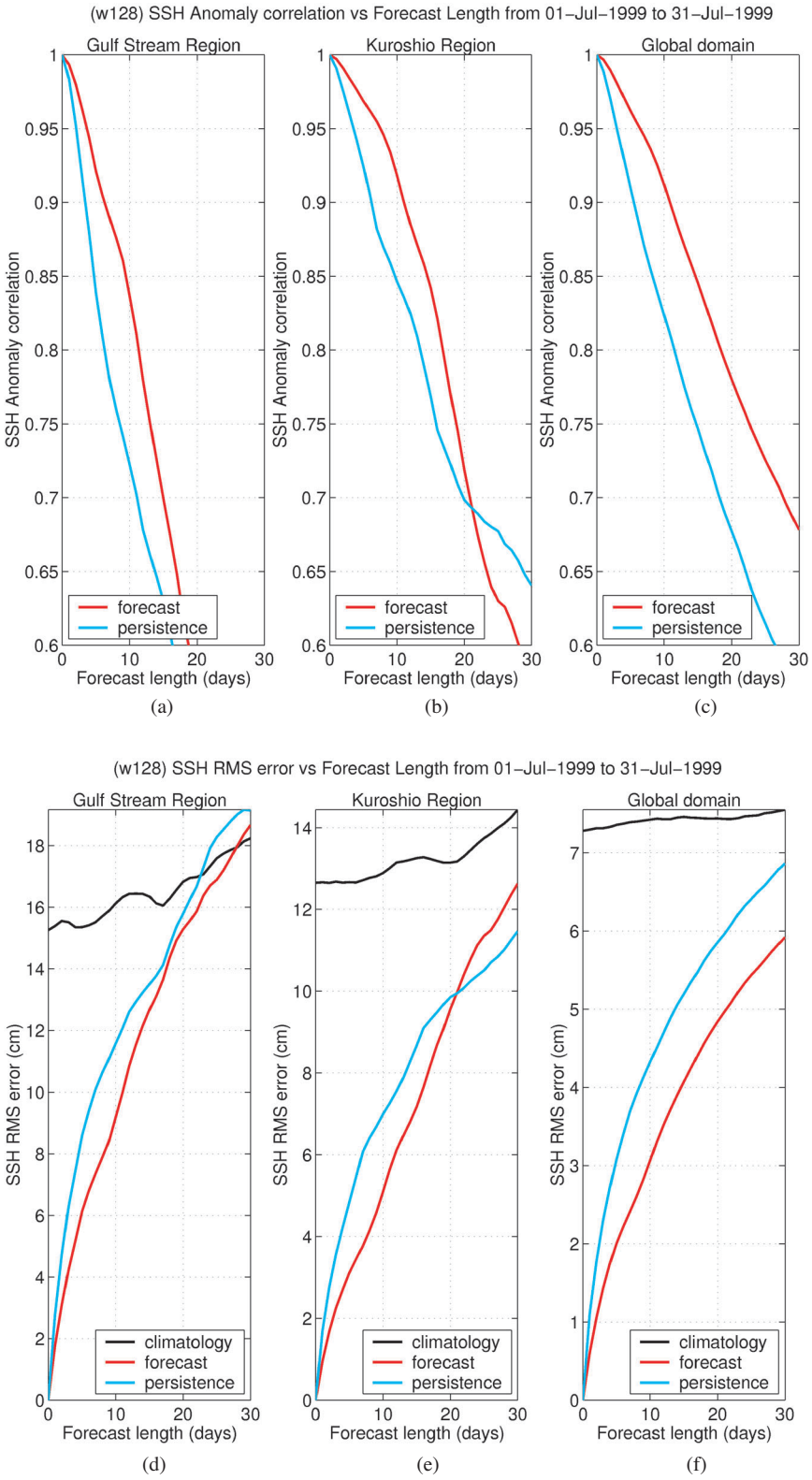

Fig. 45 — Forecast verification statistics for July 1999 from the 1/16° global NLOM SSH forecasts. SSH anomaly correlation vs forecast length (days) for NLOM forecast (red curve) and persistence forecast (blue curve) in (a) the Gulf Stream region, (b) the Kuroshio region, and (c) the entire Global domain; and SSH RMS error (cm) vs forecast length (days) for NLOM forecast (red curve), persistence forecast (blue curve), and climatology forecast (black curve) in (d) the Gulf Stream region, (e) the Kuroshio region, and (f) the entire Global domain.

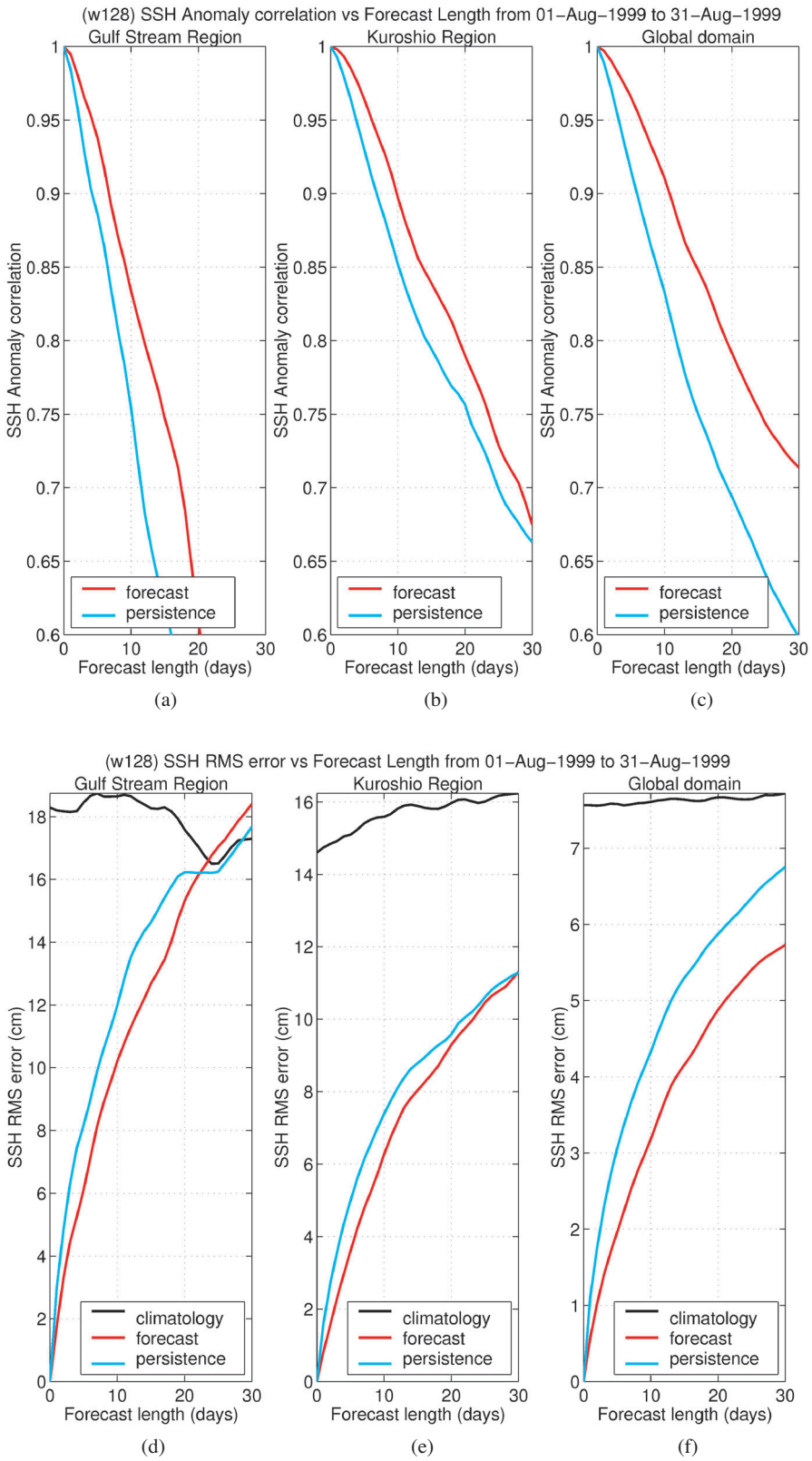

Fig. 46 — Forecast verification statistics for August 1999 from the 1/16° global NLOM SSH forecasts. SSH anomaly correlation vs forecast length (days) for NLOM forecast (red curve) and persistence forecast (blue curve) in (a) the Gulf Stream region, (b) the Kuroshio region, and (c) the entire Global domain; and SSH RMS error (cm) vs forecast length (days) for NLOM forecast (red curve), persistence forecast (blue curve), and climatology forecast (black curve) in (d) the Gulf Stream region, (e) the Kuroshio region, and (f) the entire Global domain.

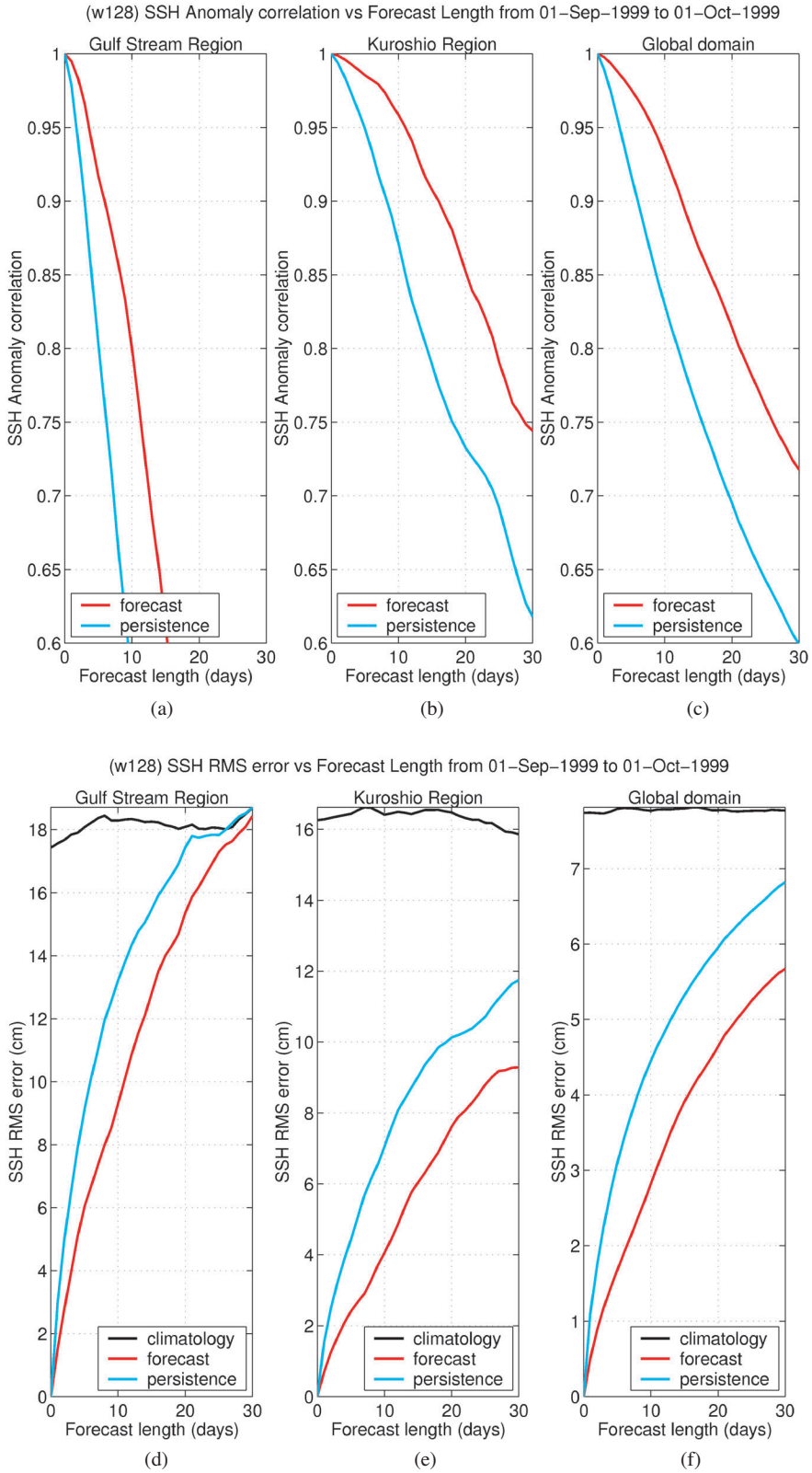

Fig. 47 — Forecast verification statistics for September 1999 from the 1/16° global NLOM SSH forecasts. SSH anomaly correlation vs forecast length (days) for NLOM forecast (red curve) and persistence forecast (blue curve) in (a) the Gulf Stream region, (b) the Kuroshio region, and (c) the entire Global domain; and SSH RMS error (cm) vs forecast length (days) for NLOM forecast (red curve), persistence forecast (blue curve), and climatology forecast (black curve) in (d) the Gulf Stream region, (e) the Kuroshio region, and (f) the entire Global domain.

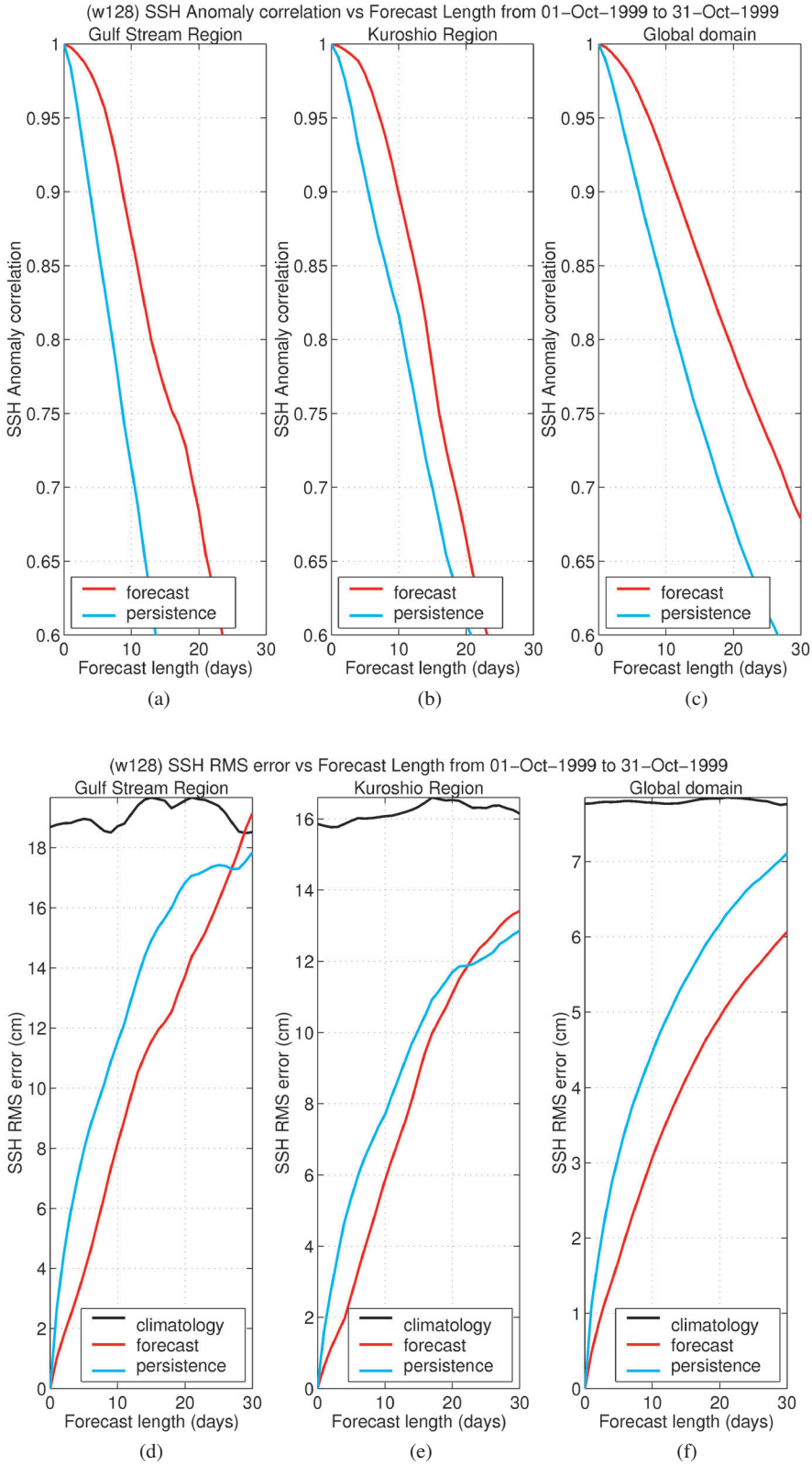

Fig. 48 — Forecast verification statistics for October 1999 from the 1/16° global NLOM SSH forecasts. SSH anomaly correlation vs forecast length (days) for NLOM forecast (red curve) and persistence forecast (blue curve) in (a) the Gulf Stream region, (b) the Kuroshio region, and (c) the entire Global domain; and SSH RMS error (cm) vs forecast length (days) for NLOM forecast (red curve), persistence forecast (blue curve), and climatology forecast (black curve) in (d) the Gulf Stream region, (e) the Kuroshio region, and (f) the entire Global domain.

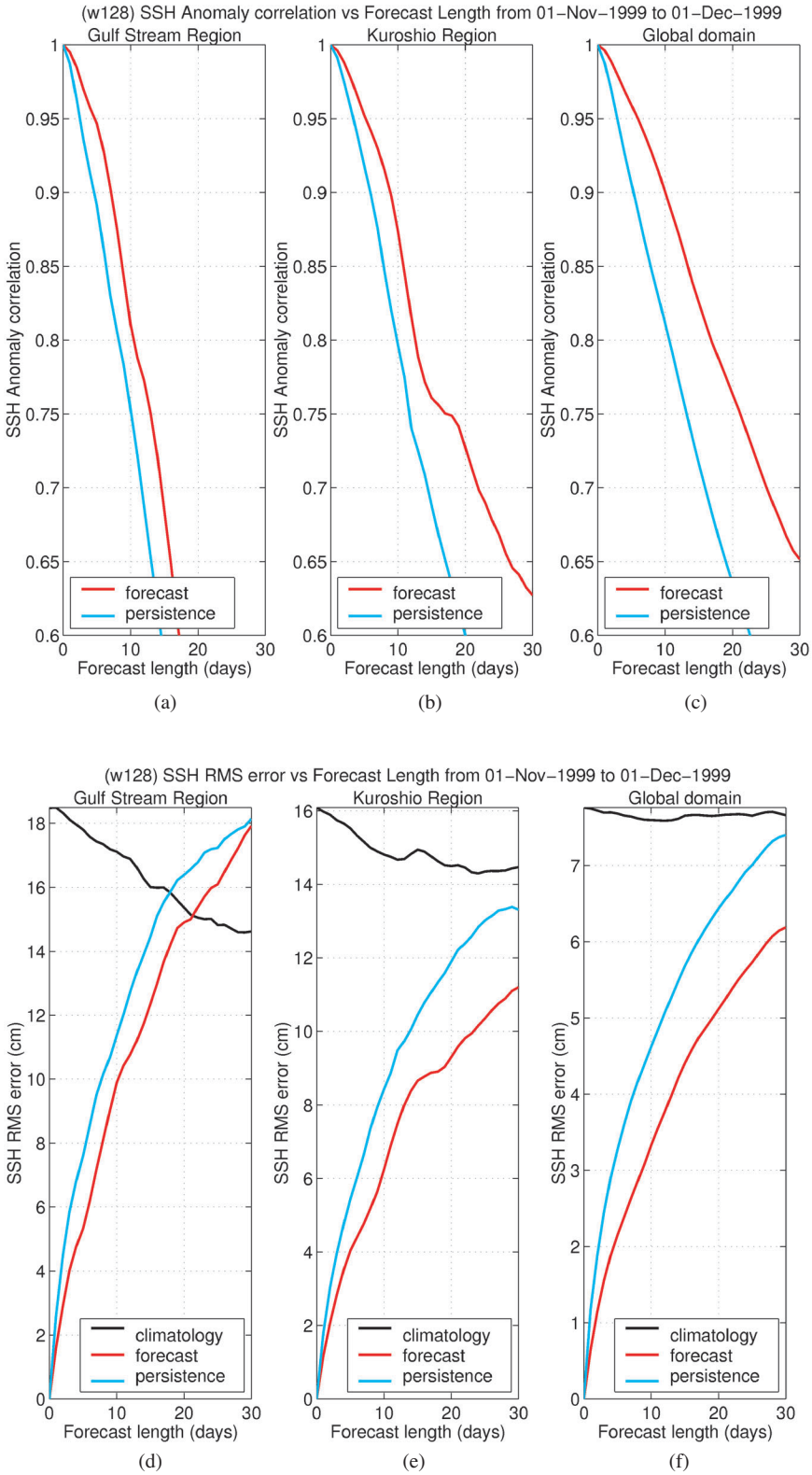

Fig. 49 — Forecast verification statistics for November 1999 from the 1/16° global NLOM SSH forecasts. SSH anomaly correlation vs forecast length (days) for NLOM forecast (red curve) and persistence forecast (blue curve) in (a) the Gulf Stream region, (b) the Kuroshio region, and (c) the entire Global domain; and SSH RMS error (cm) vs forecast length (days) for NLOM forecast (red curve), persistence forecast (blue curve), and climatology forecast (black curve) in (d) the Gulf Stream region, (e) the Kuroshio region, and (f) the entire Global domain.

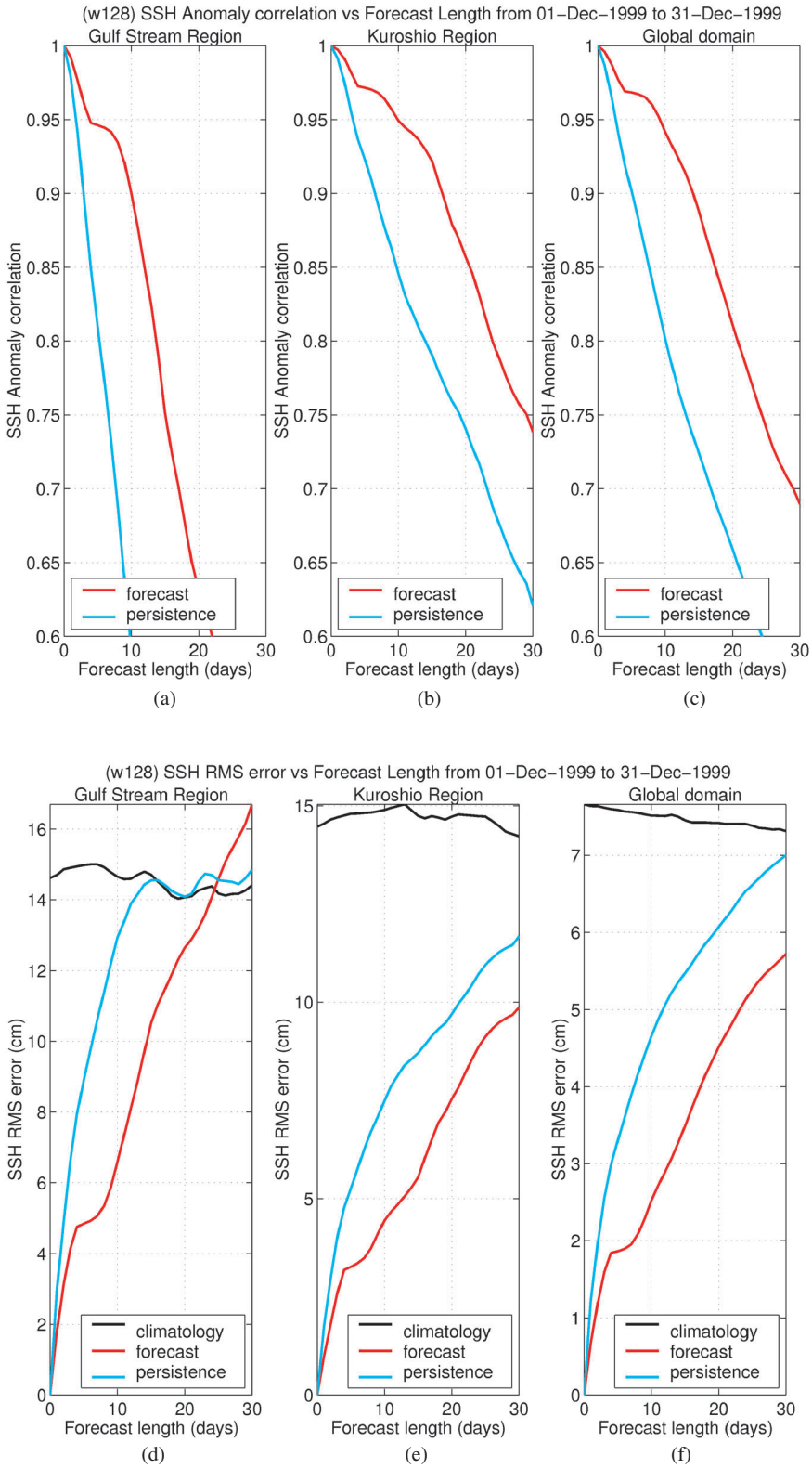

Fig. 50 — Forecast verification statistics for December 1999 from the 1/16° global NLOM SSH forecasts. SSH anomaly correlation vs forecast length (days) for NLOM forecast (red curve) and persistence forecast (blue curve) in (a) the Gulf Stream region, (b) the Kuroshio region, and (c) the entire Global domain; and SSH RMS error (cm) vs forecast length (days) for NLOM forecast (red curve), persistence forecast (blue curve), and climatology forecast (black curve) in (d) the Gulf Stream region, (e) the Kuroshio region, and (f) the entire Global domain.